

AD-769 338

A NUMERICAL MODEL OF SURFACE RECESSION
PHENOMENA OF METAL SUBJECTED TO LASER
RADIATION IN AN AERODYNAMIC ENVIRONMENT

Richard G. Wigglesworth

Air Force Institute of Technology
Wright-Patterson Air Force Base, Ohio

December 1972

DISTRIBUTED BY:

NTIS

National Technical Information Service
U. S. DEPARTMENT OF COMMERCE
5285 Port Royal Road, Springfield Va. 22151

**Best
Available
Copy**

AD 769338



UNITED STATES AIR FORCE
AIR UNIVERSITY
AIR FORCE INSTITUTE OF TECHNOLOGY
Wright-Patterson Air Force Base, Ohio

Q

UNCLASSIFIED
Security Classification

DOCUMENT CONTROL DATA - R & D

(Security classification of title, body of abstract and indexing annotation must be entered when the overall report is classified)

1. ORIGINATING ACTIVITY (Corporate author)

Air Force Institute of Technology
Wright-Patterson AFB, Ohio 45433

2a. REPORT SECURITY CLASSIFICATION

Unclassified

2b. GROUP

3. REPORT TITLE

A NUMERICAL MODEL OF SURFACE RECESSION PHENOMENA OF METALS
SUBJECTED TO LASER RADIATION IN AN AERODYNAMIC ENVIRONMENT

4. DESCRIPTIVE NOTES (Type of report and inclusive dates)

AFIT Thesis

5. AUTHOR(S) (First name, middle initial, last name)

Richard G. Wigglesworth
Major USAF

6. REPORT DATE

December 1972

7a. TOTAL NO. OF PAGES

136

7b. NO. OF REFS

21

8a. CONTRACT OR GRANT NO.

b. PROJECT NO.

c.

d.

9a. ORIGINATOR'S REPORT NUMBER(S)

GAW/MC/72-17

9b. OTHER REPORT NO(S) (Any other numbers that may be assigned
to this report)

10. DISTRIBUTION STATEMENT

Approved for public release; distribution unlimited

11. ABSTRACT BY NOTE

Approved for public release; IAW AFR 190-17

JERRY C. HIX, Captain, USAF
Director of Information

12. SPONSORING MILITARY ACTIVITY

AIR FORCE WEAPONS LABORATORY
KIRTLAND AIR FORCE BASE, NEW MEXICO

13. ABSTRACT

A two-dimensional numerical model of the surface recession dynamics and transient heating of metal plates simultaneously subjected to high intensity laser radiation and aerodynamic frictional forces is developed. The model employs heat and force balance calculations over successive finite time increments on an array of finite elements constructed within the plate's cross-sectional profile lying parallel to the wind vector and bisecting the laser beam spot. A computer program of the model in FORTRAN Extended is provided. The model, exercised at various mach numbers, was found to give results consistent with simplified limiting cases of instantaneous melt removal. Melt-through times for 0.05, 0.10, and 0.20 centimeter thick sheets of aluminum, magnesium, stainless steel, and titanium absorbing 1 and 10 kilowatts of power over spots of 1 cm² and 10 cm² at mach numbers ranging from 0.0 to 4.0 are presented.

Reproduced by
NATIONAL TECHNICAL
INFORMATION SERVICE
U.S. Department of Commerce
Springfield VA 22151

UNCLASSIFIED

Security Classification

14. KEY WORDS	LINK A		LINK B		LINK C	
	ROLE	WT	ROLE	WT	ROLE	WT
Numerical Model Laser Effects Surface Recession Aerodynamic Effects Metals						

UNCLASSIFIED

AD 769338

A NUMERICAL MODEL OF SURFACE RECESSION
PHENOMENA OF METALS SUBJECTED TO LASER
RADIATION IN AN AERODYNAMIC
ENVIRONMENT

THESIS

GAW/MC/72-17

Richard G. Wigglesworth
Major USAF

14

Approved for public release; distribution unlimited

14

A NUMERICAL MODEL OF SURFACE RECESSION PHENOMENA
OF METALS SUBJECTED TO LASER RADIATION
IN AN AERODYNAMIC ENVIRONMENT

THESIS

Presented to the Faculty of the School of Engineering
of the Air Force Institute of Technology
Air University
in Partial Fulfillment of the
Requirements for the Degree of
Master of Science

by

Richard G. Wigglesworth, B.S.
Major USAF

Graduate Air Weapons

December 1972

Approved for public release; distribution unlimited

ic

Preface

I consider myself fortunate having had the opportunity to conduct my thesis study in the fascinating and increasingly important field of lasers. Particularly satisfying to me was the challenge of probing the present frontiers of knowledge and being able to successfully create a tool whereby the bounds of ignorance might be further diminished. Although temporal and intellectual limitations did temper my initial aspirations, I am nevertheless pleased to present a finished, computer-programmed, mathematical model which I am confident can be advantageously employed to further the understanding of laser effects on metals. I stand willing to assist those who may wish to avail themselves of the model. Such gainful use of this thesis will fully compensate for the tribulations encountered and make this effort more than worthwhile.

I am deeply indebted to my friend and thesis advisor, Dr. Peter J. Torvik, for his sincere guidance and concern during the entire course of this investigation. His wisdom in the realm of scientific inquiry will not be forgotten. I am grateful to Dr. James E. Hitchcock and Captain Wesley R. Crow for the expertise that they generously gave in their respective fields of heat transfer and metallurgy. Also, I wish to express my appreciation for the assistance provided by Major John L. Kurzenberger, Major Keith Gilbert, and Captain William T. Laughlin of the sponsoring Laser Effects Branch, Laser Division, Air Force Weapons Laboratory. And finally, my family deserves a very special thanks for their patience and understanding afforded me during the prolonged work on my thesis.

Richard Glen Wigglesworth

Contents

	Page
Preface	ii
List of Figures	v
List of Tables	viii
List of Symbols	ix
Abstract	xi
I. Introduction	1
Statement of the Problem	1
Significance of the Problem	1
Definition of Terms	2
The Physical Phenomena of Laser Interaction With Metals	2
Scope of Study	7
II. Analysis of the Problem	9
Complicating Factors	9
Previous Studies and Current Knowledge	10
Method of Attacking the Problem	11
III. Modeling the Heat Transfer	12
Modeling the Flux Absorption Distribution	14
Modeling the Internal Heat Transfer	15
Modeling the Heat Transfer at the Surface	18
Modeling the Solid-Liquid Phase Change	17
Modeling the Vaporization	20
IV. Modeling the Melt Transfer	22
Modeling the Melt Transfer--Assumptions	22
Determining the Surface Shear Stresses	24
Approximating the Convective Heat Transfer Rate	26
Modeling the Melt Flow--A Numerical Algorithm	29
Assembling the Total Model	33
V. Results	35
Computer Program Specifications	35
Model Validation	37
Model Sensitivity	37

	Page
Comparison of Predicted Results with Known Solutions	39
Comparison of Predicted and Experimental Results . .	42
VI. Findings	45
Aerodynamic Effects on Melt-Through Times	45
Aerodynamic Heating/Cooling Effects	46
Melt Transfer Effects	47
The Influence of the Metal on Aerodynamic Effects . . .	52
The Influence of Metallic Properties on Melt Flow Effects	54
The Influence of Metallic Properties on Aerodynamic Cooling/Heating Effects	56
The Influence of Plate Thickness on Melt-Through Times	58
The Influence of Flux Levels and Spot Sizes on Aerodynamic Effects	61
VII. Conclusions and Recommendations	67
Conclusions	67
Recommendations	68
Bibliography	70
Appendix A: QUEST, A Computer Program of a Numerical Model of Surface Recession Phenomena of Metals Subjected to Laser Radiation in an Aerodynamic Environment . . .	72
Appendix B: A Flow Diagram of QUEST	98
Appendix C: Thermophysical and Thermodynamic Properties of Aluminum, Magnesium, Titanium, Stainless Steel (AISI 304), and Air as Used in QUEST	124
Appendix D: Numerical Results from QUEST for 0.05, 0.10, and 0.20 cm Thick Aluminum, Magnesium, Titanium, and Stainless Steel Irradiated by 1.0 and 10.0 kw Power Over Spots of 1.0 and 10.0 cm ² at Selected Mach Numbers Between 0.0 and 4.0	131
Vita	136

Figure	<u>List of Figures</u>	Page
1	Top and Cross-Sectional Views of a Metal Plate Impinged by a Gaussian Laser Beam of Radius $2c$	13
2	Heat Transfer Rates From the Top, Bottom, Left, and Right Constitute the Net Heat Transfer Rate for Each Finite Element in the Analytic Cellular Array	17
3	The Aerodynamic Boundary Layer Creates Shear Forces Over the Plate's Surface Causing the Molten Metal (Cross-Hatched) Flow	23
4	Velocity Profile Within the Melt Layer	29
5	Graphical Representation of the Computational Algorithm for Transfer of Flow to Adjacent Downstream Finite Element	31
6	A Numerical Finite Element Model (Below) of a Hypothesized Melt Flow (Above)	32
7	The Numerical Transfer of Melt Resulting in Voids and Excesses Within Certain Cells (See Above) is Corrected (Below) by a Subroutine SQUEEZE	33
8	Sensitivity of Melt-Through Times Predicted by QUEST to Changes in n , the Number of Tiers in the Analytic Array of Finite Elements	38
9	Rear Surface Temperatures of a 16 mil Stainless Steel (AISI 304) Plate as Determined from Experiment Results and as Predicted by Modeling	43
10	Dimensionless Melt-Through Times (Normalized by Dividing by the Melt-Through Time at 0.0 Mach) for 0.05, 0.10, and 0.20 cm Thick Aluminum Plates Absorbing 1 and 10 kw of Light Over 1 and 10 cm^2 Spots at Mach Numbers from 0 to 4	48
11	Dimensionless Melt-Through Times (Normalized by Dividing by the Melt-Through Time at 0.0 Mach) for 0.05, 0.10, and 0.20 cm Thick Magnesium Plates Absorbing 1 and 10 kw of Light Over 1 and 10 cm^2 Spots at Mach Numbers from 0 to 4	49
12	Dimensionless Melt-Through Times (Normalized by Dividing by the Melt-Through Time at 0.0 Mach) for 0.05, 0.10, and 0.20 cm Thick Titanium Plates Absorbing 1 and 10 kw of Light Over 1 and 10 cm^2 Spots at Mach Numbers from 0 to 4	50

Figure		Page
13	Dimensionless Melt-Through Times (Normalized by Dividing by the Melt-Through Time at 0.0 Mach) for 0.05, 0.10, and 0.20 cm Thick Stainless Steel Plates Absorbing 1 and 10 kw of Light over 1 and 10 cm ² Spots at Mach Numbers from 0 to 4	51
14	Interior Temperatures of 0.05, 0.10, and 0.20 cm Thick Aluminum and Titanium Plates at Time of Melt-Through After Exposure to 1 kw Radiation Over a 1 cm ² Spot as Modeled by QUEST	55
15	Time to Melt-Through per Unit Thickness of Stainless Steel, Titanium, Aluminum, and Magnesium as a Function of Plate Thickness	59
16	Melt-Through Times for 0.2 cm Thick Titanium and Aluminum in a Mach 2.0 Sea-Level Airstream Normalized by Dividing by the Corresponding Mach 0.0 Melt-Through Times as a Function of Power Density	63
17	Intensity of a Gaussian Flux Distribution as a Function of Radial Distance from the Center of 1 and 10 cm ² Spots Absorbing 1 and 10 kw Power ($q_0 = 2000$ joules/(sec·cm ²))	65
18	Intensity of a Gaussian Flux Distribution as a Function of Radial Distance from the Center of 1 and 2 cm ² Spots Absorbing 1 kw of Power	66
A-1	A Cross-Sectional View at Time of Melt-Through of a 0.01 cm Thick Titanium Sheet Subjected to a Mach 0.5 Sea-Level Wind and an Absorbed Gaussian-Distributed Flux of 10 kw Over a 10 cm ² Spot	92
A-2	The Temperature History at the Back Surface (Opposite the Laser Beam Axis) of a 0.1 cm Thick Titanium Sheet in a Mach 0.5 Sea-Level Airstream Absorbing 10 kw of Laser Power Over a 10 cm ² Spot	93
A-3	The Solid Surface Recession History at the Center of the Laser Beam Spot of a 0.10 cm Thick Titanium Sheet Absorbing 10 kw of Laser Power, Gaussian-Distributed, Over 10 cm ² (Time vs. Axial Distance)	94
A-4	The Solid Surface Recession History at the Center of the Laser Beam Spot of a 0.10 cm Thick Titanium Sheet Absorbing 10 kw of Laser Power, Gaussian-Distributed, Over 10 cm ² (Axial Distance vs. Time)	95

Figure		Page
A-5	The Velocity History of the Nadir of the Liquid-Solid Interface in a Laser-Formed Pit in a 0.1 cm Thick Titanium Sheet Absorbing 10 kw of Gaussian-Distributed Power Over a 10 cm ² Spot	96
A-6	The Velocity as a Function of Axial Distance of the Nadir of the Liquid-Solid Interface in a Laser-Formed Pit in a 0.1 cm Thick Titanium Sheet Absorbing 10 kw of Gaussian-Distributed Power Over 10 cm ²	97

List of Tables

Table		Page
I	Melt-Through Times (in Seconds) of Metal Plates, Assuming Instantaneously Vanishing Melt, One-Dimensional Heat Conduction, and No Wind	27
D-I	Melt-Through Times (in Seconds) as Predicted by QUEST for Aluminum	132
D-II	Melt-Through Times (in Seconds) as Predicted by QUEST for Magnesium	133
D-III	Melt-Through Times (in Seconds) as Predicted by QUEST for Titanium	134
D-IV	Melt-Through Times (in Seconds) as Predicted by QUEST for Stainless Steel	135

List of Symbols

Symbol	Mnemonic	Definition	Typical Units
c		Speed of light	$3 \times 10^8 \text{ msec}^{-1}$
C_{f_x}	CFX	Local skin friction coefficient	(dimensionless)
C_p	CP	Specific heat (at constant pressure)	$\text{cal} \cdot \text{gm}^{-1} \cdot ^\circ\text{K}^{-1}$
E		Energy	ev
h		Planck's Constant	$6.63 \times 10^{-34} \text{ j} \cdot \text{sec}$
i	H, RH, WH, RCVRYH, HBASE	Enthalpy	calories
k	CND	Conductivity	$\text{cal} \cdot \text{sec}^{-1} \cdot \text{cm}^{-1} \cdot ^\circ\text{K}^{-1}$
M	AMACH	Mach number	(dimensionless)
P_N	PRANDTL	Prandtl number	(dimensionless)
Q	FLUX	Total energy absorption rate	kw
q	Q, QO	Flux intensity (or power density)	$\text{j} \cdot \text{sec}^{-1} \cdot \text{cm}^{-2}$
q	HXFR	Heat transfer rate	$\text{cal} \cdot \text{sec}^{-1} \cdot \text{cm}^{-2}$
R_N	ARN	Reynolds number	(dimensionless)
r	RFCTR	Recovery factor	(dimensionless)
r	R	Radial distance	cm
T	T, TT, ATEMP	Temperature	$^\circ\text{K}$
$t, \Delta t$	TIME, DTIME, DELTIME	Time	sec
$t_{1/2}$		Half value thickness	cm
u		Velocity	$\text{cm} \cdot \text{sec}^{-1}$
V	AVELOX	Velocity	$\text{cm} \cdot \text{sec}^{-1}$
$x, \Delta x$	DELX	Radial distance	cm
$y, \Delta y$	DELY	Axial distance	cm

Symbol	Mnemonic	Definition	Typical Units
γ		Ratio of specific heats, C_p/C_v	(dimensionless)
Δ	DEL, D	Incremental dimension	(dimensionless)
ϵ		Hemispherical total emissivity	(dimensionless)
λ		Wavelength	angstrom
μ	VISCSTY, MU	Viscosity	centipoise
ρ	ARHO, DENSITY	Density	$\text{gm}\cdot\text{cm}^{-3}$
σ	STEFAN	Stefan-Boltzmann	$1.355 \times 10^{-12} \text{ cal/}(\text{sec}\cdot\text{cm}^2\cdot^\circ\text{K}^4)$
2σ	SIGMA2	Radius of spot	cm
τ	TAU	Shear stress	dynes cm^{-2}

Superscripts

*	R	Reference condition
---	---	---------------------

Subscripts

∞		Free stream conditions
w		Conditions at air-metal interface
r		Values at recovery temperature
0	0, BASE	Initial condition, starting point, or base value

Abstract

A two-dimensional numerical model of the surface recession dynamics and transient heating of metal plates simultaneously subjected to high intensity laser radiation and aerodynamic frictional forces is developed. The model employs heat and force balance calculations over successive finite time increments on an array of finite elements constructed within the plate's cross-sectional profile lying parallel to the wind vector and bisecting the laser beam spot. A computer program of the model in FORTRAN Extended is provided. The model, exercised at various mach numbers, was found to give results consistent with simplified limiting cases of instantaneous melt removal. Melt-through times for 0.05, 0.10, and 0.20 centimeter thick sheets of aluminum, magnesium, stainless steel, and titanium absorbing 1 and 10 kilowatts of power over spots of 1 cm² and 10 cm² at mach numbers ranging from 0.0 to 4.0 are presented.

A NUMERICAL MODEL OF SURFACE RECESSION PHENOMENA OF METALS SUBJECTED TO LASER RADIATION IN AN AERODYNAMIC ENVIRONMENT

I. Introduction

Light has long been equated with illumination; but light as a means of transmitting man-generated energy was only science fiction until the advent of the laser. Focused laser light can now deposit energy at intensities heretofore never seriously considered. The virtual void of experience has prompted a flourish of laser effect studies. This thesis presents a study concerning the problem of modeling laser effects on metals in an airstream.

Statement of the Problem

The objective of this study is to model the surface recession and transient heating of metals in aerodynamic environments under exposure to high intensity laser radiation. The proposed model shall be programmed for computer solution and be adaptable to various metals and alloys under varying initial and boundary conditions.

Significance of the Problem

No explicit means is known to exist whereby melt-through or "melt-to" times can be predicted for laser beams incident upon metals over which air is flowing. A model to predict such times and to generate ancillary data describing the transient heating and surface recession dynamics will enable various analyses of material response to laser heating. Varying the initial parameters such as laser power,

beam diameter, exposure times, metal thicknesses and properties, and aerodynamic conditions (definable by mach number and altitude in a "standard" atmosphere) in successive simulations can provide information necessary to an increased understanding of the relationships involved. Corresponding data through experiment is and can be expected to continue to be minimal due to nonexistence of lasing devices in various power/spot size regimes, difficulty in accurately and fully instrumenting actual experiments, and excessive cost and time required to conduct sufficient tests over the range of parameters of possible interest. Development of a model is thus considered to be an appropriate supplement to laser effects tests that are possible and a necessary substitute for tests which are not yet feasible.

Definition of Terms

The symbols used in this text, the corresponding mnemonic names used in the resultant computer-programmed model, and their definitions are listed on page viii. Laser radiation as treated herein is electromagnetic radiation within the infrared-visible-ultraviolet spectrum. "High intensity" refers to a laser energy flux sufficient to create significant heating effects, namely melting, when incident upon a metal under consideration; a precise numerical definition is not intended. Other terms will be defined as they occur.

The Physical Phenomena of Laser Interaction with Metals

Given a laser beam directed toward a metal, only a fraction of the photons constituting the initial beam energy emitted from the lasing device will be absorbed by the metal. First, the intervening medium

may appreciably attenuate the transmitted energy. The degree of such attenuation is dependent upon the following: the density and composition of the medium (for example, atmospheric humidity can be a strongly influential factor); the wavelength of the photon; the flux intensity within the beam; and the distance traversed by the beam. Secondly, a portion of the incident photons are reflected by the metal. The portion reflected is a function of several factors; the photon wavelength; the incidence angle; the metallic composition; the surface characteristics including degree of roughness, foreign coatings (ranging for example from a simple inadvertent fingerprint to a purposeful protective paint), surface scale from oxidizing reactions involving the metal; and surface temperature which in turn governs the physical state (solid or liquid) of the metal's face.

The phenomenon by which the absorbed photons impart heat to the metal is primarily by the successive mechanisms of internal photo-electric effect and electron de-excitation to either optic or acoustic phonons (Ref 1:1-2). The process occurs essentially instantaneously at the immediate surface of the metal. The accuracy of this approximation can be evaluated by considering a "worst case"--one in which penetration by the photon should be maximal--where highly energetic photons impinge upon a comparatively light metal. For the case of magnesium subjected to far ultraviolet photons of 12.4 angstrom (\AA) wavelength λ , the photons have an energy E expressed by

$$E = \frac{hc}{\lambda} \quad (1)$$

where h is Planck's constant ($h = 4.136 \times 10^{-15}$ ev·sec), and c is the speed of light ($c = 3.00 \times 10^8$ m/sec). In this example E equals 1 Kev

(one thousand electron volts). From Ref 2, the total mass attenuation coefficient μ/ρ for 1 Kev photons is $993.3 \text{ cm}^2/\text{gm}$ with the photoelectric effect accounting for all but 0.21% of the value of the mass attenuation coefficient (Ref 2:49). The half-thickness $t_{1/2}$, which is the penetration depth by which one-half of all the nonreflected photons are absorbed is (Ref 3:92)

$$t_{1/2} = \frac{\ln 2}{\mu} \quad (2)$$

where μ is the linear attenuation coefficient found by multiplying the mass attenuation coefficient previously noted by the density ρ of the metal (ρ for magnesium is 1.740 gm/cm^3). Thus, for magnesium $t_{1/2}$ equals 0.0004 cm , a very small distance relative to even thin sheets of metals used in practical applications.

Electrons excited by the photoelectric absorption mechanism in turn de-excite by transferring their excess energy to phonons, or vibrational energy within the crystalline lattice of the solid, and thereby complete the transformation of light to heat. The total time of photon to phonon conversion is the time to absorption (after passing the face of the metal) plus the electron de-excitation time. The order of magnitude of the time to absorption may be calculated by dividing the half-thickness $t_{1/2}$ by the speed of light; and, in the "worst case" considered above, the time to absorption is about $1.33 \times 10^{-14} \text{ sec}$. The "worst case" for de-excitation times, that is where the relaxation takes the longest, occurs where the incident photons have much less energy than the 1 Kev used to calculate the half-thickness $t_{1/2}$ above (Ref 1:21). It is also hypothesized that transition metals have longer relaxation

times than do simple metals. Typical de-excitation times have been calculated to be about 10^{-7} to 10^{-6} sec for transition metals such as stainless steel and titanium compared to 10^{-11} to 10^{-10} sec for simple metals such as aluminum and magnesium (Ref 1:v).

The combined times to absorption and to de-excitation can be approximated, due to its dominance, solely by the time to de-excite; that is, the "worst case" total time for conversion of light to heat is about 10^{-6} sec. Such times are large when compared to the duration of a typical single 10^{-8} sec pulse from a Q-switched laser (Ref 4:8), and the assumption of instantaneous light to heat conversion in this case is inappropriate; but for continuous wave (cw) lasers, for pulsed lasers where the individual pulse is much longer than 10^{-6} sec, and possibly for repetitively pulsed lasers where the pulse repetition rate is very high, the assumption of "instantaneous" conversion of light to heat is approximate for most analytic purposes.

Subsequent to the optical-to-thermal energy transformation, heat is transferred from the laser beam-metal interface, or "spot," by four mechanisms, three of which are: conduction within the metal, radiation from the surface, and convection to (or from) the adjoining air. If the absorbed energy flux is sufficiently intense, a finite element within the laser spot receiving the greatest flux will after some initial interval of time reach the melting temperature; and after accumulating an additional amount of energy (the latent heat of fusion) the element transforms to the molten state. As a liquid, the metal is subject to mass flow due to the surface shear forces created by aerodynamic skin friction; this is the fourth mechanism by which heat is transferred.

The rate of the liquid transfer (and consequential heat transfer) is a function of the magnitude of the drag forces, the viscosity of the liquid metal, and the depth of the molten layer. Transfer of the melt along the surface of the metal to a region of lower flux absorption and correspondingly cooler surface temperatures may result in either freezing of the liquid metal or melting of the underlying solid layer. As time progresses, heat will continue to be absorbed and conducted such that interior temperatures will continue to rise and additional incremental layers will continue to melt thereby causing the solid-liquid interface to recede until melt-through occurs.

Additional phenomena which can further complicate the total modeling problem include vaporization of the liquid metal and oxidation at the metal's surface. Vaporization can occur when incident flux exceeds the combined modes of heat dissipation. If vaporization does occur, any vapor within the laser beam may strongly attenuate the oncoming laser energy flux (Ref 1:2). Oxidizing reactions liberate heat of combustion at rates dependent upon the temperature-time history of the metal and the ambient air and wind conditions. The rates may be insignificant except for certain metals such as magnesium and titanium, where at elevated temperatures in a high velocity airstream catastrophic oxidation may occur. The conditions under which this ignition begins are not well-defined (Ref 5:1), but when ignited the liberated heat of combustion combined with the laser flux will accelerate the melting process to one of burning. The rate of the process is highly dependent upon the oxygen available and the temperature of the combustive metal; thus the combustion should propagate faster to

the leeward but may not be self-sustaining beyond the area influenced by the laser radiation.

Scope of Study

This study includes the two-dimensional, numerical modeling of the surface erosion dynamics and the transient heating within metal plates given the mach number, the altitude, the distance from the plate's leading edge, the energy absorption rate (flux) distribution, and the physical and thermodynamic properties of the metal. Attenuation of the laser energy from the lasing device to the plate and reflection of the light at the surface of the metal are not treated in this work. Transport of molten metal due to gravity and energy release from any surface oxidation or combustion were not studied sufficiently to permit inclusion of their respective effects in the resultant model. Only the shear stresses from aerodynamic skin friction are incorporated within the model; pressure drag forces on the molten metal are neglected. The model assumes an axially symmetric flux distribution within a normally incident laser beam. Heat conduction in the axial and windward/leeward directions is included; heat conduction perpendicular to the plane formed by the wind vector and the normal to the plate surface is disregarded.

Four metals (aluminum, magnesium, stainless steel, and titanium) were specifically modeled, including variation of their physical and thermodynamic properties as a function of temperature. Other metals can be accommodated upon appropriately incorporating their respective properties within the model. Although it was originally intended to

GAW/MC/72-17

model continuous wave (cw) laser radiation, the resultant model appears adaptable to certain pulsed laser radiation where the duration and repetitive rate of the pulses are consonant with the approximation of instantaneous photon to phonon conversion as discussed earlier in this chapter.

II. Analysis of the Problem

Although lasers have provided a novel mode of transmitting intensive energies by means of photons, analysis of the surface recession and transient heating of metals coincidentally subjected to such laser energy and aerodynamic friction reduces to using fundamentals of heat transfer and mass flow--established fields of science. Justification for such analytic methods lies in the nature of light absorption by metals, as described in Chapter I, whereby the absorbed light is approximately instantaneously converted to thermal heat at the immediate surface of the metal. Such thermal heat is subject to all of the conventional equations employed in the field of heat transfer. Thus the total phenomenon being modeled conveniently divides itself into (1) a problem of heat transfer within a static two- (or, including the vapor phase, a three-) phase metal, and (2) a problem of mass flow within the liquid metal resulting from shear forces generated by aerodynamic friction over the plate's surface.

Complicating Factors

The problem of modeling the heat transfer within a two-phase metal has defied a general solution (Ref 6:477). The primary obstacle has been the complexity of the mathematics involved (Ref 7:951). Complicating factors include the following: unree-dimensional, unsteady temperature distributions within the solid and liquid phases; temperature-dependent thermodynamic properties; diverse initial and boundary conditions found in practical applications; and the presence of two moving physical boundaries.

The second problem, that of determining the molten mass flow rate and skin frictional heating due to aerodynamic flow over the metal plate relates to boundary layer studies that have been extensively pursued since the requirement arose for determining heat and mass transfer effects on reentry vehicles. While even though most existent solutions to these problems are approximate ones, it does appear that adequate investigative study has been accomplished for now and that the relations obtained have been verified sufficiently to give reasonable tools for the purpose of this study (Refs 8 and 9). Factors that in general can complicate the calculations of drag forces and convective heat transfer due to aerodynamic friction are as follows: arbitrary shapes of the objects to be modeled, imprecise ability to predict the transitional Reynolds number between laminar and turbulent flow, and locally varying temperatures along the line of flow.

Previous Studies and Current Knowledge

A study on polar ice thickness including a mathematical treatise on the associated heat conduction with freezing was published by Josef Stefan in 1891; and, although it was Franz Neumann who first found the particular solution for freezing of a semi-infinite slab with a constant boundary temperature, the general problem of conduction with freezing or melting has become known as "Stefan's Problem." Muehlbauer and Sunderland (Ref 7), the source of the above historical note, have published a comprehensive literature review of works covering "Stefan's Problem" to 1965. Reference 10 refers to a survey of later works.

While Stefan's Problem is relevant to numerous contemporary processes, perhaps the most studied of these have been metal casting,

welding, and reentry vehicle ablation. Despite the general similarity of all these problems to that of laser heating, subtle differences do exist; and no single solution to any of these problems was found to be readily adaptable to modeling melt-through by laser heating.

Several mathematical approaches have been employed in seeking solutions to Stefan's Problem. They include the variational, heat-balance and contour integral, analogue, and numerical techniques (Ref 7:951-6). Of these, numerical analysis using the finite difference and finite element approaches was selected for the purposes of this study--primarily on the basis of the availability of a large, high-speed, digital computer (such a computer is nearly mandatory for the large array of elements necessary for any satisfactory degree of accuracy). This approach in part paralleled the work of Torvik (Ref 10) who has recently modeled laser heating exclusive of aerodynamic effects.

Method of Attacking the Problem

The final model of this study, as found in Appendix A, evolved from a rudimentary, one-dimensional, constant flux, constant thermodynamic/physical properties, instantaneous melt removal, finite difference model by progressively removing the enumerated qualifications. The next two chapters review the logic employed in constructing the final model. Chapter III deals with heat transfer by absorption, radiation, conduction, and vaporization, and Chapter IV with heat transfer by convection and melt flow.

III. Modeling the Heat Transfer

Assuming a normally incident laser beam in still air with axially symmetric energy deposition, no heat transfer occurs circumferentially about the beam axis. An array consisting of concentric annuli, as shown in Fig. 1, can be used to model the resulting transient heating and progressive melting phenomena two-dimensionally (radially and axially) in a cylindrical coordinate system with no loss in accuracy occurring by ignoring the circumferential direction (Ref 10:6).

The presence of wind-driven melt flow, however, contravenes the two-dimensionality of the total surface recession problem since the axial symmetry of temperatures is lost as soon as melting commences. Nevertheless, thermal and topographical symmetry should theoretically be maintained about the spot-bisecting, wind-parallel line. Furthermore, deepest penetration should occur within the plane directly beneath this same line. A two-dimensional array to become the basis of the finite element, numerical approach to modeling the total phenomenon was therefore constructed, as shown in Fig. 1, from the volume lying directly beneath an infinitesimal strip lying along the wind line and intersecting the beam axis. The origin of the array is taken to be the element furthest downwind at the back surface of the metal plate. The first subscript of an i,j th element refers to the column and the second to the row in the array where the array is divided into m columns and n tiers. With an implement for the numerical, finite element analysis thus established, distribution of the flux absorption is next modeled.

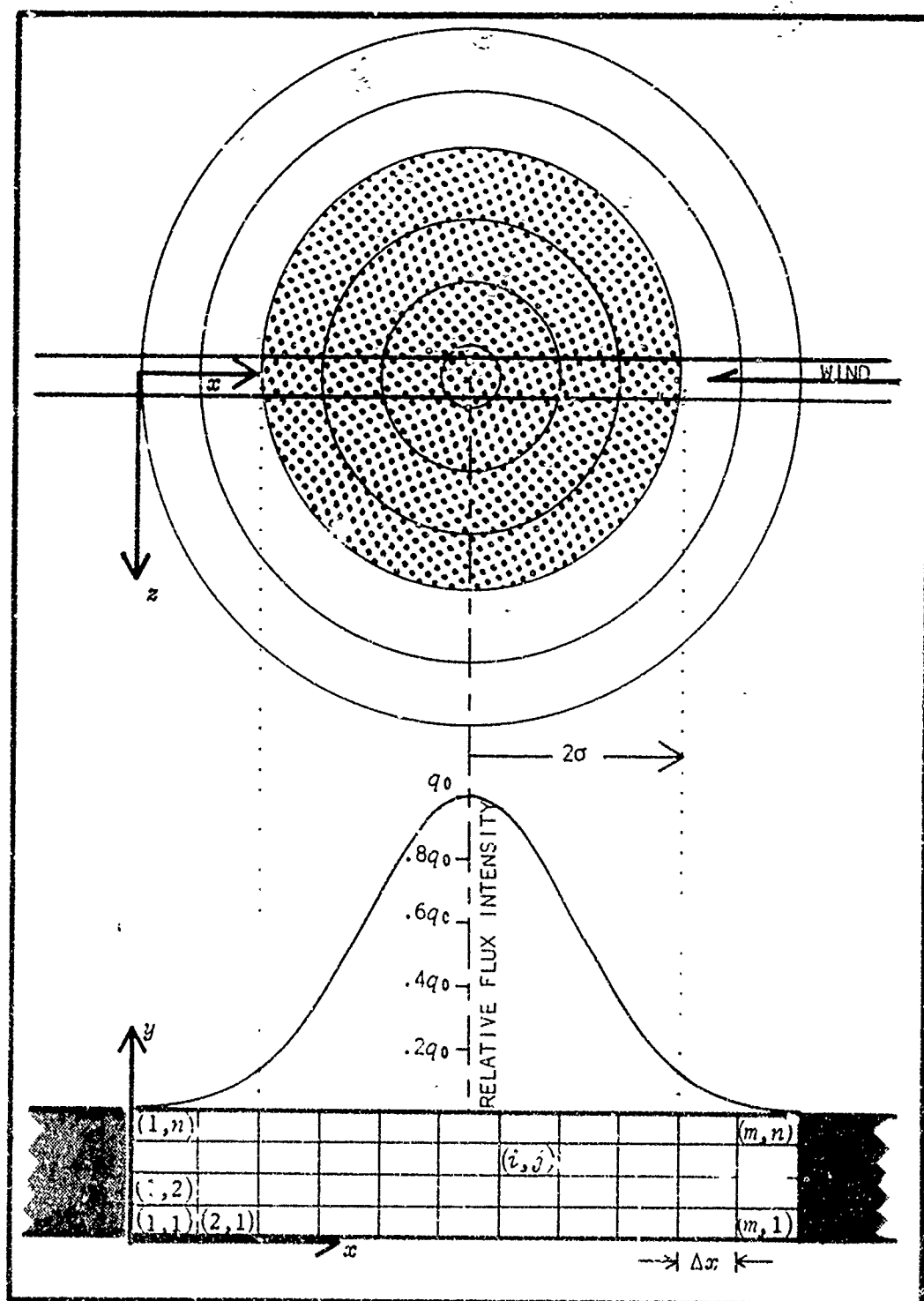


Fig. 1. Top and Cross-Sectional Views of a Metal Plate Impinged by a Gaussian Laser Beam of Radius 2σ . The radius thus defined is the distance at which the local flux density is 0.135 of the intensity at the beam axis as is illustrated by flux distribution along the cellularly arrayed cross section of plate underlying the beam-bisecting, wind-parallel strip.

Modeling the Flux Absorption Distribution

The incident laser energy was assumed to be absorbed as a Gaussian distribution; that is, the intensity at any point on the surface of the metal is

$$q_i(x) = q_0 e^{-(1/2)(x^2/\sigma^2)} \quad (3)$$

where q_0 is the absorbed flux intensity at the beam axis which, in turn, is

$$q_0 = \frac{2Q}{\pi(2\sigma)^2} \quad (4)$$

Q is the total absorbed flux from the lasing device, and 2σ is defined as the radius of the laser beam spot. The spot radius defined in this manner is the distance from the beam axis at which the locally absorbed flux intensity is e^{-2} , or 13.5%, of its value at the axis. The spot so defined absorbs approximately 86.5% of the total absorbed incident laser energy.

The above representation is reputed to approximate the spatial distribution for the flux of cw gas lasers in general (Ref 4:13). Experience has shown that in actuality hot spots can occur within such laser beams; but, because of the unpredictability of the intensity, size, and location within the beam of such hot spots, the Gaussian distribution was deemed the most appropriate. If more precise information is available on the spatial flux distribution from a particular lasing device, the affected subroutine (FLUXX) within the computer-programmed model (see Appendix A) may be modified accordingly.

Modeling the Internal Heat Transfer

The transient heat conduction within the metal, which transfers energy both axially and radially from the area of deposition (the laser spot), is mathematically described in Cartesian coordinates for a volume element by the following parabolic partial differential energy balance equation (Ref 11:31):

$$c_p \rho \frac{\partial T}{\partial t} = \frac{\partial}{\partial x} \left(k \frac{\partial T}{\partial x} \right) + \frac{\partial}{\partial y} \left(k \frac{\partial T}{\partial y} \right) + \frac{\partial}{\partial z} \left(k \frac{\partial T}{\partial z} \right) + q \quad (5)$$

where

T = temperature ($^{\circ}$ Kelvin),

c_p = specific heat (cal/gm/ $^{\circ}$ K),

ρ = density (gm/cm³),

k = conductivity (cal/sec/cm/ $^{\circ}$ K),

t = time (sec),

q = rate of energy gain/loss due to laser flux absorption, surface radiation, or convection (cal/sec/cm³), and

x, y, z = orthogonal directions.

The restriction in dimensionality to the analysis, as imposed by the two-dimensional finite element array, in essence ignores the heat conduction in the z direction when x and y are taken as the windward and axial directions respectively (or, equivalently, the restriction assumes an invariant flux q in the z direction). Some heat is indeed transferred in this direction since, even though the crosswind temperature gradient at the plane of symmetry is theoretically zero, its derivative is not. The consequences of ignoring conduction in the z direction are slightly faster melt-through times and somewhat elevated

temperatures, particularly close-in to the beam axis where $\partial^2 T / \partial z^2$ is larger in magnitude than at outlying radii. The two-dimensional modeling thus becomes more nearly exact with increasing distance from the beam axis and with increasing spot size. The approximation is, however, more precise than a strictly one-dimensional model which in turn, as is indicated in Ref 12, gives close approximations to three-dimensional conduction for large total absorbed powers in thin metal sheets. From these considerations, a two-dimensional finite element array, as constructed, should not in itself severely restrict the resultant model's applicability.

Using the numerical technique of finite elements, Eq (5) can be reduced to a more tractable, algebraic equation for an i,j th element as follows:

$$\Delta T_{i,j} \rho c_p \Delta x \Delta y \Delta z = \Delta t * HNET_{i,j} \quad (6)$$

where $\Delta T_{i,j}$ is the temperature change of the i,j th element over the time period Δt ; Δx and Δy are the fixed dimensions as chosen for the finite elements (Δz is taken to be a unit distance in this and subsequent equations so as to maintain dimensional integrity); and $HNET_{i,j}$ is the net heat transfer rate into the i,j th element.

This numerical equivalent to the parabolic partial differential transient heat conduction equation (Eq (5)) requires an iterative solution over finite time differences Δt . For stability and convergence of the numerical solution it is necessary that the forward time increment Δt in each iteration be limited by

$$\Delta t \leq \frac{\rho c_p}{2k} \left(\frac{1}{(1/\Delta x^2) + (1/\Delta y^2)} \right) \quad (7)$$

The net heat transfer rate $HNET_{i,j}$ is the summation of the heat flow rates through the top, bottom, right, and left of the element as illustrated for the middle column of a 3×3 array in Fig. 2. The heat flows through the right face $HXFRR$ and through the top $HXFRT$ for an i,j th embedded element are

$$HXFRR_{i,j} = k \frac{\Delta y}{\Delta x} \frac{\Delta z}{\Delta x} (T_{i+1,j} - T_{i,j}) \quad (8)$$

$$HXFRT_{i,j} = k \frac{\Delta x}{\Delta y} \frac{\Delta z}{\Delta y} (T_{i,j+1} - T_{i,j}) \quad (9)$$

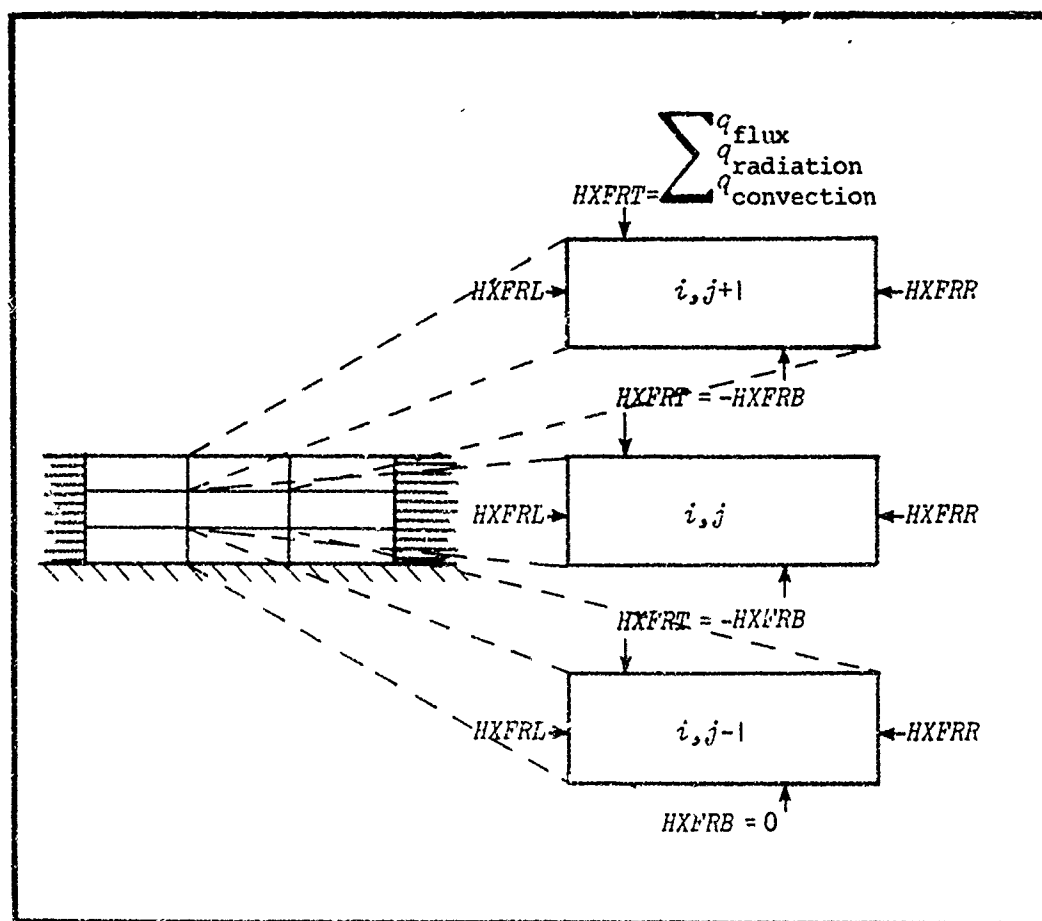


Fig. 2. Heat Transfer Rates From the Top, Bottom, Left, and Right Constitute the Net Heat Transfer Rate for Each Finite Element in the Analytic Cellular Array

The corresponding equations for the heat transfer through the left face $HXFRL_{i,j}$ and bottom face $HXFRB_{i,j}$ are identical to Eqs (8) and (9) with the exception that the plus signs in the temperature subscripting are replaced with minus signs. Adiabatic conditions, which are assumed at the back surface of the metal plate, require that all $HXFRB_{i,1}$ values equal zero. Left or right faces of elements which are coincident with the respective ends of the analytic array or which form a portion of the boundary of the melted hole or lip are likewise assumed to be adiabatic.

The conductivity k in Eqs (8) and (9) is temperature-dependent; but, since two finite elements and therefore two temperatures are associated with each of the heat transfer equations, calculation of an average conductivity between the centers of adjacent elements is called for. Such an expression, derivable from the concept of thermal resistance, is analogous to the conductance of two series resistors in an electrical circuit (Ref 11:10), and for two radially adjacent elements is

$$k_{[(i,j),(i+1,j)]} = \frac{2}{(1/k_{i,j}) + (1/k_{i+1,j})} \quad (10)$$

The average conductivity for two axially adjacent elements is identical except for appropriate changes of subscripts.

Modeling the Heat Transfer at the Surface

The non-embedded elements at the front surface in the finite element array, in addition to transferring heat by conduction to adjacent elements, absorb laser energy, radiate heat, and transfer by convection an additional amount of heat. The rates of transferring

energy by these additional means were lumped into the term " q " in Eq (5).

Energy deposition from the lasing device was modeled for an assumed Gaussian distribution in an earlier subsection. The absorption rate for a surface element, using Eq (3), is

$$\begin{aligned} q_{\text{flux}} &= q_i \Delta x \Delta z \\ &= \frac{2Q}{\pi(2\sigma)^2} e^{-2(r/2\sigma)^2} \Delta x \Delta z \end{aligned} \quad (11)$$

where r is the distance from the beam axis to the center of the element and the other terms are as previously defined.

The total hemispherical radiative heat transfer rate from any surface element is

$$q_{\text{radiation}} = \epsilon \sigma T^4 \Delta x \Delta z \quad (12)$$

where ϵ is the emissivity of the metal (nondimensional), T is the surface temperature, and σ is the Stephan-Boltzmann constant ($= 5.67 \times 10^{-8} \text{ w/m}^2/\text{°K}^4$). The emissivity ϵ is a function of the metallic and alloying elements, the surface temperature, and the surface condition. Emissivity values in general were found to be both limited and inconsistent (see Appendix C).

Modeling the convective heat transfer rate $q_{\text{convection}}$ is closely allied to determining surface shear stresses from aerodynamic friction. The derivation of the expression for $q_{\text{convection}}$ is therefore deferred (see Eq (23)) until Chapter IV.

Combining these three modes of heat transfer, the total energy transfer rate for the exposed face of a surface element is

$$HXFRT = q_{\text{flux}} + q_{\text{radiation}} + q_{\text{convection}} \quad (13)$$

It should be noted that $q_{\text{convection}}$ may be either positive or negative depending upon whether aerodynamic heating or cooling takes place.

Modeling the Solid-Liquid Phase Change

The transition from the solid to liquid phase occurs differently for alloys than for pure metals in that while the temperature of a pure metal remains at a constant melting temperature throughout a steady influx of the latent heat of fusion, the temperature of an alloy rises, quite slowly initially but later at an increased rate, from a solidus to a liquidus temperature. This phenomenon was modeled by means of a quasi-phase, coined the "slush" phase, whereby the heat of fusion was accounted for by incorporating it with the specific heat of the metal to give a "pseudo-specific heat" $c_{p\text{slush}}$, defined as

$$c_{p\text{slush}} = \frac{1}{2} \left(c_{p@T_{\text{solidus}}} + c_{p@T_{\text{liquidus}}} \right) + \frac{\text{Heat of Fusion}}{(T_{\text{liquidus}} - T_{\text{solidus}})} \quad (14)$$

To better approximate the increasing rate of the temperature rise, a more elaborate formula could be devised; but, more simply, the solidus temperature may be manipulated upward so as to in effect account for the entire temperature rise over an upper portion of the $T_{\text{solidus-liquidus}}$ temperature range.

Modeling the Vaporization

A sufficiently intense laser flux will vaporize a portion of the subjected metal during the melt-through process. The lower limit of the flux intensity necessary to cause vaporization is dependent upon the air

flow as well as the thermophysical and thermodynamic properties of the metal. Reduced air flow and a poorly conductive, highly viscous metal having a small latent heat of vaporization and a low specific heat in the liquid phase enhances vaporization at lower flux intensities.

Using the postulation of instantaneous vapor removal, no vapor phase need be provided for in modeling the melt-through process. Instead, the mass and thermal energy removed from finite elements undergoing vaporization can be fully accounted for by allowing the temperatures of such elements to "overshoot" the vaporization temperature. Each "superheated" element will possess energy in excess to the heat content of the same element at the vaporization temperature. The excess energy divided by the latent heat of vaporization gives the mass removed by vaporization. A subroutine "VAPORIZ" (see Appendix A), within the computer programmed model determines if there are any "superheated" elements; how much mass, or equivalently thickness, is removed; appropriately reduces the thickness of the affected elements; and sets the temperature of the remaining mass to the vaporization temperature.

IV. Modeling the Melt Transfer

The slush phase, as modeled in the previous chapter, is considered to consist of a solid matrix interspersed with liquid metal. Thus the slush phase is assumed to be unaffected by surface shear forces generated by aerodynamic friction. Once at the liquidus temperature, however, the molten metal is subject to the influence of aerodynamic drag forces; and at this point several postulations will facilitate the ensuing analysis of the melt flow process.

Modeling the Melt Transfer--Assumptions

First, for the purposes of this study, the airflow is assumed to be parallel to the profile of the hole as the hole deepens and enlarges with continued melting (see Fig. 3). This approximation will overestimate drag forces on the windward edge of the hole and the leeward side of the lip (see Fig. 3). Similarly, pressure forces on the lip's windward side are neglected. As the diameter-to-depth ratio of the hole decreases, this assumption becomes less plausible. While the qualitative effect of this approximation on the hole's cross-sectional profile is easily surmised (i.e., the modeled hole and lip will appear deeper and steeper, respectively, and the nadir of the modeled hole will lie slightly more windward than should actually occur), the quantitative effect of the parallel air flow approximation on the melt-through time is not so apparent. The insulative effect of the thicker modeled lip should counteract to some extent the heat flow enhanced by the thinner-than-actual liquid layer within the windward side of the modeled hole. A

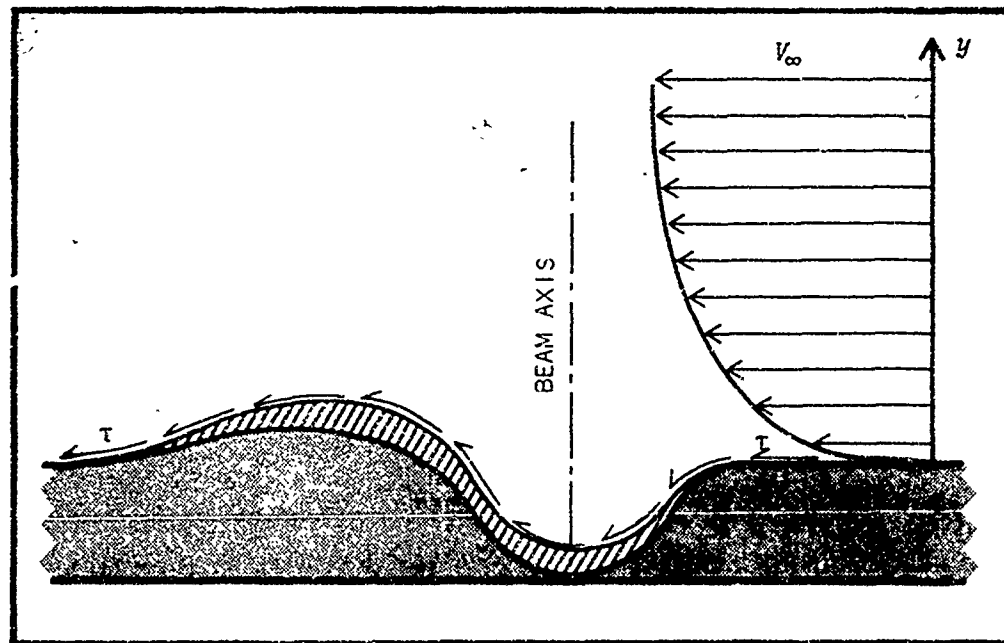


Fig. 3. The Aerodynamic Boundary Layer Creates Shear Forces Over the Plate's Surface Causing the Molten Metal (Cross-Hatched) Flow

slightly faster-than-actual melt-through time is probably the overall effect of the assumed parallel-to-the-surface airflow.

Secondly, it is postulated that the molten metal adheres to the solid (or slush) surface of the plate rather than entering the airstream as droplets. This is believed to be a good approximation for flow from the leading edge of the hole to as far as the lip. At that point pressure forces acting on the leading edge of the lip, combined with the frictional drag forces, conceivably could exceed the opposing surface tension and internal shear forces; if so, consequent "blow-off" would result. The effect of blow-off would be a smaller-than-predicted lip size and faster, but probably insignificantly so, melt-through times. The argument for this latter effect is that a thinner lip would allow

slightly faster conductive heat transfer to the underlying and inwardly situated material.

A third assumption made to facilitate the analysis is that of instantaneous melt flow acceleration. That is, it is assumed that the flow of molten metal reaches steady state in a time that is small compared to the total time of the flow. While this approximation tends to overpredict mass removal rates, it eliminates a formidable task of maintaining an account of momentum and changes thereto throughout the flow.

Determining the Surface Shear Stresses

The surface shear forces, in conjunction with the viscosity of the liquid metal, determine the mass removal rate of the molten metal. The shear forces τ at the atmospheric-metallic interface, or "wall" as indicated by the subscript "w," are determined by the following equation (Ref 8:30):

$$\tau_w = \frac{1}{2} \rho^* V_\infty^2 c_{f_x} \quad (15)$$

where ρ^* is the air density at a reference enthalpy to be defined later (see Eq (19)); V_∞ is the free stream wind velocity; and c_{f_x} is the local skin friction coefficient at a distance x from the leading edge of the plate. The form of the solution for c_{f_x} is dependent upon whether the aerodynamic boundary layer is laminar or turbulent. One set of solutions which has been found to give good results (Ref 8:30,35) is

$$c_{f_x \text{ laminar}} = 0.664 / \sqrt{(R_N^*)} \quad (16)$$

$$c_{f_x \text{ turbulent}} = 0.370 / (\log_{10} R_N^*)^{2.584} \quad (17)$$

where the Reynolds number

$$R_N^* = x \rho^* V_\infty / \mu^* \quad (18)$$

and ρ^* and μ^* are the density and dynamic viscosity, respectively, of the air at a reference enthalpy i^* (the asterisk indicating the reference condition), defined by

$$i^* = \frac{i_\infty + i_w}{2} + 0.22 r_i \frac{\gamma - 1}{2} M_\infty^2 i_\infty \quad (19)$$

The subscripts ∞ and w refer respectively to the conditions in the free stream beyond the aerodynamic boundary layer and at the wall; M is the mach number, or the velocity of the wind divided by the speed of sound, γ is the ratio of the specific heats at constant pressure c_p^* and at constant volume c_v^* (for air $c_p/c_v \approx 1.4$); and r_i is a recovery factor defined for laminar and turbulent boundary flow conditions as

$$r_{i_{\text{laminar}}} = \sqrt{(P_N^*)} \quad (20)$$

$$r_{i_{\text{turbulent}}} = \sqrt[3]{(P_N^*)} \quad (21)$$

where the Prandtl number at the reference enthalpy conditions is

$$P_N^* = c_p^* \mu^* / k^* \quad (22)$$

and k is the conductivity of the air at i^* .

Turbulence along flat plates generally occurs at a Reynolds number in the range of 3.5×10^5 to 10^6 (Ref 14:435). An arbitrary value of 4×10^5 for the transition Reynolds number was tentatively incorporated within the numerical model. Note that the Prandtl number, used to compute the recovery factor and in turn the reference enthalpy (Eq (19)), must also be computed at the reference enthalpy conditions (Eq (22)). A two-step iteration was employed within the model to accomplish this.

Equations (16) to (22) were in large part empirically derived. Equation (16), with R_N^* replaced by $R_{N\infty}$, is Blasius' 1908 exact solution for a laminar boundary layer assuming constant properties, independent of pressure and temperature, throughout the thickness of the boundary layer (Ref 14:128). Equation (17), less the asterisk, is by Schulz-Grunow (Ref 8:35). Modification of the equations by computing various properties at a reference enthalpy i^* so as to make Eqs (16) and (17) valid through hypersonic mach numbers was devised by Eckert (Refs 8 and 9). These modifications correct for the variation of the air density and viscosity with changes in temperature as actually occurs in boundary layers associated with high speed flow.

Approximating the Convective Heat Transfer Rate

Solution of the skin friction coefficient c_{f_x} according to Eqs (16) or (17), above, facilitates determination of the convective heat transfer rate at the same local area. The appropriate formula for a flat plate with a constant surface temperature (Ref 8:30-31) is

$$q_{\text{convection}} = c_{f_x} \rho^* V_{\infty} \frac{(i_r - i_w)}{2P_N^{*2/3}} \quad (23)$$

where i_w is the enthalpy of the air at the wall temperature and i_r is the enthalpy at a recovery temperature T_r defined by

$$T_r = \frac{r i_{\infty}^2}{2c_p^*} + T_{\infty} \quad (24)$$

Although Eq (23) has been exclusively used to approximate the local convective heat transfer rate in the model presented in Appendix A,

further elaboration has since appeared necessary to fully account for the effects of temperature variation along the plate as would be encountered with localized laser heating. Treatment of such surface temperature variation may be divided into that of an essentially unheated starting length and the temperature variation encountered subsequent to that distance.

Corrective factors for unheated starting lengths x_0 (i.e., the distance between the plate's leading edge and the point where significant temperature changes commence) are treated in Ref 15. The factors $C.F.$ given for laminar and turbulent flow (Ref 15:217,242) to be applied to Eq (23) are

$$C.F._{\text{laminar}} = [1 - (x_0/x)^{0.75}]^{-1/3} \quad (25)$$

$$C.F._{\text{turbulent}} = [1 - (x_0/x)^{0.9}]^{-1/9} \quad (26)$$

For a laser beam having a 10 cm^2 cross section, directed at a point five feet from the leading edge (this same distance was used in all test cases) and assuming a radial distance of one inch from the laser beam axis at which the temperature rise begins, the turbulent flow corrective factor is computed to be

$$\begin{aligned} C.F._{\text{turbulent}} &= [1 - (59/60)^{0.9}]^{-1/9} \\ &= 1.6 \end{aligned} \quad (27)$$

That is, the convective heat transfer rate should, under the given situation, be 1.6 times that approximated by Eq (23). However, this correction applies for unheated starting lengths which would occur only if the initial temperature T_0 of the plate was at the recovery temperature T_r .

(see Eq (24)). For other initial temperatures, Eq (25) may not be entirely appropriate; and additional investigation is considered necessary before adopting the factor as is for cases in general.

To account for the effect of significant variation in surface temperature subsequent to modest variations along an "unheated" starting length on the convective heat transfer rate, Eckert (Ref 9:16-21) offers a numerical procedure which could prove adaptable in refining Eq (23). The compatibility of this correction procedure in conjunction with the previous correction for unheated starting lengths remains to be determined however. The change on the convective heat transfer rates for turbulent flow due to the local temperature variation alone (neglecting unheated starting lengths) should not exceed $\pm 40\%$ (Ref 9:18,19). More pronounced effects should occur with laminar flow. For the sake of expedience, pending further development and evaluation of a composite correction factor to account for the combined effects of relatively unheated starting lengths followed by intense temperature variations, Eq (23) was provisionally incorporated within the numerical model. The consequence of this oversimplification should not be overly adverse to most of the modeling results for turbulent flow (no laminar flow results are presented in this thesis) since for most cases the convective heat transfer rate will be insignificant when compared to the absorbed flux intensity. However, for laminar flow and for very low flux intensities, modification of Eq (23) appears to be warranted.

Solution to the convective heat transfer rate, by the use of Eq (23), combined with Eqs (11) and (12), the solutions to the absorbed flux and radiative heat transfer rates, completes the means of solving

the rate of total heat transfer (reference Eq (13)) through the exposed face of any surface element in the model's elemental array. Having thus purposefully digressed from this chapter's titled content in order to complete the modeling of the heat transfer proper, attention is returned to modeling the melt transfer.

Modeling the Melt Flow--a Numerical Algorithm

With a means to calculate the shear stress τ_w at the surface of the molten metal (reference Eq (15)), the mass flow within the melt layer is derivable from Newton's equation (Ref 11:124)

$$\tau = \mu \frac{du}{dy} \quad (28)$$

where μ is the dynamic viscosity of the liquid metal, u is the velocity of the assumed laminar flow, and y is the normal distance from the solid-liquid interface within the metal plate as depicted in Fig. 4.

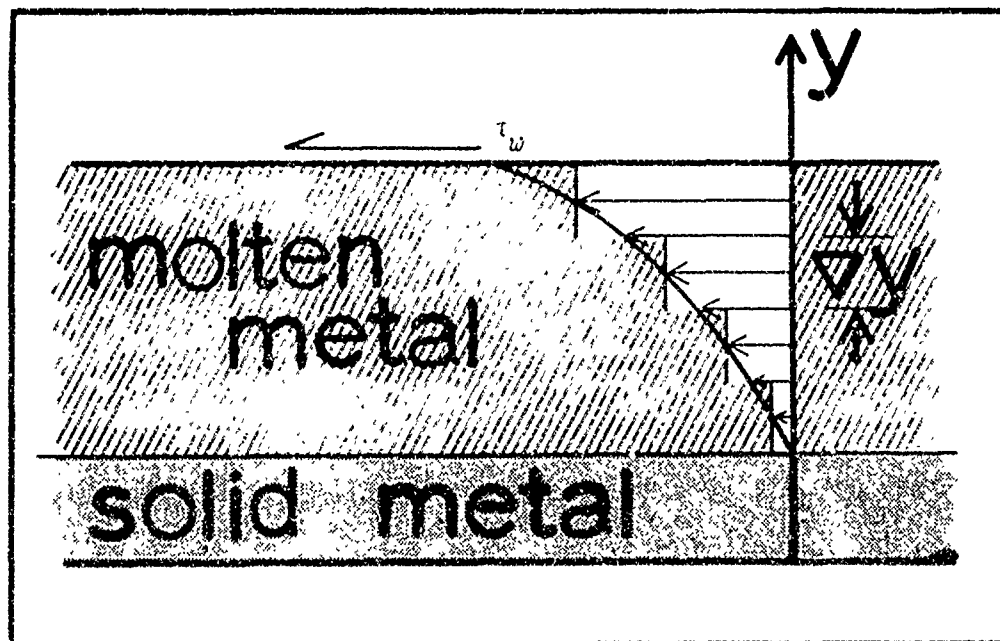


Fig. 4. Velocity Profile Within the Melt Layer

With an assumed steady flow, the shear stress remains essentially constant throughout the melt layer while the dynamic viscosity varies with the temperature of the liquid. The velocity at any point within the melt layer can be determined by solving Eq (28) for u as a function of y .

$$u(y) = \tau_w \int_0^y \frac{1}{\mu(y)} dy \quad (29)$$

A numerical approximation to the above equation, for the velocity midway in an i,j th finite element, is

$$u_{i,j} = \left[\sum_{l=1}^{l=j-1} \frac{\tau_w \Delta y}{\mu_{i,l}} \right] + \frac{\tau_w \Delta y}{2\mu_{i,j}} \quad (30)$$

Within an increment of time Δt the i,j th element is transferred downstream a distance,

$$x_{tfr} = u_{i,j} \Delta t \quad (31)$$

Equivalently, allowing the array of spatial cells to remain stationary and merely transferring the proper mass from one cell to its adjacent downstream cell, the "mass transfer" from the i,j th cell to the $i-1,j$ th cell is

$$TFR_{i,j} = \frac{x_{tfr}}{\Delta x} \Delta y_{i,j} \quad (32)$$

where $TFR_{i,j}$ is, for computational purposes, expressed as thickness. This accountability of the mass flow is illustrated in Fig. 5. The scheme portrayed is consistent with reality only if the downstream element is also molten or is void. Thus to assure that the melt has a valid cell in which to flow, and to simulate laminar flow conditions,

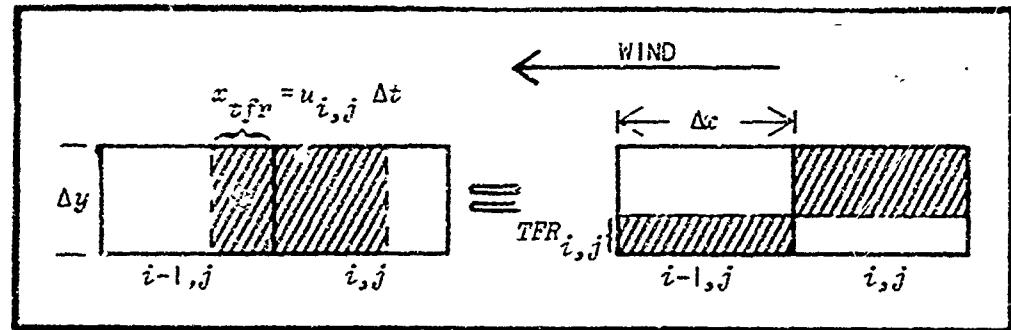


Fig. 5. Graphical Representation of the Computational Algorithm for Transfer of Flow to Adjacent Downstream Finite Element

the model was programmed to transfer the flow as hypothetically exemplified in Fig. 6. Note that the array of finite elements representing the initial cross section of the plate must be augmented with initially empty cells to accommodate the melt flow and the subsequent lip formation.

After one time increment Δt the bottom array in Fig. 6, depending upon the surface shear forces and viscosities within the elements, might appear as the top array in Fig. 7. Observe that some of the cells are only partially filled while others are "overflowing." A subprogram SQUEEZE (see Appendix A) was devised to redistribute the liquid among the axially adjacent elements in each array column to eliminate the voids and/or overflow while ensuring that mass and thermal energy were conserved and that the temperature gradient was valid. After execution of subroutine SQUEEZE, the hole's modeled profile might appear as in the bottom array of Fig. 7.

The uppermost element in each column is allowed to range in thickness only between $\Delta y/2$ and $3\Delta y/2$, where Δy is the constant axial dimension of all embedded cells. This range ensures stability in the numerical solution to the partial differential heat conduction equation without

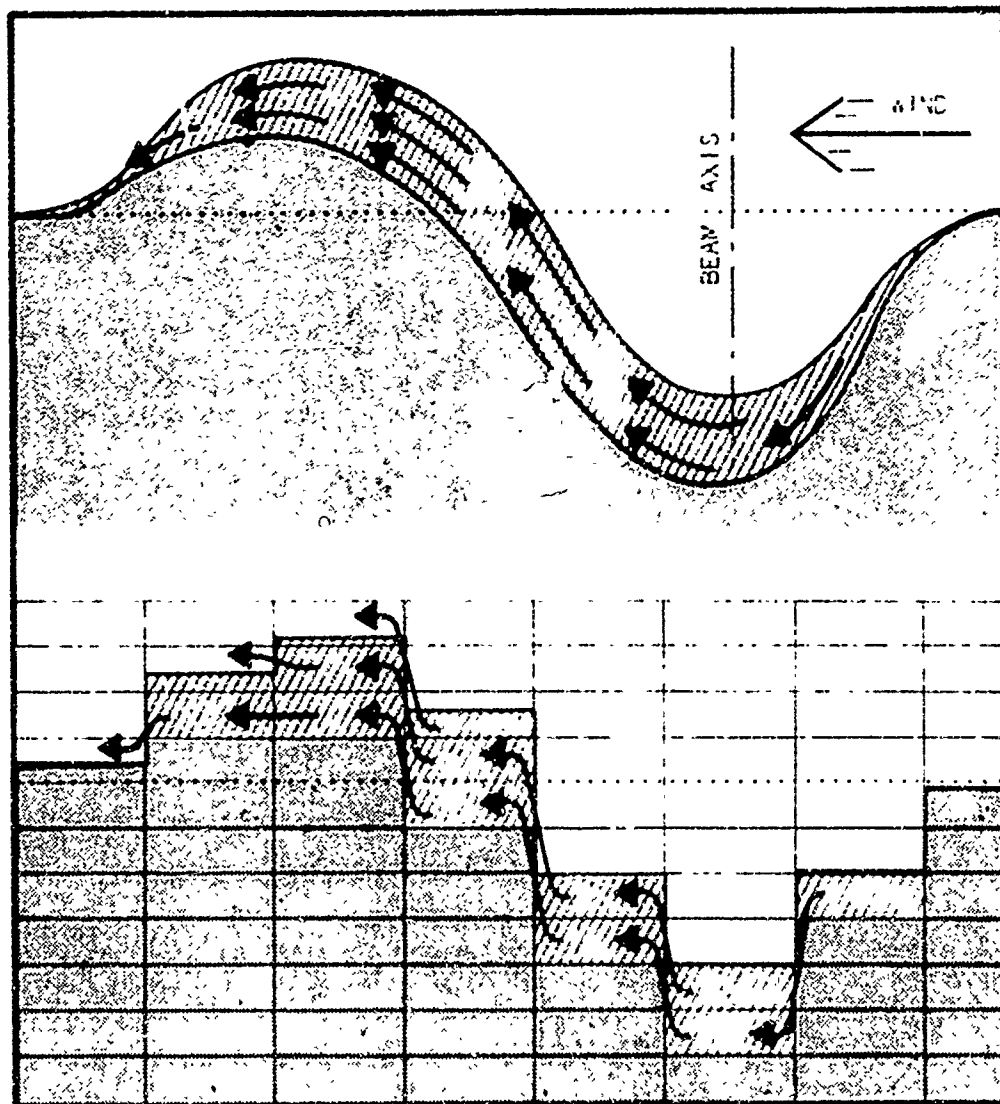


Fig. 6. A Numerical Finite Element Model (Below) of a Hypothesized Melt Flow (Above)

undue degradation in modeling accuracy (reference Eq (7)). When, after execution of subroutine SQUEEZE, an uppermost element is less than $\Delta y/2$ thick, its energy and mass must be combined with those of its underlying element. If the underlying element is nonmolten, the resultant merged element may be molten or frozen dependent upon the combined mass and thermal energy involved. A subroutine FREEZE (see Appendix A), actuated

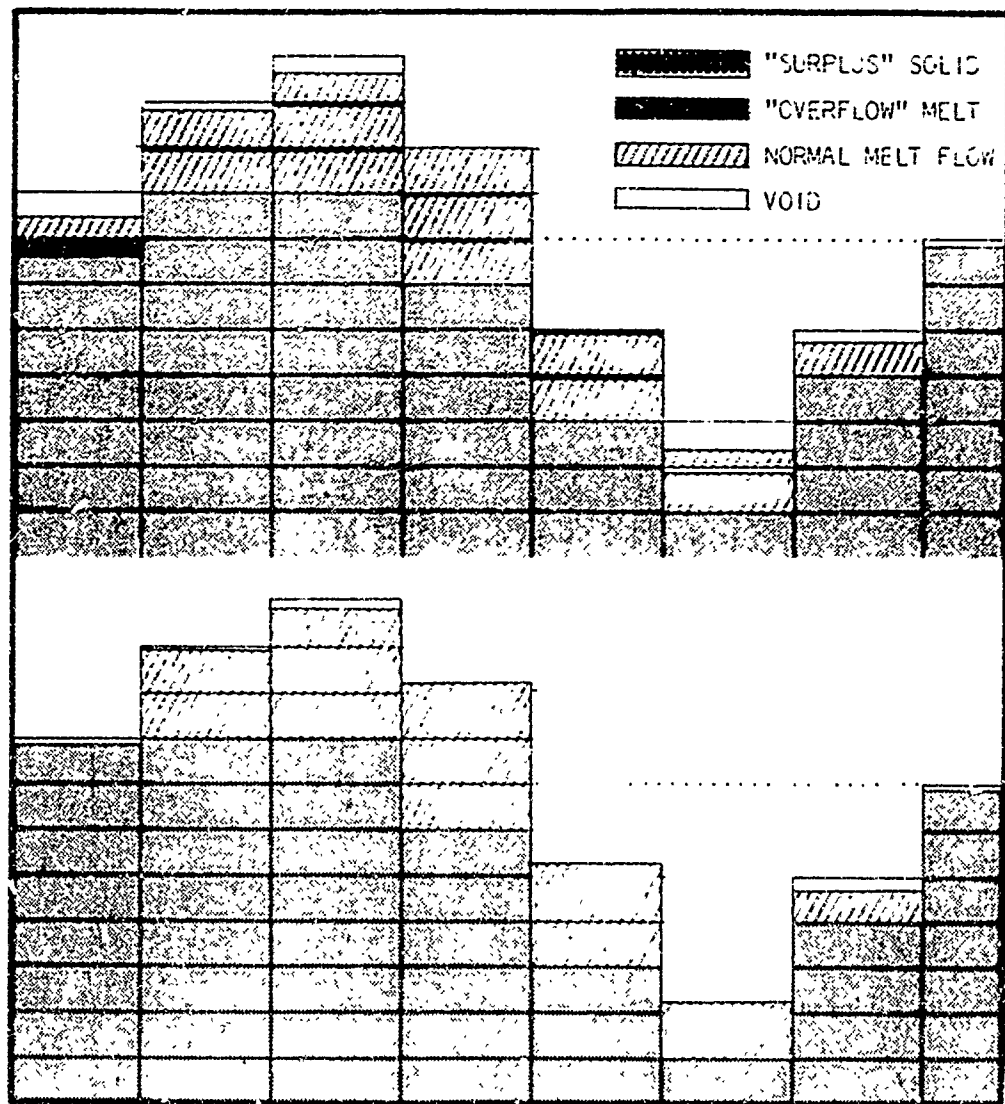


Fig. 7. The Numerically Modelled Transfer of Melt Resulting in Voids and Excesses Within Certain Cells (See Above) is Corrected (Below) by a Subroutine SQUEEZE

within the model for such exigencies, computes the resultant temperatures of such merged elements.

Assembling the Total Model

The total model of this study consists of an iterative sequencing through the various component models which, as previously outlined,

approximate the several phenomena comprising the total melt-through process of laser light incident upon a metal plate. The sequential order of the component models, within each iteration of the total model, starts with the temperature and mass of every finite element known. Supplementary matrices store tentative temperature and thickness values pending successful completion of each iteration. Property values of the elements at their known temperatures are calculated in subroutines CONDUCT, SPHEAT, and VISCSTY (the density of the metal has been taken as invariant with temperature). Heat transfer rates q_{flux} , $q_{\text{convection}}$, and $q_{\text{radiation}}$ at the exposed face are computed in subroutines FLUXX, FRCTION, and SCHMIDT. Heat balances for all elements over the maximal time increment Δt (reference Eq (7)) are also computed in the subroutine SCHMIDT (titled after E. Schmidt, the developer of a numerical and graphical method for the solution to one-dimensional transient heating (Ref 16:294)). Solid-to-slush and slush-to-liquid phase changes are searched for within the cellular array in the subroutine XACTIME; and, if found, the subroutine calculates the exact time increment at which the affected element changes to slush or liquid as the case may be and reexecutes SCHMIDT with the revised time increment. A subsequent check for liquid-to-slush or slush-to-solid phase changes is performed in subroutine COOLIT. If such a temperature drop in any cell is detected, the new temperature of the cell is recalculated using the specific heat of the cooler phase over that portion of the time increment after which the phase change occurs. Next, vaporization, as previously treated, is accounted for in the subroutine VAPORIZ. The melt flow, also dealt with earlier and modeled in subroutines TRNSFRX, SQUEEZE, and FREEZE, concludes the sequence of modeled effects constituting the total surface recession phenomenon.

V. Results

The essential result of this thesis study is "QUEST," a model to predict melt-through times and generate supplementary data concerning the transient heating and surface recession dynamics for laser beams impinging upon flat metal plates in an aerodynamic environment. The model, computer programmed in FORTRAN Extended (a variant of FORTRAN IV), is presented in Appendix A. The version presented is for a 0.1 cm thick titanium sheet at sea level subjected to a mach 0.50 wind and absorbing a Gaussian-distributed energy flux of 10 kw over a 10 square centimeter spot. QUEST was additionally exercised for aluminum, magnesium, and stainless steel and for various thicknesses, wind velocities, absorbed laser powers, and spot sizes. Numerical results from these computer runs are tabulated in Appendix D. Qualitative findings from those results are presented in the following chapter.

Computer Program Specifications

QUEST consists of 13 program subroutines and approximately 500 executable statements. Twenty-three library subroutines are employed, including six used in producing graphical plots of output data. The program requires less than 50,000 octal word memory capacity. Although thus far run exclusively on a CDC 6600 computer, QUEST should be adaptable to other digital computers, with perhaps the exception of the CALCOMP plotting feature. However, the data that are plotted are also printed, and thus this feature could be eliminated.

Input, which includes mach number, altitude, distance from the leading edge of the plate to the laser spot, initial temperature of the metal, and the total rate of energy absorption, is by data cards. Other parameters peculiar to each metal are incorporated directly within the appropriate program subroutines.

Execution time for the program varies with the input parameters. Thicker metals, lower energy flux intensities, and finer stratification of the plate's cellular array all require additional computation time. Total run times have ranged from less than 10 to over 500 seconds. The example presented in Appendix A compiled in 17 seconds and required an additional 253 seconds for execution. Conversion of the source deck from the FORTRAN IV programming language to binary machine language eliminates the compilation time.

Output, as programmed and an example of which may be found in Appendix A, consists of an abbreviated three line diagnostic printout after each occurrence of a phase change within the finite element array plus an extended printout of analytic data at the conclusion of melt-through. In addition to the melt-through time, the final printout provides the input parameters; selected thermodynamic property values of the metal; the final temperature array; comparative values of the incident (absorbed) laser energy, convective and radiative heat transferred, and energy consumed by vaporization along the spot-bisecting, wind line; the remaining total and non-molten thicknesses of the plate along the same diagnostic line; the temperature history of the plate's back surface opposite the center of the laser beam spot; the position of solid-liquid interface at the center of the spot versus time; and

the surface recession rate history at the center of the hole. Additional output information, if needed, may be extracted with additional programming.

Model Validation

The numerical results from any complex simulation must be suspect until proven true. Unfortunately, if the results could be fully validated, there probably would have been no need for a model in the first place. Such is the case with QUEST--only limited means exist to even partially substantiate the results. Despite these inherent obstacles, great care was taken in programming QUEST to attain what is believed to be mathematical and logical integrity. QUEST was additionally tested for sensitivity and results were compared with theoretical values and experimental findings.

Model Sensitivity. The sensitivity of the model QUEST to various axial dimensions of the diagnostic cellular array was tested in order to find an acceptable trade-off between the accuracy of the results and required computer processing time. The combined test results for aluminum, 0.05, 0.10, and 0.20 cm thick at mach numbers of 0.0, 0.1, and 0.5 and for 10 kw of power over a 1 cm² spot, are shown in Fig. 8.

Deviations of melt-through times from those predicted with a 20-tiered array were less than 1% for reductions in the axial array dimension n to 10. With n reduced to 5, however, the deviation increased to about 5%. In making trade-offs between accuracy and computer run times, a rough guide to the computations--and the computer time required--is Eq (7); halving the number of tiers will approximately quadruple the incremental time in each forward time step and thus reduce by four

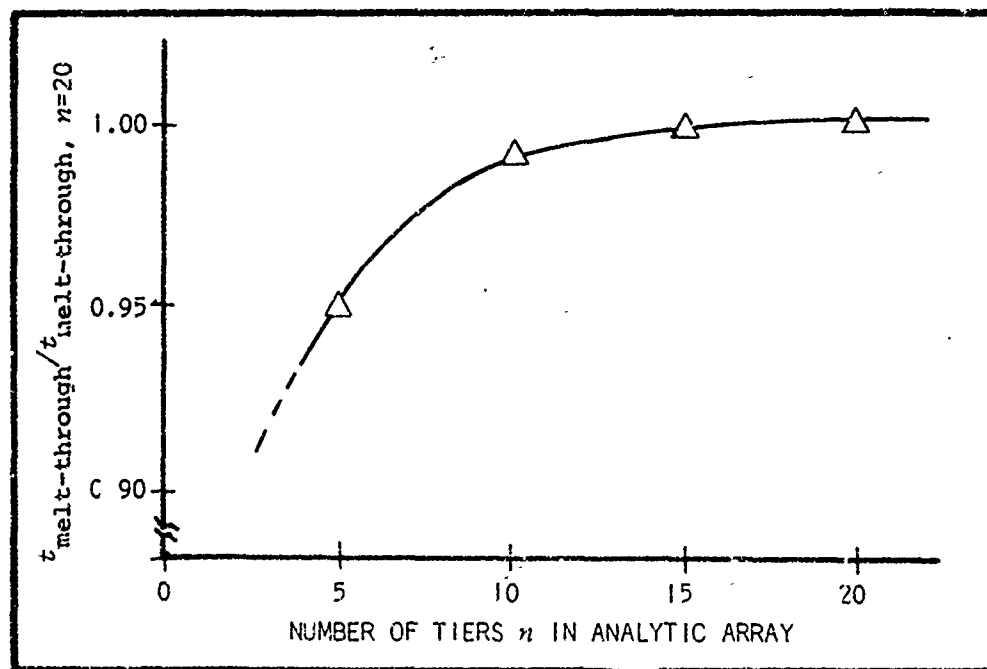


Fig. 8. Sensitivity of Melt-Through Times Predicted by QUEST to Changes in n , the Number of Tiers in the Analytic Array of Finite Elements

times the computer processing time required. The results presented in Appendix D were obtained with 10-tiered arrays (exclusive of the augmentation required for mass flow and lip formation) for 1 cm² incident beam spots and with 5-tiered arrays for 10 cm² spots. The array was limited to 5 tiers in these latter cases to reduce computer run times.

The computer-programmed model QUEST is dimensioned for a 30-tiered array. Approximately one-third of these tiers, however, must be reserved for modeling the lip formation, thus allowing up to 20 tiers for the initial plate thickness. If less accuracy, both in modeling the hole and lip profile and in predicting the melt-through time, is permissible and the array's axial dimension were accordingly halved, the central computer memory required by QUEST could be reduced by

approximately 6000 octal words. If, in addition, the CALCOMP plotting feature were removed and the FORTRAN programming were replaced with binary machine language, the total memory core required by QUEST reduces to less than 30,000 octal words--a significant reduction in computer requirements with only limited restriction in achievable accuracies of predicted melt-through times.

Comparison of Predicted Results with Known Solutions. A complete absence of known solutions to the total phenomenon of melt-through in an aerodynamic environment and a dearth of exact solutions to even fictitiously simplified melt-through processes restrict the ability to validate the results of QUEST. The most satisfactory of the simplified known solutions found to gauge the soundness of QUEST is that of melt-through with no wind but with "instantaneously-vanishing" melt and one-dimensional (axial) heat conduction. Solutions to melt-through times under such simplifying assumptions reduce to

$$t_{\text{melt-through}} = \frac{\Delta H \rho y}{q_0 (\text{mol wt})} \quad (33)$$

where

ΔH = the difference in the heat content between the melting point and the initial temperature of the metal (calories/gm-mole),

ρ = density (gm/cm³),

y = thickness of plate,

q_0 = absorbed flux intensity at mid-beam (see Eq (4)), and

mol wt = molecular weight of the metal.

Heat contents for aluminum, magnesium, and titanium were computed from applicable formulas presented by Wicks and Block in Ref 17 (see Appendix C). The values for stainless steel were approximated by those found for

iron. The melt-through times according to Eq (33) for the metals, spot sizes, and laser powers presented in Appendix D are given in Table I.

For all but near-hypersonic conditions, the tabulated melt-through times in Table I are less than the corresponding times modeled by QUEST and presented in Appendix D. Times from QUEST ranged to 300% of the corresponding times arrived at from Eq (33)--the maximum difference occurring for 0.20 cm thick titanium absorbing 1 kw power over a 10 cm² spot subjected to mach 2 airflow. The significant difference in this cited case is primarily attributable to aerodynamic cooling. The convective heat losses, as computed by QUEST, were over half (56%) of the laser energy absorbed (which alone would more than double the melt-through time as gauged by Eq (33)). Additional heat loss by radiation (5% of that absorbed) and by radial heat conduction combined with the heating of the liquified metal account for the balance of the additional incident power required and the consequential longer melt-through times. Titanium, as opposed to the other metals modeled, exhibits greater convective heat losses due to its high melting temperature. Its melting point exceeds the recovery temperature within the boundary layer (reference Eqs (23) and (24)) at sea level wind velocities of up to mach 4.0. It must be pointed out that for this particular case, if corrective factors for unheated starting lengths and variant surface temperatures had been applied to the convective cooling as presently approximated by Eq (23), melt-through could possibly have been precluded altogether. This would happen if the corrections increased the convective cooling to a point where the absorbed flux and the combined heat losses were equal. Thus, as previously recommended, further refinement to Eq (23) appears to be in order for modeling cases involving very low flux intensities.

TABLE I
Melt-Through Times (in Seconds) of Metal Plates Assuming
Instantaneously Vanishing Melt, One-Dimensional
Heat Conduction, and No Wind

Metal	Spot Size (cm ²)	Absorbed Power (kw)	Thickness of Plate (cm)		
			0.05	0.10	0.20
Al	10	1	0.6525	1.3050	2.6100
		10	0.0653	0.1305	0.2610
	1	1	0.0653	0.1305	0.2610
		10	0.0065	0.0131	0.0261
Mg	10	1	0.4772	0.9544	1.9087
		10	0.0477	0.0954	0.1909
	1	1	0.0477	0.0954	0.1909
		10	0.0048	0.0095	0.0191
Ti	10	1	1.6916	3.3833	6.7665
		10	0.1692	0.3383	0.6766
	1	1	0.1692	0.3383	0.6766
		10	0.0169	0.0338	0.0677
Fe	10	1	2.6413	5.2825	10.5650
		10	0.2641	0.5283	1.0566
	1	1	0.2641	0.5283	1.0566
		10	0.0264	0.0528	0.1057

Comparison of Predicted and Experimental Results. An experimental result as reported in Ref 10 was compared with the predictions of QUEST. The experiment involved a 16 mil sheet of stainless steel irradiated over a 4.676 cm² spot by a 9 kw laser beam. Melt-through was judged from high-speed movie photography to occur at 0.40 seconds. The thermal history of the rear surface was recorded by means of a transducer aligned with the beam axis and affixed to the back of the plate.

Corresponding melt-through times predicted from QUEST, assuming constant absorptances of 0.2 and 0.3 with no wind (and thus no melt removal), were 0.51 and 0.34 seconds, respectively. The rear surface temperature histories as experimentally and predictively obtained are compared in Fig. 9. Also included are rear surface temperatures as predicted by Torvik (Ref 10:30) assuming identical absorptances but with instantaneous melt removal. As pointed out by Torvik (Ref 10:31-32), the comparative results indicate that the absorptance of stainless steel must increase significantly during the heating to account for the nonlinearity in the experimentally obtained temperature history.

Differences also appear between the rear surface temperature histories as predicted by Torvik and by QUEST. The differences are primarily attributed to the fact that QUEST utilizes temperature-dependent property values as opposed to constant properties assumed in the former model. In this case of stainless steel (AISI 304), QUEST employs a specific heat varying from 0.106 cal/gm/°K at 300°K to 0.166 cal/gm/°K at just below the melting temperature, while Torvik (Ref 10:31) assumed a constant specific heat of 0.100 cal/gm/°K over

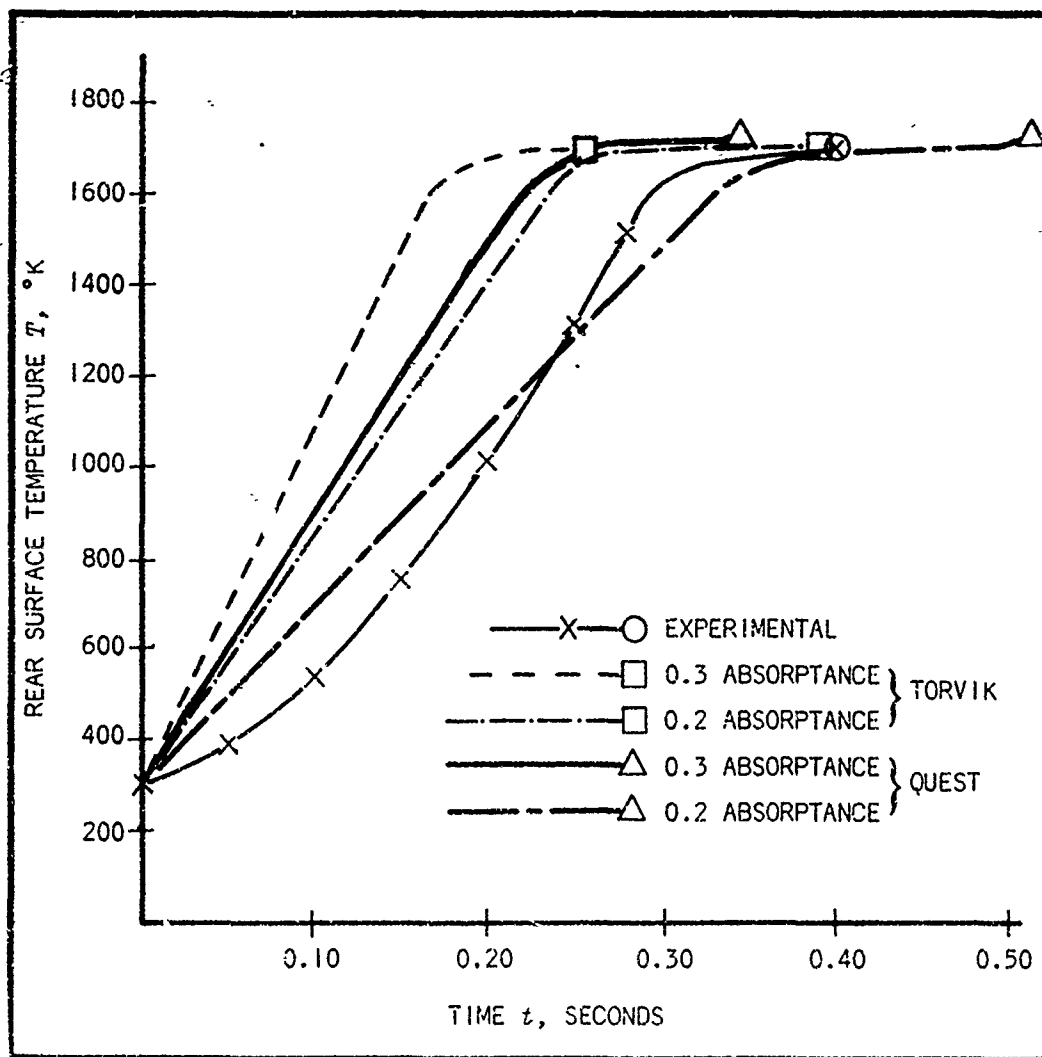


Fig. 9. Rear Surface Temperatures of a 16 mil Stainless Steel (AISI 304) Plate as Determined from Experiment Results and as Predicted by Modeling

the entire temperature range. (Equations used in QUEST for thermodynamic values of metals as a function of temperature appear in Appendix C.)

The validity of QUEST cannot be ascertained with this single comparison to experimental results due to the necessity of assuming an absorptivity of photons by the metal. The absorptivity itself is a phenomenon requiring temperature-dependent modeling. Despite being

limited at present to constant absorptivities, however, QUEST does predict melt-through times of the same order as the experimentally obtained results. Such results, coupled with the comparisons to known solutions in the previous section, are at least indicative of the model's credibility.

VI. Findings

The limited numerical results thus far computed by QUEST (see Appendix D) have been evaluated in part to determine qualitatively the general effects of wind on melt-through and the influence of other parameters on these effects. These findings must be considered as tentative, pending further validation of the model, and should be extrapolated to cases not yet tested with extreme caution.

Aerodynamic Effects on Melt-Through Times

The melt-through times computed by QUEST for the metals, thicknesses, wind velocities, energy fluxes, and beam sizes as tabulated in Appendix D are graphically presented in normalized form in Figs. 10 through 13 with mach number being the independent variable. The graphs reveal no simple relationship between melt-through time and mach number; that is, the overall effect of air flow on the melting process must in turn be a function of the remaining parameters. For instance, with spot size and energy flux unspecified, one cannot even predict whether wind will retard or speed melt-through. To wit, 0.2 cm thick titanium in a mach 2.0 airstream required from over twice (for 1 kw Gaussian absorption over a 10 cm² spot) to about one-fourth, (for 10 kw/1 cm² spot) the time to melt-through when compared to the same metal sheet subjected to the same conditions in still air (see Fig. 12). A further indication of the complicity involved in analyzing the aerodynamic effects is found with 0.2 cm thick titanium and stainless steel absorbing 1 kw/1 cm². In these two cases, instead of a monotonic decrease

in melt-through time with increase in wind velocity, the time to melt-through actually increased as the mach number increased from 1.0 to 2.0. Other apparent anomalies occurred for 0.05 cm thick sheets absorbing 1 kw/1 cm² and 10 kw/10 cm² where a slight increase in melt-through times was often noted at low subsonic velocities followed by the otherwise characteristic decrease in time to melt-through. All of these apparent anomalies can be rationalized by reconsidering the two basic mechanisms by which wind affects laser-induced melting.

Aerodynamic Heating/Cooling Effects. The first mechanism, aerodynamic heating or cooling by convective heat transfer, either hastens or retards melt-through by respectively augmenting or detracting from the laser-absorbed energy. Which effect occurs is dependent upon the relative surface and aerodynamic boundary layer recovery temperatures and their respective enthalpies (reference Eq (23)). The dependence of the recovery temperature upon the square of the free airstream velocity (Eq (24)) plus the strong dependence of the magnitude of the convective heat transfer on an additional power of the free stream velocity (Eq (23)) forces the effect of this first mechanism to vary significantly with mach number. At low mach numbers aerodynamic cooling is to be expected within the heated spot; but because of the relatively slow free airstream velocity the magnitude of such cooling will be limited. Often, because of the limited cooling, the retardation effect on melt-through times was found to be masked by a stronger melt transfer effect. One set of cases where such masking did not occur was for 1 kw of power absorption over 10 cm² spots. In these cases, for all metals (see lower, left graph in Figs. 10-13), aerodynamic cooling exceeded all other effects for mach numbers up to and, in the cases of titanium and stainless steel,

in excess of 2.5. Thereafter, increases in aerodynamic heating with increased wind velocities accelerated melt-through to times approaching or less than melt-through times in still air. Other cases where aerodynamic heating effects are evident are for 1 kw absorption over 1 cm² spots (upper left graphs in Figs. 10-13). The decrease in melt-through times observed at mach numbers greater than 3.0 is attributed, for these particular cases, nearly exclusively to aerodynamic heating. Such aerodynamic heating was found possible to reduce melt-through times to even less than those theoretically possible with one-dimensional (axial) heat flow and instantaneous melt removal (viz 0.1 and 0.2 cm thick Mg exposed to 1 kw over 10 cm² at mach 4.0--reference Table I and Appendix D).

Melt Transfer Effects. Mass flow, or "melt transfer," the second mechanism by which wind affects melt-through times, generally hastens melt-through by removing a portion of the melt over the hottest portion of the spot and thereby eliminating it from further heating. The energy thus "saved" is absorbed by the underlying elements which heat and consequently melt faster, thus perpetuating the accelerated melting process. The effect was most evident in the thicker metals (as can be seen in all but the lower left graph in Figs. 10-13). This characteristic is explainable due to the fact that for a given laser beam in still air, thicker plates either attain higher front face and interior temperatures or consume a greater portion of the incident energy in vaporization than do thinner sheets. Stated differently, in the absence of wind, thicker sheets will at melt-through exhibit a higher average heat content per unit mass than will a thinner sheet exposed to an identical laser beam. Prompt removal of melt from thicker metals at or close to the liquidus temperature thus has a proportionally greater effect in reducing

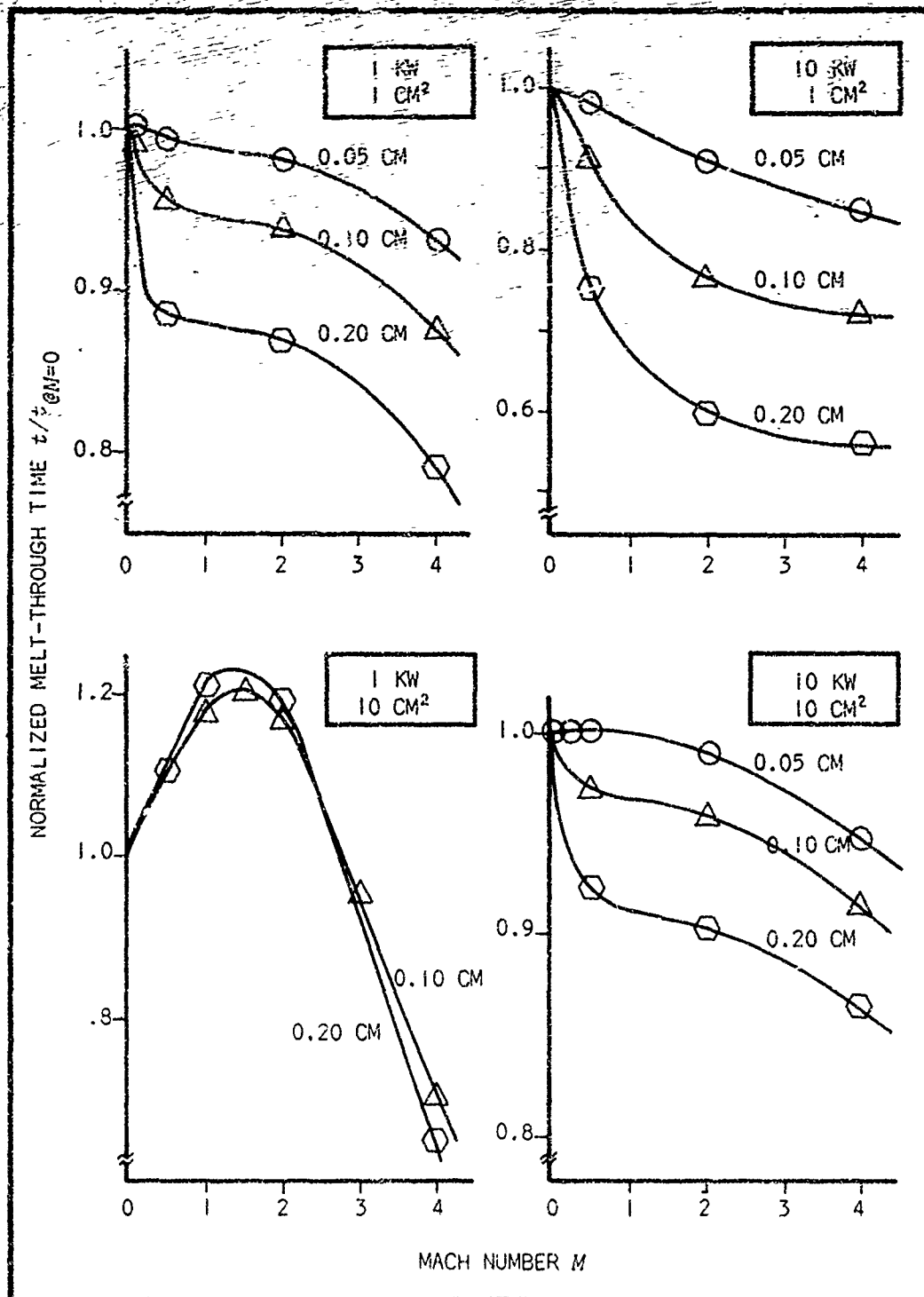


Fig. 10. Dimensionless Melt-Through Times (Normalized by Dividing by the Melt-Through Time at 0.0 Mach) for 0.05, 0.10, and 0.20 cm Thick Aluminum Plates Absorbing 1 and 10 kw of Light over 1 and 10 cm² Spots at Mach Numbers from 0 to 4

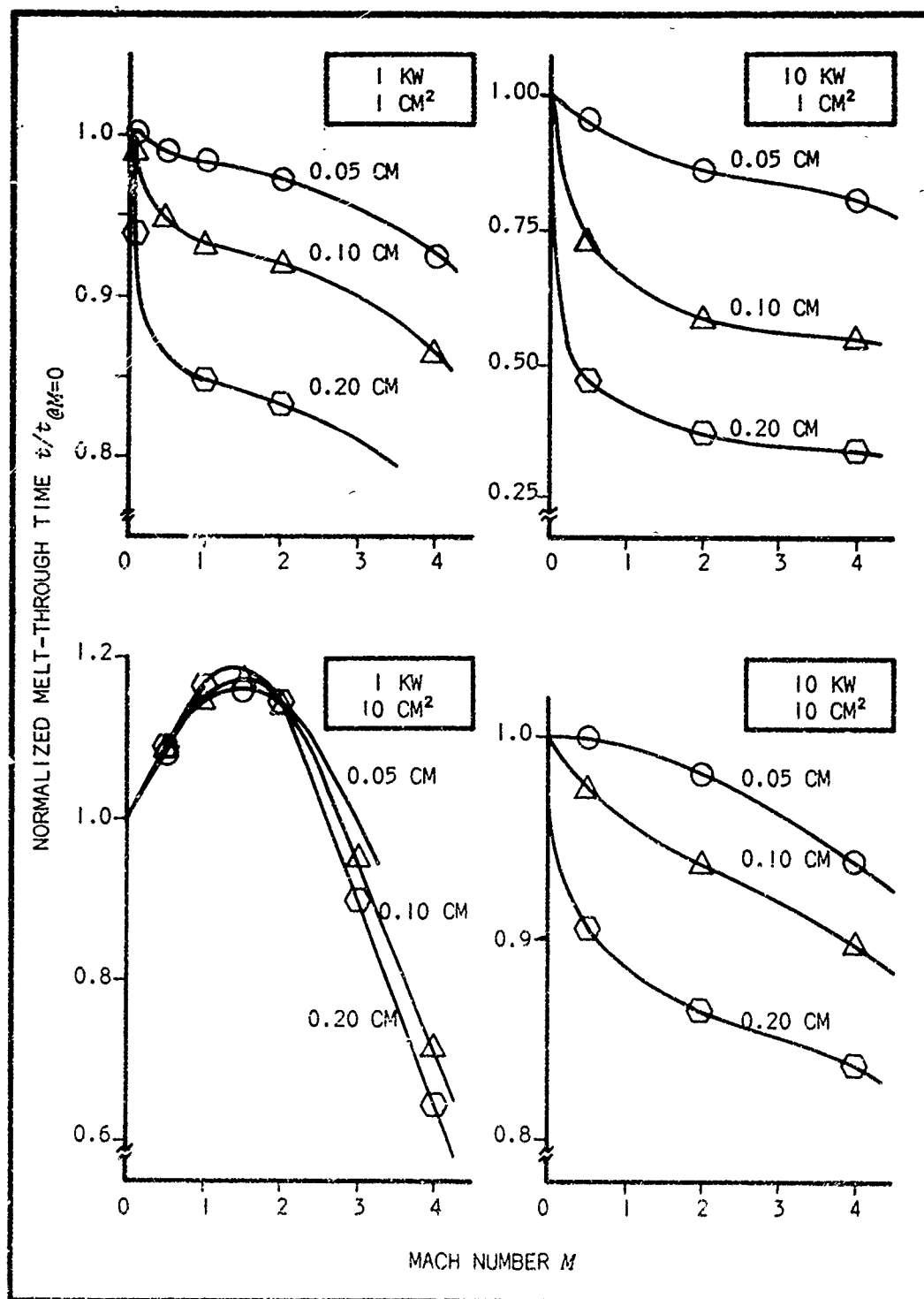


Fig. 11. Dimensionless Melt-Through Times (Normalized by Dividing by the Melt-Through Time at 0.0 Mach) for 0.05, 0.10, and 0.20 cm Thick Magnesium Plates Absorbing 1 and 10 kw of Light over 1 and 10 cm² Spots at Mach Numbers from 0 to 4

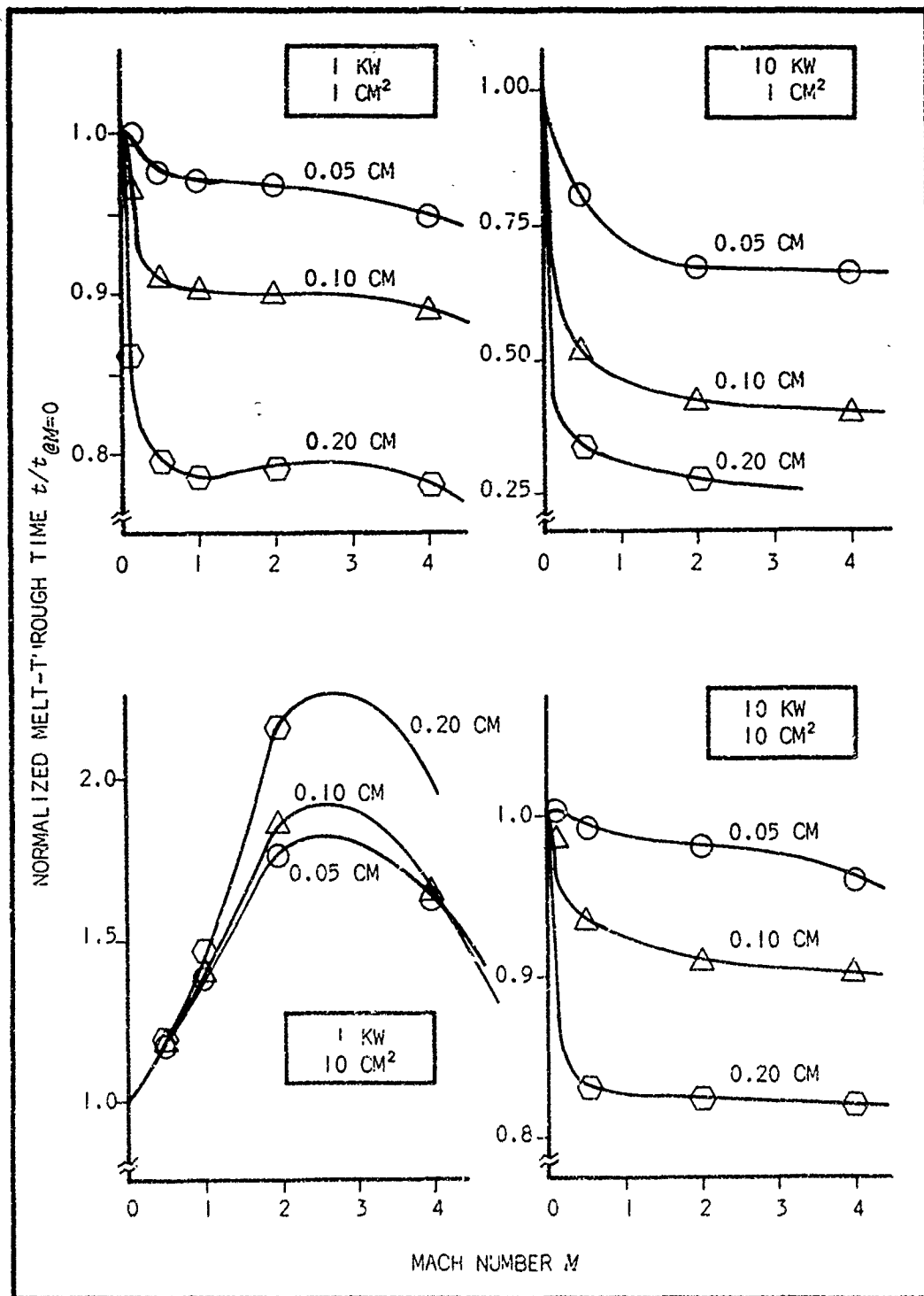


Fig. 12. Dimensionless Melt-Through Times (Normalized by Dividing by the Melt-Through Time at 0.0 Mach) for 0.05, 0.10, and 0.20 cm Thick Titanium Plates Absorbing 1 and 10 kw of Light Over 1 and 10 cm² Spots at Mach Numbers from 0 to 4

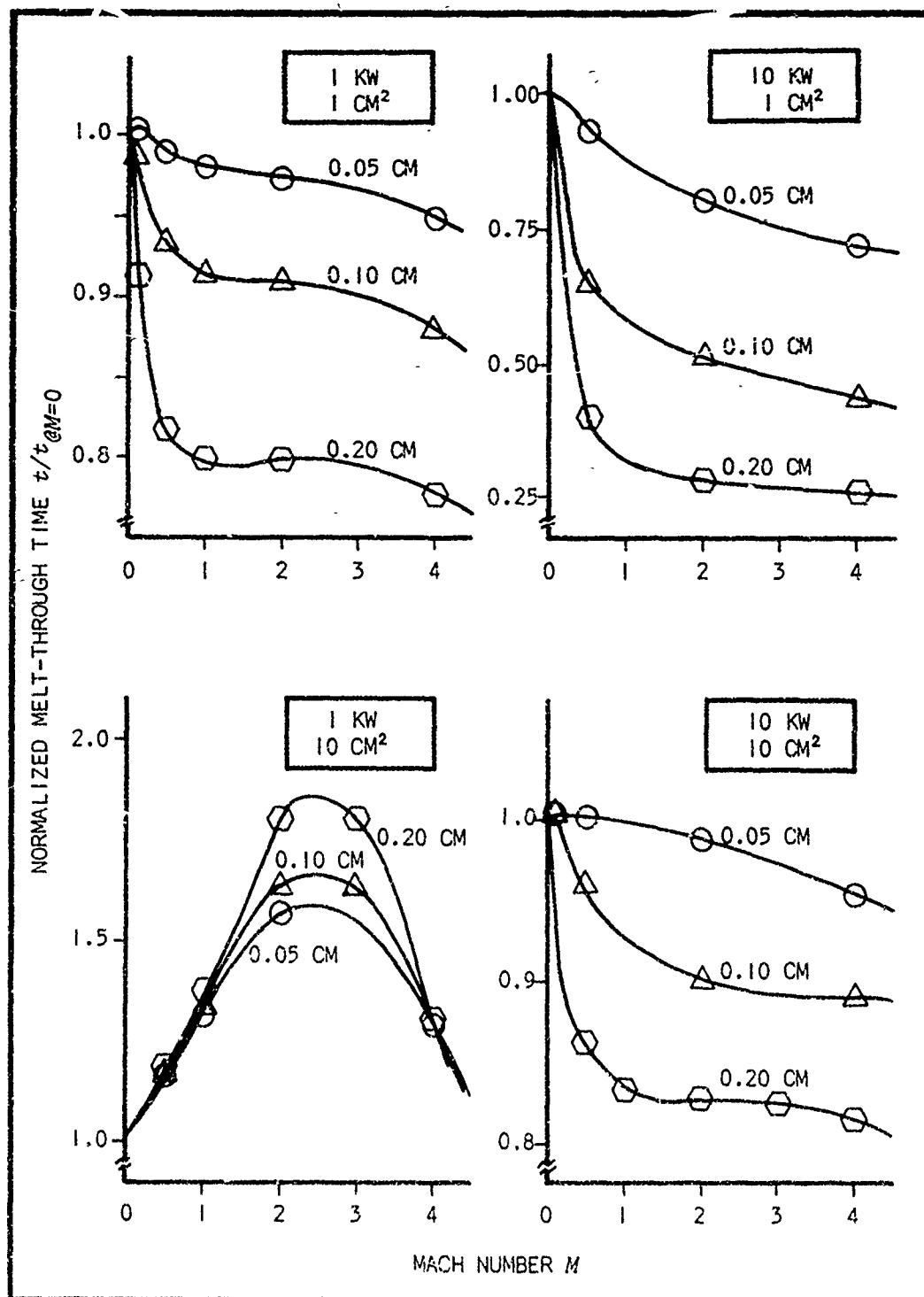


Fig. 13. Dimensionless Melt-Through Times (Normalized by Dividing by the Melt-Through Time at 0.0 Mach) for 0.05, 0.10, and 0.20 cm Thick Stainless Steel Plates Absorbing 1 and 10 kw of Light Over 1 and 10 cm² Spots at Mach Numbers from 0 to 4

melt-through times than with similar melt removal from thinner sheets identically radiated. Another characteristic of the mass flow mechanism is that its effect quickly increases with increased wind velocity until it approaches a maximum. The theoretical maximum effect would be instantaneous melt removal; but, for the spot sizes tested, this maximum was virtually achieved as early as sea level mach 0.5 (in the cases of extremely high flux intensities, i.e., 10 kw/l cm^2 , the maximum was approached at about mach 1.0). Further increases in wind velocities did not appreciably hasten melt-through due to the effect of mass flow. The changes that are noted in melt-through times at higher mach numbers are attributed instead to aerodynamic heating/cooling effects which are, as previously stated, strongly a function of wind velocity particularly at the higher mach numbers.

The overall effect of wind on melt-through is simply the summation of the two individual effects noted above. But, since the individual effects can vary considerably with changes in the metal, the metal thickness, the flux, and the beam or spot size, these other parameters must also be examined as to their influence on melt-through and the aerodynamic effects.

The Influence of the Metal on Aerodynamic Effects

The corresponding melt-through time versus mach number curves for the four metals in Figs. 10-13 exhibit definite similarities in form and in some of the cases in magnitude as well. These similarities indicate that the metals have similar influences, qualitatively, on the effects of air flow on laser-induced melting. The curves of Figs. 10-13 in their normalized form do, however, discount quantitative differences between

the metals. Therefore, the effect of the metal on "aerostatic" (meaning in still air) melt-through times is necessary to appreciate the magnitude of those differences that do exist in the influence of the metal on aerodynamic effects.

Briefly, the relative times for aerostatic melt-through for identical thicknesses and energy absorption, taking the value for magnesium as 1.0, were found to be approximately 1.5 for aluminum, 3.5 for titanium, and 4.5 for stainless steel. Interestingly, the densities of the same respective metals, relative to magnesium, are 1.5, 2.5, and 4.5. The correspondence of the relative densities to relative melt-through times indicates that it is the difference in density that largely accounts for the variation between these four metals in times to melt through in still air. Titanium, the only exception to the above curiosity, requires additional time for melt-through due to its high melting point (1988°K cf 923°K for Mg). Stainless steel also has a high melting point (approximately 1730°K), but a low specific heat (≈ 0.166 cal/gm/°K cf ≈ 0.312 cal/gm/°K for Mg) keeps the heat content per unit mass at melting comparable to that of magnesium. Other properties of metals that can influence aerostatic melt-through times, but which in the case of the above metals apparently "balanced out" in the net effect, are the heat of fusion, the boiling point, the heat of vaporization, and conductivity. Viscosity, in addition to several of the above properties, can influence aerodynamic effects on melt-through times.

Aerodynamic effects on melt-through were observed to be most pronounced on titanium and stainless steel (see Figs. 10-13). Lesser effects were noted on magnesium and aluminum. The causes of these differences between the four metals were traced to three properties: the respective

conductivities, specific heats, and melting temperatures of the metals. The conductivity and specific heat were found to indirectly affect the mass flow effect while the melting point was determined to directly influence aerodynamic heating/cooling.

The Influence of Metallic Properties on Melt Flow Effects. In the case of mass flow, poor conductivity forces an increased temperature gradient and consequently higher average heat content in any melt not removed by aerodynamic frictional forces. As previously explained, the faster the removal of such heat-cumulating material, the faster the melt-through. The most heat-cumulative of the molten metals are those with the poorest conductivities and the highest specific heats. Liquid titanium, stainless steel, and magnesium have approximately 0.15, 0.25, and 0.75 the conductivity of molten aluminum, and the corresponding relative axial temperature gradients, disregarding radial heat conduction, will be approximately proportional to the reciprocals of the relative conductivities. Temperature gradients at time of melt-through for 0.05, 0.10, and 0.20 cm thick titanium and aluminum as modeled by QUEST for 1 kw power absorption over a 1 cm² spot (see Fig. 14) clearly demonstrate the significant differences possible in temperature gradients between metals. The products of the relative temperature gradients and the relative specific heats (see Appendix C for property values of the metals) should provide an index of the potential amount of heat acquirable by unremoved melt ΔH_{melt} for a given flux intensity and plate thickness (low boiling points combined with small heat of vaporization in the case of relatively thick metals could reduce the accuracy of such an index). The resultant products are Ti, 6.8; stainless steel, 4.3; Mg, 2.6; and Al, 1.6.

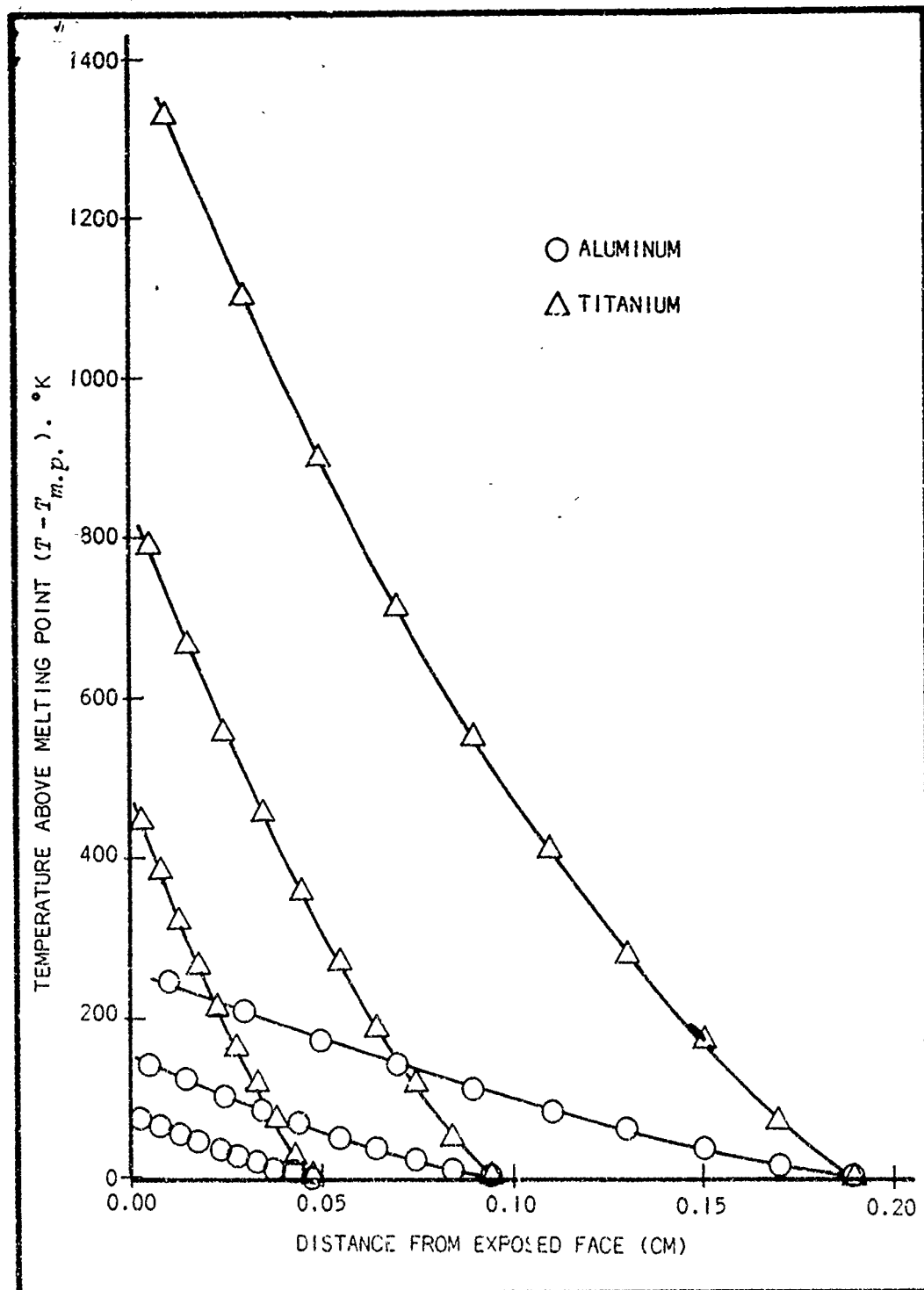


Fig. 14. Interior Temperatures of 0.05, 0.10, and 0.20 cm Thick Aluminum and Titanium Plates at Time of Melt-Through After Exposure to 1 kw Radiation Over a 1 cm² Spot as Modeled by QUESi

Another property of metal, viscosity, intuitively should determine the mach number at which melt flow achieves a given percentage of its ultimate potential effect. However, despite titanium and stainless steel having viscosities at the melting temperature about four times as great as magnesium and aluminum, no significant shift between metals was observable from Figs. 10-13 in the mach number at which melt flow produced similar effects. It appears, from the limited data available, that mass flow in general approached its maximum effect between mach 0.5 and 1.0. However, it is anticipated that further sensitivity testing in the subsonic regime will reveal that viscosity does have some discernible but limited influence in the mach number-mass flow effect relationship.

The Influence of Metallic Properties on Aerodynamic Cooling/Heating Effects. As indicated previously, the melting point is the primary determinant of a metal's influence on the convective heat transfer effects. From Eq (23), it is the difference between the aerodynamic boundary layer recovery enthalpy and the surface enthalpy (or the difference between their related temperatures) that not only determines whether cooling or heating occurs but also affects the magnitude of whichever effect takes place. Since the melting point serves as a lower limit to the surface temperature at the spot's center during the latter, and in most cases the major portion of the melt-through process, this property is strongly influential in the aerodynamic heating or cooling effect. Titanium and stainless steel, with high melting points (approximately 1988°K and 1730°K, respectively), demonstrate their influence on aerodynamic cooling in the lower left graphs of Figs. 12-13. Compared to the corresponding graphs for aluminum and magnesium

(Figs. 10-11) the magnitude of the cooling effect on delaying melt-through for titanium and stainless steel is significantly amplified and peaks at nearly twice the mach number. The elevated melting temperatures of titanium and stainless steel also manifest their influence on aerodynamic cooling in the cases of 0.2 cm thick sheets exposed to 1 kw over 1 cm² where melt-through times actually increased from mach 1.0 to mach 2.0. No similar effect was noted with cooler melting (933°K and 923°K) aluminum and magnesium. Conversely, aerodynamic heating effects are enhanced by the lower melting temperatures of aluminum and magnesium. The enhancement is manifested by faster melt-through at reduced free-airstream velocities. Such is evidenced in the cases of 1 kw/1 cm² and 10 kw/10 cm² power absorption per spot size (upper left and lower right graphs of Figs. 10-11) where appreciable reductions in melt-through times commenced as early as mach 2.0 for these two metals while little or no reduction occurred in stainless steel and titanium until after mach 3.0.

The Influence of Plate Thickness on Melt-Through Times

In Ref 12 Torvik determined that the ratio of total power to plate thickness was the criterion that decided the accuracy of a one-dimensional (axial) approximation to interior heat flow as opposed to three-dimensional reality. That is, for a given power, it is the thickness, with the spot size having essentially no influence, that determines the proportion of radial heat loss to the heat retained directly beneath the laser spot. These findings were based on instantaneous melt removal. However, another influence of plate thickness, in addition to its effect

on radial heat loss, must be accounted for in non-instantaneous melt removal cases. This additional factor is the heat content within the molten metal. As can be seen from Fig. 14, the heat content in the melt for a particular metal in the aerostatic case approximately quadruples in magnitude with a doubling of thickness (this can be viewed as doubling the base and nearly doubling the height of the approximate triangles formed from the graph's axes and the interior temperatures within the molten slab--the area of which is proportional to the added heat content of the metal above the melting point). This nonlinear heat requirement, combined with similarly nonproportional heat requirements for radial heat conduction with increases in thickness, accounts for the increase in melt-through time per unit thickness with increased plate thickness as calculated from the results tabulated in Appendix D and as presented in Fig. 15. The ratio of aerostatic melt-through times per cm of thickness (t_1/cm)/(t_2/cm), due to the nonlinear heating requirements of the melt for different plate thicknesses should be approximately

$$\frac{t_2/\text{cm}}{t_1/\text{cm}} \approx \frac{\left[\Delta H_{\text{melt}_2} + (H_{\text{m.p.}} - H_{\text{start}}) \right]}{\left[\Delta H_{\text{melt}_1} + (H_{\text{m.p.}} - H_{\text{start}}) \right]} \quad (34)$$

where ΔH_{melt} refers to the heat acquired per unit mass of melt in excess to the heat content of the same metal at the melting point $H_{\text{m.p.}}$, and H_{start} is the heat content of the metal prior to heating. For the case of titanium plates 0.05 and 0.2 cm in thickness, the above equation becomes

$$\begin{aligned} \frac{t(0.2 \text{ cm Ti})/\text{cm}}{t(0.05 \text{ cm Ti})/\text{cm}} &\approx \frac{[(1150^\circ\text{K}/2)(0.167 \text{ cal/gm}^\circ\text{K}) + (341 \text{ cal/gm})]}{[(400^\circ\text{K}/2)(0.167 \text{ cal/gm}^\circ\text{K}) + (341 \text{ cal/gm})]} \\ &\approx 1.165 \end{aligned} \quad (35)$$

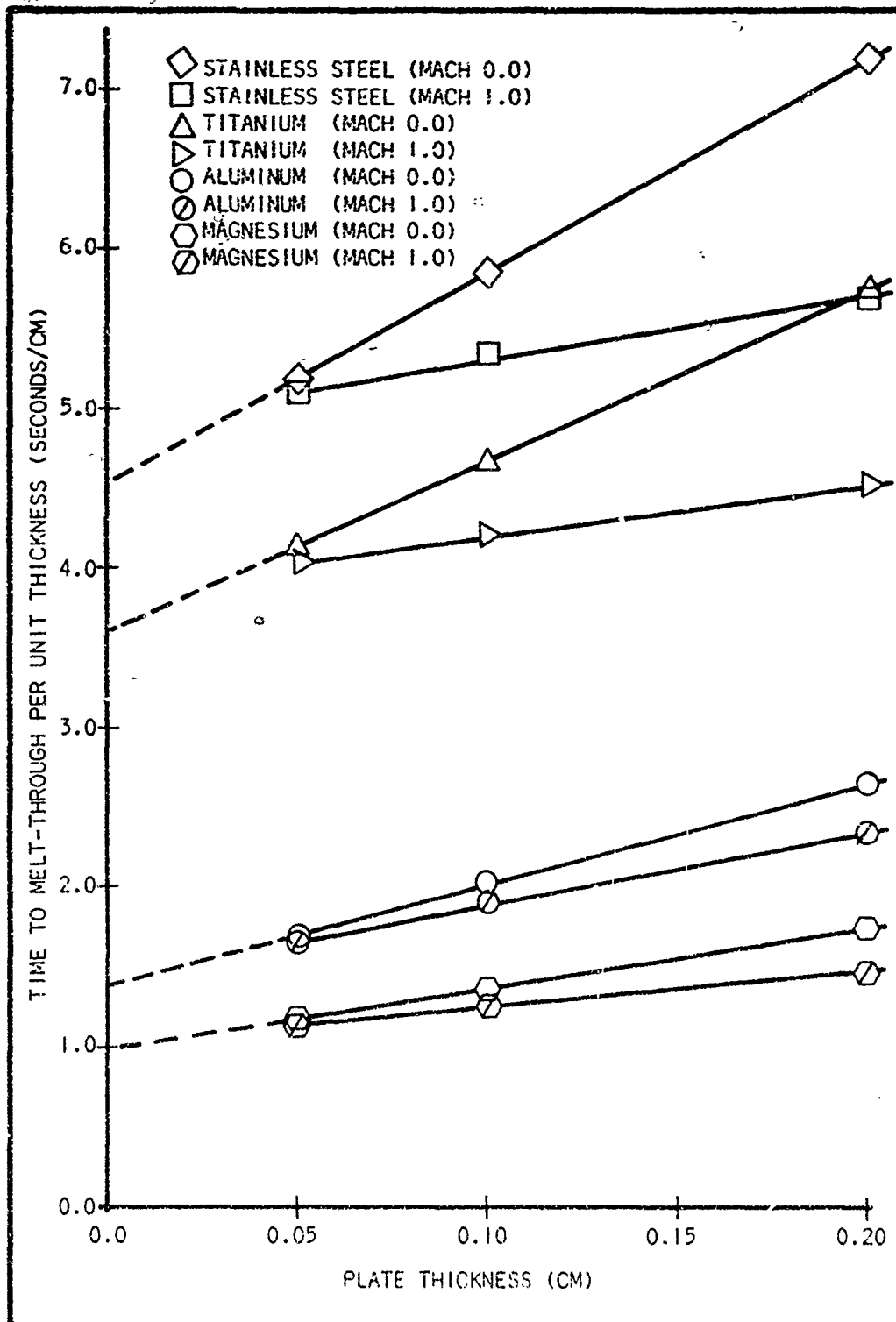


Fig. 15. Time to Melt-Through per Unit Thickness of Stainless Steel, Titanium, Aluminum, and Magnesium as a Function of Plate Thickness

where ΔH_{melt_1} and ΔH_{melt_2} were approximated from the temperature profiles in Fig. 14 in conjunction with the specific heat for titanium (see Appendix C). The actual predicted ratio, from Fig. 15, is 1.38. The difference is attributed to the additional retardation effect of increased radial heat conduction with increased plate thickness. If such is the case, the retardation from radial heat loss as modeled by QUEST and from melt heating are roughly the same for the aerostatic melt-through case. However, it must be remembered that QUEST is only a two-dimensional model and thus does not account for all radial heat loss; and that, therefore, radial heat flow should have an even greater effect than melt heating.

It was noted that extrapolation of the aerostatic melt-through time per thickness curves in Fig. 15 to the point of zero thickness nearly coincided with the corresponding values computed for one-dimensional heat flow and instantaneous melt removal from Table I. This seems reasonable, but similar extrapolation of the aerodynamic (for mach equal to 1.0) curves gives values indicating longer melt-through times per unit thickness. A possible explanation for this curiosity would be a retardation effect on melt-through due to aerodynamic cooling as was noted at lower mach numbers for 0.05 cm thick plates absorbing 1 kw of power over 1 cm² (see Figs. 10-13).

The aerodynamic curves of Fig. 15 also have less slope, representing the fact that with increasing plate thickness the wind negates, through melt removal, more and more of the potential retardation effect of heat accumulation within the melt layer. The remaining slope in the aerodynamic curves is mostly attributed to radial heat losses since

mach 1.0, sea level air flow should provide near-instantaneous melt removal over a 1 cm^2 spot.

The Influence of Flux Levels and Spot Sizes on Aerodynamic Effects

Since just two power levels (1 and 10 kw) and beam sizes (1 and 10 cm^2) have thus far been tested by QUEST in the simulation of laser melt-through, only limited inferences are possible as to the influence of each of these parameters on the aerodynamic effects on laser-induced melting. Notwithstanding, the similarity in form and magnitude of the corresponding curves within the upper left and lower right graphs of Figs. 10-13 (which depict the aerodynamic effects for $1 \text{ kw}/1 \text{ cm}^2$ and $10 \text{ kw}/1 \text{ cm}^2$) suggests that the ratio of power to spot size, or flux intensity, may serve as a gauge in determining the effect of wind on melt-through. It is clear, not only from comparisons between the above two and the remaining two graphs within each of Figs. 10-13 but also from logical considerations, that flux intensity is strongly, and possibly predominantly, influential in determining the effect of wind on melt-through. Low intensities allow aerodynamic cooling or heating (which one depends upon the mach number and the melting point of the metal) to strongly manifest their respective effects of melt-through retardation or acceleration. At very low flux intensities convective heat transfer due to aerodynamic cooling (and to a lesser extent, radiation*)

*For example, for flux intensities of $0.1 \text{ kw}/\text{cm}^2$ on 0.2 cm thick titanium and aluminum at mach 2.0 and evaluated for conditions at the spot center, heat losses due to radiation accounted for 6.0 and 0.01% respectively of the heat absorbed (the higher melting point of titanium primarily accounted for the three order of magnitude difference). Thus radiation was found to be insignificant except for metals with high melting points which are exposed to very low ($<0.1 \text{ kw}/\text{cm}^2$) flux intensities.

could even counteract laser heating prior to the metal rising to the solidus temperature such that melt-through would never occur. On the other hand, increasing the flux intensity influences the melt transfer effect in a manner quite similar to that of reducing the metal's conductivity. That is, for aerostatic melt-through, increased flux forces an increased axial temperature gradient within the molten metal. Equation (9) manipulated to the form of Eq (36), mathematically illustrates the effect on the axial temperature gradients by changes in either conductivity or flux intensity. That is,

$$\left(\frac{HXFRT_{i,j}}{\Delta x \Delta z} \right) \left(\frac{1}{K} \right) = \left(\frac{T_{i,j+1} - T_{i,j}}{\Delta y} \right) \quad (36)$$

or equivalently,

$$\frac{q}{k} = \frac{\Delta T}{\Delta y} \quad (37)$$

An ultimate consequence of large temperature gradients within a sufficiently thick melt layer is vaporization. But even if vaporization does not occur, removal by aerodynamic friction of potential "heat-robbing" melt will reduce melt-through times. The extent of the reduction is approximated by Eq (34).

Quantitative evaluation of the influence of flux intensity on aerodynamic effects, difficult due to the limited data points and the simultaneous influences of other parameters, was attempted by plotting dimensionless melt-through times for 0.2 cm thick titanium and aluminum at sea level mach 2.0 against logarithmically scaled flux intensities as shown in Fig. 16 (the corresponding times for stainless steel and magnesium, although not plotted, approximated those of titanium

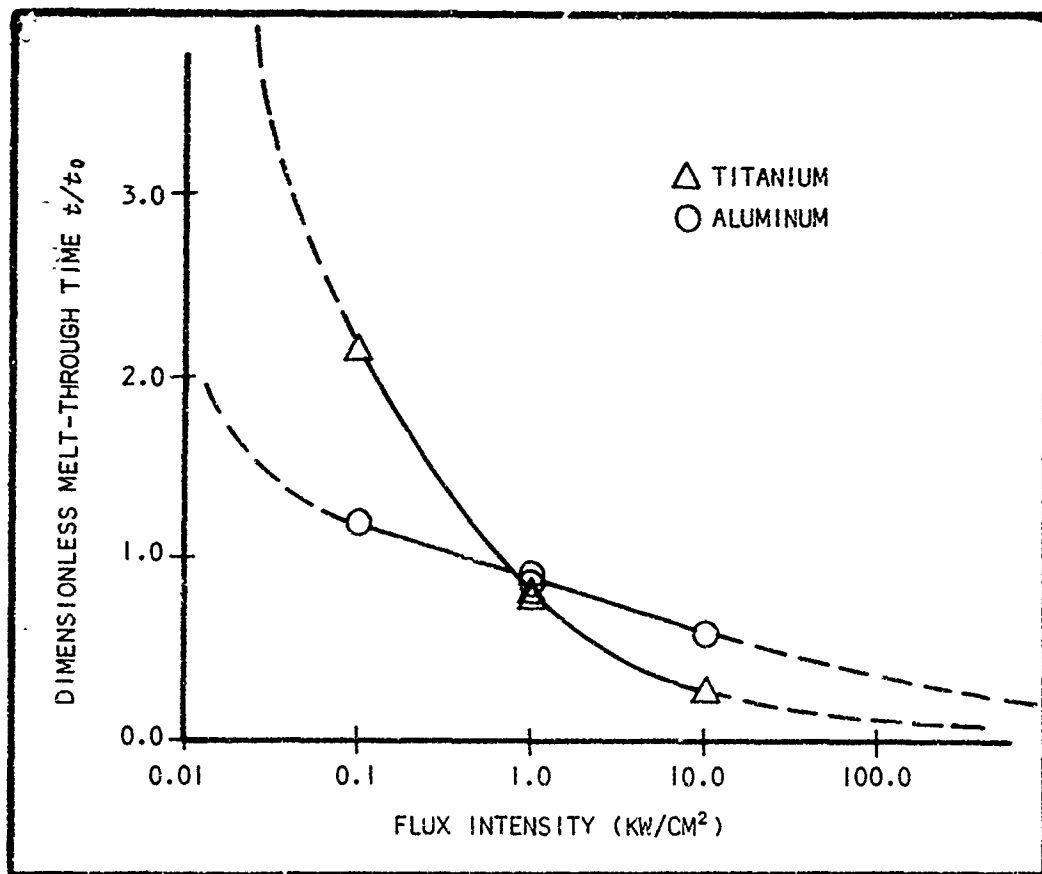


Fig. 16. Melt-Through Times for 0.2 cm Thick Titanium and Aluminum in a Mach 2.0 Sea-Level Airstream Normalized by Dividing by the Corresponding Mach 0.0 Melt-Through Times as a Function of Power Density

and aluminum respectively). The solid curves as deduced from each of the two sets of data differ in form--that for titanium (and stainless steel) implies a decreasing reduction in melt-through time with each magnitude increase in flux intensity while the one for aluminum (and magnesium) indicates a constant reduction. As previously stated, however, with aerodynamic cooling and some small flux intensity, the melt-through time for aluminum must go to infinity. And, no matter how intense the flux, melt-through will require some positive finite time.

Thus, the curve for aluminum in Fig. 16 cannot remain linear, but must asymptotically approach both the abscissa and the vertical to the maximum flux intensity at which no melt-through occurs for the given mach number and the other initial conditions. Such curvature is suggested by the dashed lines of Fig. 16, but computation of additional data points is essential prior to any additional postulations in quantitatively relating flux intensity and aerodynamic effects.

It may be noted that the two data points for each metal at the 1.0 kw/cm² flux intensity in Fig. 16 differed slightly. Further investigation of the data in Appendix D will reveal that for similar metals, thicknesses, and mach numbers the 1 kw/1 cm² power-to-spot-size ratios always required longer to melt-through than did power-to-spot-size ratios of 10 kw/10cm²--this occurred despite identical flux intensities of 2000 joules per second per cm² at the spot center (reference Eq (4)). The differences, up to 50 percent of the smaller time, are ascribed to lesser radial heat transfer rates within the larger spot due to smaller radial temperature gradients which in turn is a consequence of the assumed Gaussian flux distribution described by Eq (3). Differentiation of Eq (3) with respect to the radial distance r provides the radial gradient of flux intensity as a function of the spot size σ ; radial distance; and flux intensity at the beam axis q_0 . That is,

$$\frac{\partial q}{\partial r} = \frac{-q_0 r}{\sigma^2} e^{-(1/2)(r^2/\sigma^2)} \quad (38)$$

Easier to visualize than Eq (38) is Fig. 17 which shows the local flux intensity along the radii of 1 and 10 cm² spots absorbing 1 and 10 kw of power, respectively. The intensities and their gradients are identical

at the spot centers, but the magnitude of the radial gradient can otherwise be seen to be less for the larger spot at any point within the smaller spot. The radial temperature gradients within the metal plate and the consequential radial heat losses will approximately correspond to the relative radial gradients of the flux intensities. Thus, larger radial heat losses should account for much of the added time required for melt-through in the 1 kw/1 cm² total power-to-spot-size cases.

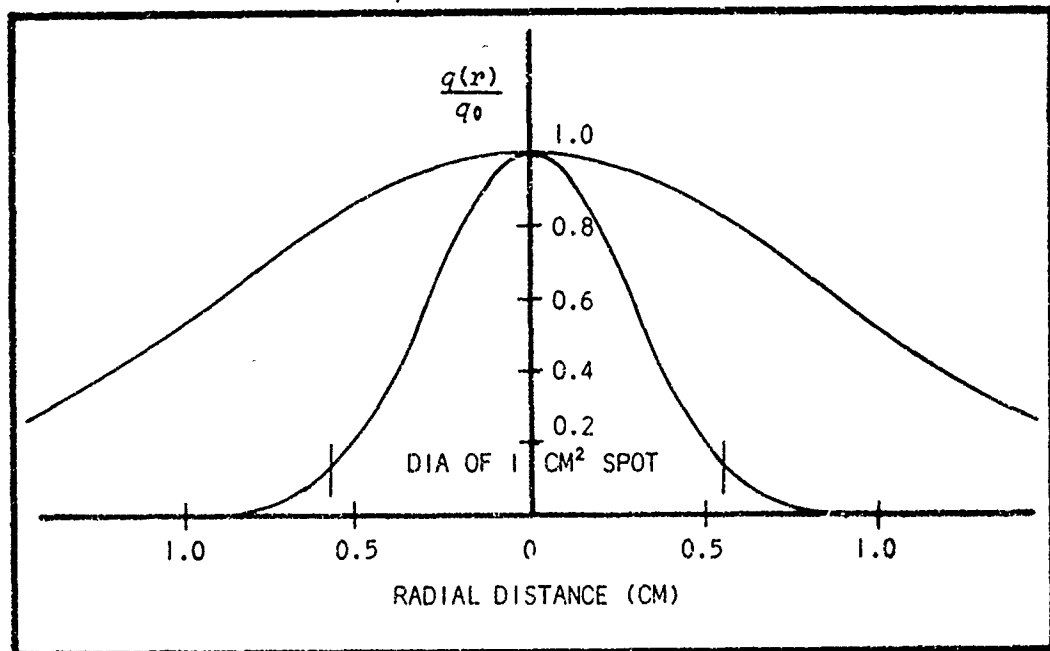


Fig. 17. Intensity of a Gaussian Flux Distribution as a Function of Radial Distance from the Center of 1 and 10 cm² Spots Absorbing 1 and 10 kw Power ($q_0 = 2000$ joules/(sec·cm²))

Extending the above analysis to the case of a constant total flux, for example 1 kw, and a varying spot size helps to explain why spot size may be safely ignored in gauging the accuracy of a one-dimensional heat flow approximation for laser heating (Ref 12). Doubling the spot area from 1 to 2 cm² exactly halves the flux intensity at the spot's center q_0 while roughly halving the radial gradient of

the flux intensity (see Fig. 18). Halving q_0 will about double the time required to melt-through, whereas halving the radial gradient should reduce the radial heat transfer rate by a factor of approximately two. The result is an approximately equal radial heat loss despite the doubling of the spot size. Postulating further, varying the spot size for a constant laser power and plate thickness would have negligible influence in the total heat lost through radial conduction; or, as discovered by Torvik and reported by him in Ref 12, the accuracy in approximating laser heating by one-dimensional (axial) heat flow is independent of spot size.

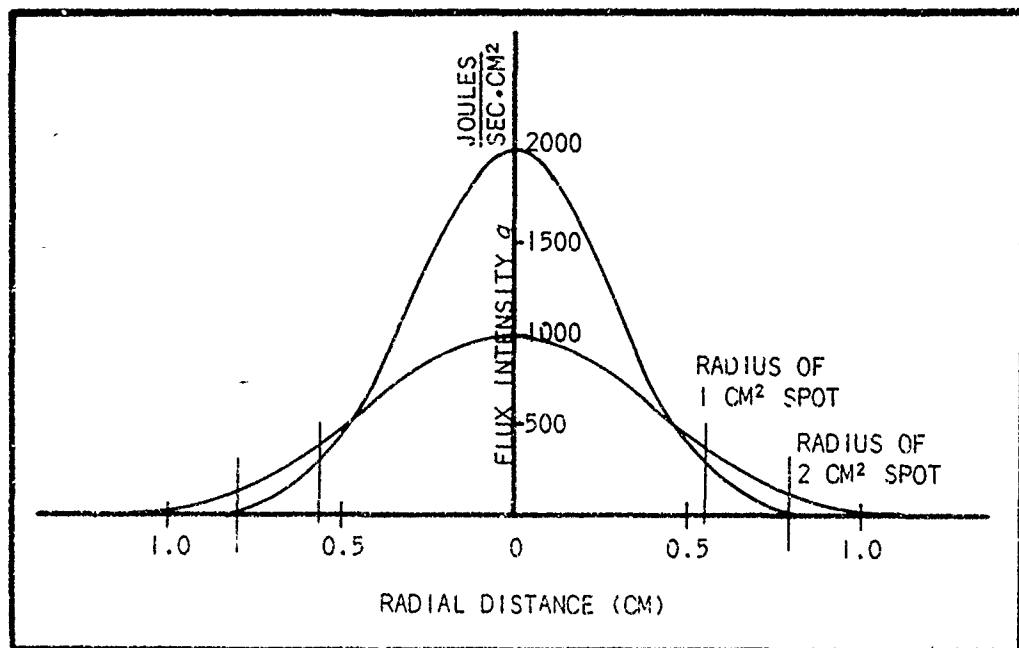


Fig. 18. Intensity of a Gaussian Flux Distribution as a Function of Radial Distance From the Center of 1 and 2 cm² Spots Absorbing 1 kw of Power

VI. Conclusions and Recommendations

Based on the results and findings to date, QUEST appears to be a viable model capable of closely estimating the melt-through times and approximating the surface recession phenomena of laser-induced, wind-affected melting of metal plates when the energy absorption rate is known. From this premise, the following conclusions and recommendations are submitted.

Conclusions

1. The model, as comprised in the computer program QUEST, has met the objective of this thesis study. That is, it stands ready as a tool for further investigation of laser effects. Substantial data, ancillary to the melt-through times as were primarily reported upon in the preceding chapter, are provided by QUEST to further assist in comprehending the nature of melt-through. The computer program is adaptable to a wide range of input parameters and is capable of accuracies commensurate with the computer processing time available.

2. The findings thus far indicate that significant utility can be obtained from QUEST in determining aerodynamic influences on laser-induced melting that would otherwise be unpredictable.

3. The effects of wind on laser-caused melting were found to be by two mechanisms--melt transfer and convective heat transfer. Either can predominate at a given altitude; which one depends primarily upon the flux intensity and the mach number. The magnitude of the aerodynamic effects likewise depends upon the mach number and flux intensity,

but also varies considerably with the plate thickness, the metal and the size of the laser beam. Further use of QUEST will enable a clearer understanding of these interrelationships over a wider range of parameters.

4. Without question, the computer program QUEST can be improved on. A major restriction (that was recognized but which was accepted since resolution thereof was beyond the scope of this study) is the requirement to specify the flux absorbed by the metal as opposed to the flux incident upon the metal. Incorporation of a reflectivity model within QUEST which would account for the change of absorptivity as a function of the metal, its surface condition, its temperature, and any other significant parameters would enhance the practicality of QUEST in the overall study of laser effects.

5. Another restriction, similarly accepted, is the exclusion of catastrophic oxidation effects in the model. Lesser restrictions are those inherent with limited available data on the properties of metals, particularly at the elevated temperatures approaching, and in excess of, melting. The basic logic used within the present model, however, is unaffected by such property value functions and therefore will accommodate revisions as they may become available.

Recommendations

It is recommended that:

1. QUEST be gainfully employed to further the knowledge of laser effects on metals in an aerodynamic environment.
2. Modeling the reflectivity of laser light on melting metals be attempted and any successful results be incorporated within QUEST.

3. Further study be given to modifying the convective heat transfer rate as presently embodied in QUEST by including effects of unheated starting lengths and variable surface temperatures (reference Eq (23)), particularly for modeling effects from low flux intensities or with laminar air flow.

4. The effect of melt transfer due to gravity be compared with the effect of similar melt transfer from aerodynamic friction and if the effect of the former is significant that it be modeled within QUEST.

5. Catastrophic oxidation as a predictable event within laser-induced, aerodynamic-influenced melting be investigated and if possible a model of such be included within QUEST.

6. Continued efforts be made to further validate QUEST through experimental results; and, despite the consistent results to date and the scrutiny to which the logic and mathematics of QUEST have been repeatedly subjected, that the numerical results from QUEST continue to be treated as suspect (as should be the case with any computer-programmed model).

7. The model be extended to other metals of interest.

8. Modeling of aerodynamically influenced, laser-induced melting of metals of other shapes be attempted.

Bibliography

1. Yura, H. T. The Interaction of Laser Light with Metals. Memorandum RM-3560-PR. Santa Monica: The Rand Corporation, March 1963.
2. McMaster, W. H., et al. "Compilation of X-Ray Cross Sections." UCRL-50174-Sec 2. Livermore, California: Livermore Radiation Laboratory, undated (released about 1968).
3. Meyerhof, Walter E. Elements of Nuclear Physics. New York: McGraw Hill Book Co., 1967.
4. Ready, John F. Effects of High-Power Laser Radiation. New York: Academic Press, Inc., 1971.
5. AD 609342. Fire Hazards Associated with the Use of Titanium in Aircraft. DMIC Technical Note. Columbus, Ohio: Defense Metals Information Center, June 1964.
6. Masters, Joseph I. "Problem of Intense Surface Heating of a Slab Accompanied by Change of Phase." Journal of Applied Physics, 27: 477-484 (May 1956).
7. Muehlbauer, John C., and J. Edward Sunderland. "Heat Conduction with Freezing or Melting." Applied Mechanics Reviews, 18: 951-959 (December 1965).
8. Eckert, Ernst R. G. Survey on Heat Transfer at High Speeds. WADC TR 54-70. Wright-Patterson Air Force Base, Ohio: Wright Air Development Center, April 1954.
9. Eckert, Ernst R. G. Survey of Boundary Layer Heat Transfer at High Velocities and High Temperatures. WADC Technical Report 59-624. Wright-Patterson Air Force Base, Ohio: Wright Air Development Center, April 1960.
10. Torvik, Peter J. A Numerical Procedure for Two-Dimensional Heating and Melting Calculations with Applications to Laser Effects. AFIT TR 72-2. Wright-Patterson Air Force Base, Ohio: Air Force Institute of Technology, March 1972.
11. Eckert, Ernst R. G., and Robert M. Drake, Jr., Heat and Mass Transfer (2nd ed.). New York: McGraw-Hill Book Co., 1959.
12. Torvik, Peter J. "A Practical Approach to Laser Heating Calculations" Laser Division Digest, LRD-72-1, Kirtland Air Force Base, New Mexico: Air Force Weapons Laboratory, June 1972.

13. Ketter, Robert L., and Sherwood P. Prawel, Jr. Modern Methods of Engineering Computation. McGraw-Hill Book Co., 1969.
14. Schlichting, Dr. Hermann. Boundary-Layer Theory (6th ed.). New York: McGraw-Hill Book Co., 1968.
15. Kays, W. M. Convective Heat and Mass Transfer. New York: McGraw-Hill Book Co., 1966.
16. Welty, James R., et al. Fundamentals of Momentum, Heat and Mass Transfer. New York: John Wiley and Sons, 1969.
17. Wicks, C. E., and F. E. Block. Thermodynamic Properties of 65 Elements--Their Oxides, Halides, Carbides, and Nitrides. Washington: U.S. Government Printing Office, 1963.
18. Touloukian, Y. S. Recommended Values of the Thermophysical Properties of Eight Alloys, Major Constituents and Their Oxides. NASA N6623802. Lafayette, Indiana: Purdue University, February 1966.
19. Christian, James Wm. "Real Gas Property Effects on Flow and Heat Transfer in the Entrance Region of a Parallel-Plate Channel." Master's Thesis, Air Force Institute of Technology, Wright-Patterson AFB, Ohio, 1967.
20. Hansen, C. Frederick. Approximations for Thermodynamic and Transport Properties of High-Temperature Air. NACA Technical Note 4150. Moffet Field, California: Ames Aeronautical Laboratory, March 1953.
21. Keenan, Joseph H., and Joseph Kaye. Gas Tables. New York: John Wiley and Sons, 1948.

APPENDIX A

QUEST, a Computer Program of a Numerical Model of Surface Recession
Phenomena of Metals Subjected to Laser Radiation
in an Aerodynamic Environment

PROGRAM QUESTI

CDC 6600 FTN V3.0-320A OPT=1 11/15/72

```

PROGRAM QUESTI (INPUT,OUTPUT,TAPE 7)
COMMENT***TITANIUM***TITANIUM***TITANIUM***TITANIUM***TITANIUM***TITANIUM***
COMMON T(30,35),TT(30,35),DY(30,35),CNDAXL(30,35),CNDPDL(30,35),
5 2 TFR(30,35),RA(30),NB(30),NZ(30),NAT(30),NBT(30),TIX(35),T8X(35),
3 ATXFR(30),BTXFR(30),TAU(30),TOCNV(30),TORAD(30),TVANISH(30),Q(30)
4 ,QOUT(30),ORAD(30),SUMDY(30),REQ(35),COEFF,AENTHLP,AMACH,AVELOX,
5 APRSURE,ARHO,ARN,ATEMP,CPI,CPSLUSH,CPV,DELX,DELY,DTIME,E,HF,HV,I,
6 J,MIDINT,MINT,NINT,NB21,NXTRA,NZ1,PRANDTL,RHO,STHMLT,TML,TMU,TV,
7 TISTMLT,TIME,VIS,XFROMLE,STOP,DELTIME
10 EQUIVALENCE (DDTIME,XFMCL,YIN),(XTIME,ATXFR),(TBACK,BTXFR,YMELT),
,ZVELOX),(TFR,CND),(YSOL10,REQ)
DIMENSION ZVELOX(30),TBACK(30),XFMCL(30),XTIME(30),YIN(30),
: 'MELT(30),CND(30,35),DATA(1024),YSOL10(30)
15 DATA TML3,TMUP,TVP,HFS,HVP/1975.,1988.,3550.,93.94572,2108.5595/
DATA YPPNDTL/0.7113/
CALL PLOTS (DATA,1024,7)
READ 993,ALT,AMACH,XFROMLE,TO
20 READ 993,PWR,SIGMA2,RADIUS,THICK
READ 992,MINT,NINT
992 FORMAT(4I20)
993 FORMAT(4F20,10)
CALL ATMOS(ALT,ATEMP,ASIGMA,ARHO,ATHETA,DELTA,CA,AMU,ACND)
ACOEFF=0.2*AMACH**2
25 APRSURE=DELTA*2116.22
AVELOX=CA*AMACH
ARN=ARHO*AVELOX*XFROMLE/AMU
ATRATIO=ATEMP/500.
AENTHLP=.01836064*ATRATIO*(0.9395396*ATRATIO*(0.03243428-ATRATIO*
30 : 0.000991742))
10 DELX=RADIUS*2./MINT
DELY=THICK/NINT
E=0.0001
HF=HFS
35 HV=HVP
MIDINT=(MINT+1)/2
NINTT=NINT+1
NINTTT=NINT+2
NXTRA=35
40 PRANDTL=PPPNOTL
RHO=DENSITY
STOP=0.
SUMQCNV=0.0
SUMORAD=0.0
45 TML=TMLO
TMU=TMUP
TV=TVP
CALL SPHEAT((TML+TMU)/2.,CPSLUSH)
CALL SPHEAT (TML-2.*E,CPI)
50 CALL SPHEAT (TV,CPV)
CALL SPHEAT (TO,CP0)
DELTIME=0.5*RHO*CP0/CNDMAX*(1./((1./DELX**2+1./DELY**2))
FLUX=PWR*238.9
CALL FLUXX(FLUX,SIGMA2)
55 20 DO 30 I=1,MINT
NAT(I)=NINT
NB(I)=NINT
60 NZ(I)=NINT
QOUT(I)=0.0
ORAD(I)=0.0
TOCNV(I)=0.0
TORAD(I)=0.0
TVANISH(I)=0.0
DO 25 J=1,NINT
65 T(I,J)=TO
TT(I,J)=TO
DY(I,J)=DELY
25 CONTINUE
DO 30 J=NINT1,NXTRA
70 T(I,J)=0.0
TT(I,J)=0.0
DY(I,J)=0.0
30 CONTINUE

```

PROGRAM	QUESTI	PAGE	2
75	CALL CONDUCT DTIME=0.5*RHO*DELY*DELY*CP0/CND(1,1)		
38	DO 40 I=1,MINT		
40	T(I,NZ(1))=T0+DTIME2(RHO*CP0*DY(1,NZ(1)))*Q(I) IF(T(MIDINT,NZ(MIDINT)).LT.(TML-E)) GO TO 42 DTIME=(TML-T0)/(T(MIDINT,NZ(MIDINT))-T0)*DTIME GO TO 38		
80	42 DO 45 I=1,MINT IF(T(I,NZ(1)).GT.TML-E) NA(I)=NA(I)-1 T(I,NZ(1))-1=(T(I,NZ(1))-T0)/4.0*T0 TIME=(T(MIDINT,NZ(MIDINT))-1)-T0)*CP0*RHO*DELY/Q(MIDINT) GO TO 60		
85	50 CONTINUE DO 55 I=1,MINT TOCNV(I)=QOUT(I)*DTIME+TOCNV(I) TORAD(I)=ORAD(I)*DTIME+TORAD(I) SUNDY(I)=0.0		
90	DO 53 J=1,NXTRA 53 SUNDY(I)=SUNDY(I)+DY(I,J) DO 55 I=1,MINT IF(NS(I).LE.0) GO TO 100		
95	55 CONTINUE DTIME=DTIME CALL FRICTION CALL SCHMIDT CALL XACTIME CALL COOL IT CALL VAPORIZ IF (NS(MIDINT).LE.0) GO TO 50 CALL RNSFRX CALL SQUEEZE		
100	DO 70 I=1,MINT 65 DO 70 J=1,NXTRA 70 T(I,J)=T(I,J) GO TO 50		
105	100 CONTINUE		
110	200 PRINT 1000,THICK,PWR,SIGMA2,DELX,DELY,ARN,ALT,AMACH,XFROMLE,TO, TMU,TV,HF,HV,CP0,CPI,CPSLUSH,CPV,CNDMAX 1000 FORMAT(1H1,'TITANIUM *F12.8,' CENTIMETERS THICK*// 1H,'*TOTAL BEAM POWER*F9.1,' KILOWATTS*// 1H,'*BEAM RADIUS (2 SIGMA)*F10.5,' CM*// 1H,'*DELX(RADIAL DIMENSION OF ELEMENTS)*F9.6,' CM*// 1H,'*DELY(AXIAL DIMENSION OF ELEMENTS)*F9.6,' CM*// 1H,'*REYNOLDS NUMBER*F12.0,/ 1H,'*ALTITUDE*F7.0,' FEET*// 1H,'*MACH NUMBER*F5.3,/ 1H,'*DISTANCE FROM LEADING EDGE*F6.2,' FEET*// 1H,'*INITIAL TEMPERATURE*F8.2,' DEGREES KELVIN*// 1H,'*MELTING POINT*F14.2,' DEGREES KELVIN*// 1H,'*BOILING POINT *F13.2,' DEGREES KELVIN*// 1H,'*HEAT OF FUSION*F14.3,' CALORIES(GM)/GRAM*// 1H,'*HEAT OF VAPORIZATION*F8.3,' CALORIES(GM)/GRAM*// 1H,'*SPECIFIC HEAT I INITIAL T*F7.6,' CALORIES/GRAM/DEG K*// 1H,'*SPECIFIC HEAT I : T MELT*F8.6,' CALORIES/GRAM/DEG KELVIN*// 1H,'*SPECIFIC HEAT I T SLUSH*F9.6,' CALORIES/GRAM/DEG K*// 1H,'*SPECIFIC HEAT I T LIQUID*F8.6,' CALORIES/GRAM/DEG K*// 1H,'*MAXIMUM CONDUCTIVITY*F12.6,' CALORIES/SEC/CM/DEG K*// PRINT 998,((T(I,J),I=1,MINT),J=1,NXTRA) 1998 FORMAT(1X,27F5.0) PRINT 1999 1999 FORMAT(1H10,VECTOR IS TO THE LEFT (FOR TEMPERATURE ARRAY ABOVE) AND IS UPWARD (FOR PRINTOUT WHICH FOLLOWS)*// PRINT 2000 2000 FORMAT(1X,ELEMENT*9X,*Q (1N)*7X,*Q (CNVC)*8X,*Q (RAD)*8X,*Q (VPR)* 6X,*CMS VPRZD*7X,*CMS LEFT*// SUMQIN=0.0 SUMQCNV=0.0 SUMORAD=0.0 SUMQVPR=0.0 DO 300 I=1,MINT TO=Q(I)*TIME*DELX TOCNV(I)=TOCNV(I)*DELX TORAD(I)=TORAD(I)*DELX TOVPR=TVANISH(I)*DELX*RHO*HV PRINT 2001,I,TO,TOCNV(I),TORAD(I),TOVPR,TVANISH(I),SUNDY(I) 2001 FORMAT(10,7E15.6//		

PROGRAM	QUESTII	PAGE
150	SUMQIN=SUMQIN+10 SUMQCNV=SUMQCNV+TCNV(1) SUMORAD=SUMORAD+TORAD(1) SUMQVPR=SUMQVPR+TVPR	3
155	300 CONTINUE PRINT 2660,SUMQIN PRINT 2620,SUMQCNV PRINT 2640,SUMORAD PRINT 2002,SUMQVPR	
160	2660 FORMAT('TOTAL INCIDENT ABSORBED ENERGY='F25.10,' CALORIES') 2620 FORMAT('TOTAL CALORIES LOST DUE TO CONVECTION='F18.10,' CALORIES') 2640 FORMAT('TOTAL ENERGY EMITTED DUE TO RADIATION='F18.10,' CALORIES') 2002 FORMAT('CALORIES EXPENDED IN VAPORIZATION (TOTAL)='F15.10/)	
165	PRINT 2003,TIME 2003 FORMAT('TIME TO MELT THROUGH='F15.10,' SECONDS'//) DO 333 I=1,MINT YSOLID(I)=0.0 NBB1=NB(I) XFML(I)=(I-MIDINT)*DELX DO 332 J=1,NBB1	
170	332 YSOLID(I)=YSOLID(I)+DY(I,J) IF(NB(I).EQ.0) YSOLID(I)=0.0 333 CONTINUE PRINT 2004	
175	2004 FORMAT('DISTANCE FROM C/L (CMS)*5X,TOTAL THICKNESS (CMS)*5X, 'NON-MOLTEN THICKNESS (CMS)*') PRINT 2005,(XFML(I),SUMDY(I),YSOLID(I)),I=1,MINT)	
180	2005 FORMAT(F20.5,F25.12/) CALL PLOT(0.0,1.0,-3) CALL SCALE(XFML,5.00,MINT,1) CALL SCALE(YSOLID,3.00,MINT,1) SUMDY(MINT+1)=YSOLID(MINT+1) SUMDY(MINT+2)=YSOLID(MINT+2) CALL AXIS(0.0,0.0,36,RADIAL POSITION FROM BEAM AXIS (CMS),-36.5 0 '0.0,XFML(MINT+1),XFML(MINT+2))	
185	CALL AXIS(0.0,0.0,15,THICKNESS (CMS),15.3,0.90,0,SUMDY(MINT+1) 'SUMDY(MINT+2)) CALL LINE(XFML,SUMDY,MINT,1,1,1) CALL LINE(XFML,YSOLID,MINT,1,1,1) CALL PLOT(10.0,-1.0,-3)	
190	TBACK(1)=TO TBACK(2)=TISTHLT XTIME(1)=0.0 XTIME(2)=STMELT DO 334 J=3,NINTTT TBACK(J)=TIX(NINTTT-J+1) XTIME(J)=TBX(NINTTT-J+1)	
195	334 CALL PLOT(0.0,1.0,-3) CALL SCALE(XTIME,5.00,NINTTT,1) CALL SCALE(TBACK,7.00,NINTTT,1) CALL AXIS(0.0,0.0,19,ELAPSED TIME (SECS),-19.5 0,0.0,XTIME(NINTTT+1 'XTIME(NINTTT+2))	
200	CALL AXIS(0.0,0.0,35,TEMPERATURE OF BACK SURFACE (DEG K),35.7 0, '90.0,TBACK(NINTTT+1),TBACK(NINTTT+2)) CALL LINE(XTIME,TBACK,NINTTT,1,1,1) CALL PLOT(10.0,-1.0,-3)	
205	PRINT 3000 3000 FORMAT('TEMPERATURE OF BACK SURFACE (DEG K) VS TIME (SECS)') PRINT 3005	
210	3005 FORMAT('TIME (SECONDS)*10X,TEMPERATURE (DEGREES KELVIN)') PRINT 3001,(XTIME(J),TBACK(J)),J=1,NINTTT 3001 FORMAT(2E20,10/)	
215	YMELT(1)=0.0 XTIME(1)=STMELT DO 335 J=2,NINTT YMELT(J)=DELY*(J-1) 335 XTIME(J)=TBX(NINTTT-J)	
220	CALL PLOT(0.0,1.0,-3) CALL SCALE(YMELT,5.00,NINTT,1) CALL SCALE(XTIME,7.00,NINTT,1) CALL AXIS(0.0,0.0,36,DISTANCE FROM ORIGINAL SURFACE (CMS), 36.5 0,	

PROGRAM	QUEST	PAGE
	0 0, YMELT(NINTT+1), YMELT(NINTT+2) CALL AXIS(0.0,0.0,19, TIME TO MELT (SECS), -19, 7.00, 90.0, XTIME(NINTT+1), XTIME(NINTT+2)) CALL LINE (YMELT, XTIME, NINTT, 1, +1, 1) CALL PLOT(10.0, -1.0, -3) CALL PLOT(0.0, 1.0, -3) CALL SCALE(XTIME, 5.00, NINTT, 1) CALL SCALE(YMELT, 7.00, NINTT, 1) CALL AXIS(0.0, 0.0, 19, TIME TO MELT (SECS), -19, 5.00, 0.0, XTIME(NINTT+1), XTIME(NINTT+2)) CALL AXIS(0.0, 0.0, 49, DISTANCE OF INTERFACE FROM ORIGINAL SURFACE (CMS), -49, 7.00, 90.0, YMELT(NINTT+1), YMELT(NINTT+2)) CALL LINE(XTIME, YMELT, NINTT, 1, +1, 1) CALL PLOT(10.0, -1.0, -3) PRINT 3002 3002 FORMAT('SOLID-LIQUID INTERFACE POSITION (CMS) VS TIME (SECS):') PRINT 3005 3006 FORMAT(' TIME (SECONDS) * 10X, CMS FROM ORIGINAL SURFACE') PRINT 3001, ((XTIME(J), YMELT(J)), J=1, NINTT) ZVELOX(1)=DELY/(TBX(NINT)-STMELT) XTIME(1)=(TBX(NINT)+STMELT)/2.0 YIN(1)=DELY/2.0 DO 336 J=2, NINT YIN(J)=J*DELY-DELY/2.0 ZVELOX(J)=DELY/(TBX(NINTT-J)-TBX(NINTT+J)) XTIME(J)=(TBX(NINTT-J)+TBX(NINTT+J))/2.0 CALL PLOT(0.0, 1.0, -3) CALL SCALE(XTIME, 5.00, NINT, 1) CALL SCALE(ZVELOX, 7.00, NINT, 1) CALL AXIS(0.0, 0.0, 19, ELAPSED TIME (SECS), -19, 5.0, 0.0, XTIME(NINT+1), XTIME(NINT+2)) CALL AXIS(0.0, 0.0, 44, VELOCITY OF SOLID-LIQUID INTERFACE (CMS/SEC), -44, 7.0, 90.0, ZVELOX(NINT+1), ZVELOX(NINT+2)) CALL LINE(XTIME, ZVELOX, NINT, 1, +1, 1) CALL PLOT(10.0, -1.0, -3) CALL PLOT(0.0, 1.0, -3) CALL SCALE(YIN, 5.00, NINT, 1) CALL SCALE(ZVELOX, 7.00, NINT, 1) CALL AXIS(0.0, 0.0, 36, DISTANCE FROM ORIGINAL SURFACE (CMS), -36, 5.0, 0.0, YIN(NINT+1), YIN(NINT+2)) CALL AXIS(0.0, 0.0, 44, VELOCITY OF SOLID-LIQUID INTERFACE (CMS/SEC), -44, 7.0, 90.0, ZVELOX(NINT+1), ZVELOX(NINT+2)) CALL LINE(YIN, ZVELOX, NINT, 1, +1, 1) CALL PLOT(10.0, -1.0, -3) PRINT 3003 3003 FORMAT('SURFACE RECESSON RATE (CMS/SEC) VS TIME (SECS) AND POSITION OF SOLID-LIQUID INTERFACE') PRINT 3007 3007 FORMAT(5X, 'TIME (SECONDS) * 5X, VELOCITY (CMS/SEC) * 4X, CENTIMETERS') PRINT 3004, ((XTIME(J), ZVELOX(J), YIN(J)), J=1, NINT) 3004 FORMAT(3E20 10//) CALL PLOT END	4
225		
230		
235		
240		
245		
250		
255		
260		
265		
270		

SUBROUTINE ATMOS

CDC 6600 FTH v3.0-320A OPT=1 11/15/72

```

      SUBROUTINE ATMOS(Z,TH,SIGMA,RHO,THETA,DELTA,CA,AMU,K)
      ATMOS001
      C CALLING SEQUENCE
      ATMOS002
      ATMOS003
      5 C CALL ATMOS(Z,TH,SIGMA,RHO,THETA,DELTA,CA,AMU,K)
      ATMOS004
      ATMOS005
      ATMOS006
      C Z = GEOMETRIC ALTITUDE (FT)
      ATMOS007
      C TH = MOLECULAR SCALE TEMPERATURE (DEGREES RANKIN)
      ATMOS008
      C SIGMA = RATIO OF DENSITY TO THAT AT SEA LEVEL
      ATMOS009
      10 C RHO = DENSITY LB-SEC**2-FT**(-4) OR SLUGS-FT**3
      ATMOS010
      C THETA = RATIO OF TEMPERATURE TO THAT AT SEA LEVEL
      ATMOS011
      C DELTA = RATIO OF PRESSURE TO THAT AT SEA LEVEL
      ATMOS012
      C CA = SPEED OF SOUND (FT/SEC)
      ATMOS013
      C AMU = VISCOSITY COEFFICIENT (LB-SEC-FT**2)
      ATMOS014
      15 C K = 1 NORMAL
      ATMOS015
      C = 2 ALTITUDE GREATER THAN 300000. FT..
      ATMOS016
      C = 3 ALTITUDE NEGATIVE.
      ATMOS017
      ATMOS018
      ATMOS019
      20 DIMENSION HPRIMB(11),TMB(11),SIGMAB(11),ALM(11),ARAY(11,4)
      ATMOS020
      EQUIVALENCE (ARAY(1,1),HPRIMB(11),(ARAY(1,2),TMB(11),
      ATMOS021
      (ARAY(1,3),SIGMAB(11),(ARAY(1,4),ALM(11))
      ATMOS022
      ATMOS023
      ATMOS024
      25 DATA ((ARAY(1,J),J=1,4),I=1,11)/
      ATMOS025
      X 0. 518.688 1.000000E 00 -0.00356616
      ATMOS026
      X 36089.239 389.988 2.9706958E-01 0.
      ATMOS027
      X 82020.997 389.988 3.2665751E-02 0.00164592
      ATMOS028
      X 154195.480 508.788 1.2117870E-02 0.
      ATMOS029
      30 X 173804.510 508.788 5.8677311E-04 -0.00246888
      ATMOS030
      X 259186.350 298.188 1.7329156E-05 0.
      ATMOS031
      X 295275.590 298.188 1.7928595E-06 0.00219456
      ATMOS032
      X 344488.190 406.188 9.3921519E-08 0.01097280
      ATMOS033
      X 524934.380 2386.188 7.7658593E-10 0.00548640
      ATMOS034
      35 X 557742.780 566.188 5.6324877E-10 0.00274320
      ATMOS035
      X 656167.980 836.188 2.5726771E-10 0.00192024
      ATMOS036
      DATA 0 / 0.018744176 / RE / 2.0855531E 07 /
      ATMOS037
      X S / 196.72 / PZ / 2116.2 /
      ATMOS038
      40 X AMUZ / 3.712998E-07 / RHOZ / 0.0023769 /
      ATMOS039
      X THZ / 518.688 /
      ATMOS040
      ATMOS041
      K=1
      ATMOS042
      IF(Z)26,18,17
      ATMOS043
      45 26 K=3
      ATMOS044
      GO TO 13
      ATMOS045
      17 IF(Z.GT.300000) K=K+1
      ATMOS046
      18 HPRIM=(RE/(RE+Z))*2
      ATMOS047
      9 DO 10 M=1,11
      ATMOS048
      50 IF(HPRIM-HPRIMB(M))11,12,10
      ATMOS049
      10 CONTINUE
      ATMOS050
      M=12
      ATMOS051
      M=M-1
      ATMOS052
      12 IF(ALM(M))14,15,14
      ATMOS053
      55 14 TM=TMB(M)+ALM(M)*(HPRIM-HPRIMB(M))
      ATMOS054
      SIGMA=EXP((1.0+(Q/ALM(M)))*(ALOG(TMB(M)/TH)))*SIGMAB(M)
      ATMOS055
      GO TO 20
      ATMOS056
      15 TM=TMB(M)
      ATMOS057
      SIGMA=SIGMAB(M)*EXP(-(Q*(HPRIM-HPRIMB(M))/TMB(M))
      ATMOS058
      60 20 RHO=RHOZ*SIGMA
      ATMOS059
      THETA=TH/THZ
      ATMOS060
      DELTA=SIGMA*THETA
      ATMOS061
      CA=49.02177*SQRT(TM)
      ATMOS062
      AMU=AMUZ*SQRT(THETA**3)*((THZ*S)/(TM*S))
      ATMOS063
      65 13 RETURN
      ATMOS064
      END
      ATMOS065
      ATMOS066

```

SUBROUTINE CONDUCT

CDC 6600 FTN V3.0-320A OPT=1 11/15/72

```

SUBROUTINE CONDUCT
COMMENT***TITANIUM***TITANIUM***TITANIUM***TITANIUM***TITANIUM***TITANIUM***
COMMON T(30,35),TT(30,35),DY(30,35),CNDAXL(30,35),CNDROL(30,35),
5 2 TFR(30,35),NA(30),NB(30),NZ(30),NAT(30),NBT(30),TIX(35),TBX(35),
3 ATXFR(30),BTXFR(30),TAU(30),TOCNV(30),TORAD(30),TVANISH(30),O(30)
4 ,OCUT(30),ORAD(30),SUNDY(30),REQ(35),ACOEFF,AENTHLP,AMACH,AVELOX,
5 APRSURE,ARHO,ARN,ATEMP,CPI,CPSLUSH,CPV,DELX,DELY,DTIME,E,HF,HV,I,
6 J,MIDINT,MINT,NINT,NBBI,NXTRA,NZI,PRANDTL,RHO,STMELT,TML,THU,TV,
7 TISTMLT,TIME,VIS,XFROMLE,STOP,DELTIME
10 DIMENSION CND(30,35)
EQUIVALENCE (CND,TFR)
DATA CND,CN1,CN2,CN3,CN4/0.075251,-0.00010874,1.353216E-07,
:-6.294976E-11,1.083052E-14/
NZI=NZ(1)
15 DO 10 I=2,MINT
NZI=MAX0(NZI,NZ(1))
10 DO 20 I=1,MINT
DO 20 J=1,NZI
20 TIT=TT(I,J)
IF(TIT.GE.TMU-E) GO TO 15
CND(I,J)=CND+TIT*(CN1+TIT*(CN2+TIT*(CN3+TIT*CN4)))
GO TO 20
15 CND(I,J)=0.035
20 CONTINUE
25 MINT=MINT-1
DO 40 I=1,MINT
DO 40 J=1,NZI
40 CNDROL(I,J)=2./(1./CND(I,J)+1./CND(I+1,J))
DO 30 I=1,MINT
NZI=NZ(1)-1
30 DO 30 J=1,NZI
30 CNDAXL(I,J)=2./(1./CND(I,J)+1./CND(I,J+1))
RETURN
END

```

SUBROUTINE SPHEAT

CDC 6600 FTN V3 0-320A OPT=1 11/15/72

```

SUBROUTINE SPHEAT (TIT,CPIJ)
COMMENT***TITANIUM***TITANIUM***TITANIUM***TITANIUM***TITANIUM***TITANIUM***
COMMON T(30,35),TT(30,35),DY(30,35),CNDAXL(30,35),CNDROL(30,35),
5 2 TFR(30,35),NA(30),NB(30),NZ(30),NAT(30),NBT(30),TIX(35),TBX(35),
3 ATXFR(30),BTXFR(30),TAU(30),TOCNV(30),TORAD(30),TVANISH(30),O(30)
4 ,OCUT(30),ORAD(30),SUNDY(30),REQ(35),ACOEFF,AENTHLP,AMACH,AVELOX,
5 APRSURE,ARHO,ARN,ATEMP,CPI,CPSLUSH,CPV,DELX,DELY,DTIME,E,HF,HV,I,
6 J,MIDINT,MINT,NINT,NBBI,NXTRA,NZI,PRANDTL,RHO,STMELT,TML,THU,TV,
7 TISTMLT,TIME,VIS,XFROMLE,STOP,DELTIME
10 DATA C0,C1,C2,C3,C4,C5,CPL/7.194207E-02,2.820977E-04,-5.009421E-7,
5.059385E-10,-2.400367E-13,4.327858E-17,0.167/
IF(TIT.GE.TMU-E) GO TO 30
IF(TIT.GE.TML-E) GO TO 20
15 CPIJ=C0+TIT*(C1+TIT*(C2+TIT*(C3+TIT*(C4+TIT*(C5))))
GO TO 100
20 TST=(TMU+TML)/2
CPIJ=C0+TST*(C1+TST*(C2+TST*(C3+TST*(C4+TST*(C5))))+WF*(TMU-TML)
GO TO 100
30 CPIJ=CPL
20 100 CONTINUE
RETURN
END

```

SUBROUTINE COOLIT

CDC 6600 FTN V3.0-320A OPT=1 11/15/72

```

SUBROUTINE COOL IT
COMMON T(30,35),TT(30,35),DY(30,35),CNDAXL(30,35),CNDROL(30,35),
2 TFR(30,35),NA(30),NB(30),NZ(30),NAT(30),NBT(30),TIX(35),TBX(35),
3 ATXFR(30),BTXFR(30),TAU(30),YOCNV(30),TORAD(30),TVANISH(30),O(30)
5 4 ,OOUT(30),ORAD(30),SUNDY(30),REQ(35),ACOEFF,AENTH,P,AMACH,AVELOX,
5 APRSURE,ARHO,ARN,ATEMP,CPI,CPSLUSH,CPV,DELX,DELY,DTIME,E,HF,HV,I,
6 J,MIDINT,MINT,NINT,NBBI,KXTRA,NZI,PRANDTL,RHO,STHMLT,TML,THU,TV,
7 TISTHLT,TIME,VIS,XFROMLE,STOP,DELTIME
DIMENSION HNET(30,35),DOTIME(30)
10 EQUIVALENCE (TFR,HNET),(DOTIME,REQ)
DO 10 I=1,MINT
IF (DOTIME(I).NE.DTIME) GO TO 10
NA(I)=NAT(I)
NB(I)=NBT(I)
15 10 CONTINUE
DO 100 I=1,MINT
NZI=NZ(I)
DO 100 J=1,NZI
50 IF (T(I,J).GE.TT(I,J)) GO TO 100
55 IF (((T(I,J).GE.TMU-E).AND.(TT(I,J).GE.TMU-E)).OR.((T(I,J).LE.TML-
: E).AND.(TT(I,J).LE.TML-E)).OR.((T(I,J).GE.TML-E).AND.(TT(I,J).LE.
: THU-E)).AND.((TT(I,J).GE.TML-E).AND.(TT(I,J).LE.TMU-E))) GOTO 100
IF (T(I,J).LT.TML-E) GO TO 65
60 TTIME=DTIME*(THU-T(I,J))/(TT(I,J)-T(I,J))
25 T(I,J)=THU+TTIME/RHO/CPSLUSH/DELX/DY(I,J)*HNET(I,J)
IF (NB(I).EQ.J-1) NB(I)=J
GO TO 100
65 IF (TT(I,J).GT.TMU-E) GO TO 70
TTIME=DTIME*(TML-T(I,J))/(TT(I,J)-T(I,J))
30 T(I,J)=TML+TTIME/RHO/CPI/DELX/DY(I,J)*HNET(I,J)
IF (NA(I).EQ.J-1) NA(I)=J
GO TO 100
70 TTIME=DTIME*(THU-T(I,J))/(TT(I,J)-T(I,J))
35 T(I,J)=THU+TTIME/RHO/CPSLUSH/DELX/DY(I,J)*HNET(I,J)
IF (NB(I).EQ.J-1) NB(I)=J
IF (T(I,J).GE.TML) GO TO 100
TTIME=TTIME*(TML-T(I,J))/(THU-TML)
40 T(I,J)=TML+TTIME/RHO/CPI/DELX/DY(I,J)*HNET(I,J)
IF (NA(I).EQ.J-1) NA(I)=J
IF (NB(I).EQ.J-1) NB(I)=J
100 CONTINUE
TIME = TIME + DTIME
STOP=STOP+1.0
IF ((STOP.EQ.20.) .OR. (STOP.EQ.30.) .OR. (STOP.EQ.40.) .OR. (STOP.FO.50.
45 : ) .OR. (STOP.EQ.60.) .OR. (STOP.EQ.70.) .OR. (STOP.EQ.80.)) GO TO 105
IF (DTIME.EQ.DELTIME) GO TO 200
105 PRINT 999,TIME,DTIME,(NA(I),I=1,MINT),T(MIDINT,NZ(MIDINT)),
: T(MIDINT,1),(NB(I),I=1,MINT),SUNDY(MIDINT),TAU(MIDINT)
: ,(NZ(I),I=1,MINT)
50 999 FORMAT(13EH .....
: .....
: ...../* TIME=*F15.12,3X,*DTIME=*F15.12,4X,*NA(I)=*2713,
: /* T(MID,FRNT)=*F8.3,3X,*T(MID,BACK)=*F9.3,4X,*NB(I)=*2713,/
: /* THICK=*F14.12,3X,*DRAG=*E16.10,4X,*NZ(I)=*2713)
55 200 CONTINUE
RETURN
END

```


SUBROUTINE FLUXX

CDC 6600 FTM V3.0-320A OPT=1 11/15/72

```

SUBROUTINE FLUXX (FLUX,SIGMA2)
COMMON T(30,35),TT(30,35),DY(30,35),CNDAXL(30,35),CNDROL(30,35),
2 TFR(30,35),NA(30),NB(30),NZ(30),NAT(30),NBT(30),TIX(35),TBX(35),
3 ATXFR(30),BTXFR(30),TAU(30),TOCNV(30),TORAD(30),TVANISH(30),Q(30)
4 QOUT(30),ORAD(30),SUNDY(30),REQ(35),ACOEFF,AENTHLP,AMACH,AVELOX,
5 APRSURE,ARHO,ARN,ATEMP,CPI,CPSLUSH,CPV,DELX,DELY,OTIME,E,HF,HV,I,
6 J,MIDINT,MINT,NINT,NBB1,NXTRA,NZ1,PRANDTL,RHO,STHELT,TML,THU,TV,
7 TISTMLT,TIME,VIS,XFROMLE,STOP,DELTIME
10 Q0=2.*FLUX/(3.1415926536*SIGMA2**2)
MIDIN=MIDINT-1
5 DO 10 I=1,MIDIN
R=DELX*(MIDINT-I)
Q(I)=Q0*EXP(-2.0*(R/SIGMA2)**2)
Q(MINT-I-1)=Q(I)
15 CONTINUE
10 Q(MIDINT)=Q0*EXP(-2.0*(DELX/4.0/SIGMA2)**2)
RETURN
END

```

SUBROUTINE FRCION

CDC 6600 FTM V3.0-320A OPT=1 11/15/72

```

SUBROUTINE FRCION
COMMON T(30,35),TT(30,35),DY(30,35),CNDAXL(30,35),CNDROL(30,35),
2 TFR(30,35),NA(30),NB(30),NZ(30),NAT(30),NBT(30),TIX(35),TBX(35),
3 ATXFR(30),BTXFR(30),TAU(30),TOCNV(30),TORAD(30),TVANISH(30),Q(30)
4 QOUT(30),ORAD(30),SUNDY(30),REQ(35),ACOEFF,AENTHLP,AMACH,AVELOX,
5 APRSURE,ARHO,ARN,ATEMP,CPI,CPSLUSH,CPV,DELX,DELY,OTIME,E,HF,HV,I,
6 J,MIDINT,MINT,NINT,NBB1,NXTRA,NZ1,PRANDTL,RHO,STHELT,TML,THU,TV,
7 TISTMLT,TIME,VIS,XFROMLE,STOP,DELTIME
10 DATA E0,E1,E2,E3/1.036064E-02,9.395396E-01,3.243420E-02,-9.91742E
2 -04,E1N0,E1N1,E1N2,E1N3/2.710550E-02,1.012903,-2.010911E-02,
3 5.602829E-04,/,A0,A1,A2,A3/0.979006,0.00651928,0.0158536,
4 -0.00155636/,B0,B1,B2,B3/0.0306331,1.07642,-0.113979,0.00679309/,
5 CPBASE,VISBASE,CNDBASE,HBASE/0.2395,0.000255236,5.68218632E-05
6 ,66.377778/
15 DO 100 I=1,MINT
IF(AVELOX.GT.0.) GO TO 5
TAU(I)=0.0
GO TO 100
5 TIW=T(I,NZ(I))*C.0036
WH=E0+TIW*(E1+TIW*(E2+TIW*E3))
20 RFCTR=SQRT(PRANDTL)
RH=0.5*(AENTHLP*WH)+0.22*RFCTR*ACOEFF*AENTHLP
10 RT=E1N0*RH*(E1N1*RH*(E1N2*RH*E1N3))
PRANDTL=(VISBASE*SQRT(5.*(RT/9.)*CPBASE*(A0+RT*(A1+RT*(A2+RT*A3))))/
25 :CNDBASE/(B0+RT*(B1+RT*(B2+RT*B3))))
RFCTR=SQRT(PRANDTL)
IF(ARN.GT.400000.) GO TO 25
15 RH=0.5*(AENTHLP*WH)+0.22*RFCTR*ACOEFF*AENTHLP
RT=E1N0*RH*(E1N1*RH*(E1N2*RH*E1N3))
30 RTEMP=RT*500.
RNU=VISBASE*SQRT(RTEMP/900.0)
RDENSTY=APRSURE/RTEMP/53.35
RN=RDENSTY*AVELOX*XFROMLE/RNU
CFX=0.664/SQRT(RN)
35 GO TO 50
25 RFCTR=RFCTR*0.6667
RH=0.5*(AENTHLP*WH)+0.22*RFCTR*ACOEFF*AENTHLP
10 RT=E1N0*RH*(E1N1*RH*(E1N2*RH*E1N3))
RTEMP=RT*500.
40 RNU=VISBASE*SQRT(RTEMP/900.0)
RDENSTY=APRSURE/RTEMP/53.35
RN=RDENSTY*AVELOX*XFROMLE/RNU
CFX=0.370/((ALOG10(RN))**2.584)
50 TAU(I)=7.440837*ARHO*AVELOX**2*CFX
45 RCVRYH=AENTHLP*HBASE*RFCTR*0.0001110035*AVELOX**2
COMMENT QOUT IS IN CAL/SEC/CM**2
QOUT(I)=0.24412176*CFX/PRANDTL*0.6667*RDENSTY*AVELOX*(RCVRYH*
50 WH*HBASE)
CONTINUE
RETURN
END

```

SUBROUTINE FREEZE

CDC 6600 FTM V3.0-320A OPT=1 11/15/72

```

SUBROUTINE FREEZE
COMMON T(30,35),TT(30,35),DY(30,35),CM,AXL(30,35),CNDROL(30,35),
2 TFR(30,35),NA(30),NB(30),NZ(30),NAT(30),NBT(30),TIX(35),TBX(35),
3 ATXFR(30),BTXFR(30),TAU(30),TOCNV(30),TORAD(30),TVANISH(30),Q(30)
4 OOUT(30),ORAD(30),SUNDY(30),REG(35),ACOFF, AENTHP, AMACH, AVELOX,
5 APPSURE, AR'D, ARN, ATEMP, CP1, CPSLUSH, CPV, DELX, DELY, DTIME, E, HF, HV, I,
6 J, MIDINT, MINT, NINT, NBB1, NXTRA, NZ1, PRANOTL, RHO, STHELT, TML, TMU, TV,
7 TISTMLT, TIME, VIS, XEROMLE, STOP, DELTIME
IF(AVELOX.EQ.0.0) GO TO 22
10 NZ1=NZ(1)
CALL SPHEAT((TML+T(1,NZ1-1))/2.0,CPL)
CALL SPHEAT((T(1,NZ1)+TMU)/2.,CP2)
IF(T(1,NZ1-1).GE.TML-E) GO TO 10
IF((TML-T(1,NZ1-1))*CPL*DY(1,NZ1-1).LT.(TMU-TML)*CPSLUSH*(T(1,NZ1
15 :)-TMU)*CP2)*DY(1,NZ1)) GO TO 8
T(1,NZ1-1)=T(1,NZ1-1)+((TML-T(1,NZ1-1))*CPL+(TMU-TML)*CPSLUSH*(T(1
:)-TMU)*CP2)*DY(1,NZ1)/((DY(1,NZ1-1)+DY(1,NZ1))*CPL)
GO TO 20
8 T(1,NZ1-1)=TML+((TMU-TML)*CPSLUSH*(T(1,NZ1)-TMU)*CP2)*DY(1,NZ1)-
:TML-T(1,NZ1-1))*CPL*DY(1,NZ1-1)/((DY(1,NZ1)+DY(1,NZ1-1))*CPSLUSH)
NA(1)=NA(1)-1
IF(T(1,NZ1-1).GT.TMU) GO TO 9
GO TO 20
25 9 T(1,NZ1-1)=TMU*(T(1,NZ1-1)-TMU)*CPSLUSH/CP2
IF(1.EQ.MIDINT) TIX(NB(1))=T(1,1)
IF(1.EQ.MIDINT) TBX(NB(1))=TIME+DTIME
NB(1)=NB(1)-1
GO TO 20
30 10 IF((TMU-T(1,NZ1-1))*CPSLUSH*DY(1,NZ1-1).LT.(T(1,NZ1)-TMU)*CP2*
: DY(1,NZ1)) GO TO 12
T(1,NZ1-1)=T(1,NZ1-1)+((TMU-T(1,NZ1-1))*CPSLUSH*(T(1,NZ1)-TMU)*
: CP2)*DY(1,NZ1)/((DY(1,NZ1-1)+DY(1,NZ1))*CPSLUSH)
GO TO 20
35 12 T(1,NZ1-1)=TMU+((T(1,NZ1)-TMU)*CP2*DY(1,NZ1)-(TMU-T(1,NZ1-1))*
: CPSLUSH*DY(1,NZ1-1))/((DY(1,NZ1)+DY(1,NZ1-1))*CP2
IF(1.EQ.MIDINT) TIX(NB(1))=T(1,1)
IF(1.EQ.MIDINT) TBX(NB(1))=TIME+DTIME
NB(1)=NB(1)-1
40 20 DY(1,NZ1-1)=DY(1,NZ1-1)+DY(1,NZ1)
DY(1,NZ1)=0.0
T(1,NZ1)=0.0
NZ(1)=NZ(1)-1
21 IF(DY(1,NZ(1)).LE.(1.5*DELY)) GO TO 22
DY(1,NZ(1)+1)+DY(1,NZ(1))-DELY
45 T(1,NZ(1)+1)=T(1,NZ(1))
DY(1,NZ(1))-DELY
IF(T(1,NZ(1)).LT.TML) NA(1)=NA(1)+1
IF(T(1,NZ(1)).LT.TMU) NB(1)=NB(1)+1
NZ(1)=NZ(1)+1
50 GO TO 21
22 CONTINUE
RETURN
END

```

SUBROUTINE SCHMIDT

COC 6600 FTH V3.0-320A OPT-1 11/15/72

```

SUBROUTINE SCHMIDT
COMMON T(30,35),TT(30,35),DY(30,35),CNDAXL(30,35),CNDROL(30,35),
2 TFR(30,35),NA(30),NB(30),NZ(30),NAT(30),NBT(30),TIX(35),TBK(35),
3 ATXFR(30),BTXFR(30),TAU(30),TOCNV(30),TORAD(30),TVANISH(30),Q(30)
4 ,QOUT(30),ORAD(30),SUNDY(30),REQ(35),ACOEFF,AENTHLP,AMACH,AVELOR,
5 APPSRE,ARHO,ARN,ATEMP,CPI,CPBLUSH,CPV,DELX,DELY,DTIME,E,HF,HV,I,
6 J,MIDINT,MINT,NINT,NBT,NKTRA,NZI,PRANDTL,RHO,STHFLT,TML,THU,TV,
7 TISTMLT,TIME,VIS,XFRACK,STOP,DELTINE
10 DIMENSION HNET(30,35)
EQUIVALENCE (TFR,HNET)
DATA STEFAN/1.355061E-12/
CALL CONDUCT
DO 100 I=1,MINT
  NZI=NZ(I)
15 DO 100 J=1,NZI
  CALL SPHEAT(TT(I,J),CPIJ)
  IF(I.NE.1) GO TO 5
  HXFR=0.0
  GO TO 10
20 5 HXFR=CNDROL(I-1,J)/DELX*AMINI(DY(I,J),DY(I-1,J))*(TT(I-1,J)-TT(I,
  :J))
  10 IF(I.NE.MINT) GO TO 15
  HXFR=0.0
  GO TO 20
25 15 HXFR=CNDROL(I,J)/DELX*AMINI(DY(I,J),DY(I+1,J))*(TT(I+1,J)-TT(I,J)
  :J)
  20 IF(J.NE.1) GO TO 25
  HXFR=0.0
  GO TO 30
30 25 HXFR=CNDAXL(I,J-1)/DELY*DELX*(TT(I,J-1)-TT(I,J))
  30 IF(J.NE.NZI) GO TO 35
  IF(TT(I,J).GE.950.0) GO TO 32
  ORAD(I)=TT(I,J)**4*STEFAN*(0.08+0.0001818182*TT(I,J))
  GO TO 33
35 32 ORAD(I)=TT(I,J)**4*STEFAN*(0.20+0.0000117647*TT(I,J))
  33 HX*RT=(Q(I)+QOUT(I)-ORAD(I))*DELX
  GO TO 40
35 HXFR=CNDAXL(I,J)/DELY*DELX*(TT(I,J+1)-TT(I,J))
  COMMENT****TO MAKE MODEL ONE DIMENSIONAL, ELIMINATE HXFR = HXFR IN NEXT CARD
40 HNET(I,J)=HXFR+HXFR+HXFR+HXFR
  T(I,J)=TT(I,J)+DTIME/RHO/CPIJ/DY(I,J)/DELX*HNET(I,J)
  IF(J.EQ.NA(I)) ATXFR(I)=RHO*CPIJ*DY(I,J)*DELX/HNET(I,J)
  IF(J.EQ.NB(I)) BTXFR(I)=RHO*CPIJ*DY(I,J)*DELX/HNET(I,J)
100 CONTINUE
RETURN
END

```

SUBROUTINE VISCSTY

COC 6600 FTH V3.0-320A OPT-1 11/15/72

```

SUBROUTINE VISCSTY (TX)
COMMENT***TITANIUM***TITANIUM***TITANIUM***TITANIUM***TITANIUM***TITANIUM***
COMMON T(30,35),TT(30,35),DY(30,35),CNDAXL(30,35),CNDROL(30,35),
2 TFR(30,35),NA(30),NB(30),NZ(30),NAT(30),NBT(30),TIX(35),TBK(35),
3 ATXFR(30),BTXFR(30),TAU(30),TOCNV(30),TORAD(30),TVANISH(30),Q(30)
4 ,QOUT(30),ORAD(30),SUNDY(30),REQ(35),ACOEFF,AENTHLP,AMACH,AVELOR,
5 APPSRE,ARHO,ARN,ATEMP,CPI,CPBLUSH,CPV,DELX,DELY,DTIME,E,HF,HV,I,
6 J,MIDINT,MINT,NINT,NBT,NKTRA,NZI,PRANDTL,RHO,STHFLT,TML,THU,TV,
7 TISTMLT,TIME,VIS,XFRACK,STOP,DELTINE
10 DATA B10/1.E300/
  IF(TX.GE.THU-E) GO TO 10
  VIS=B10
  GO TO 100
15 10 VIS=0.06*EXP((1915.0-TX)/125.0)+0.005
  100 CONTINUE
RETURN
END

```

SUBROUTINE SQUEEZE

CDC 6600 FTN V3.0-320A OPT=1 11/15/72

```

SUBROUTINE SQUEEZE
COMMON T(30,35),TT(30,35),DY(30,35),CNDAXL(30,35),CNDROL(30,35),
2 TFR(30,35),NA(30),NB(30),NZ(30),NAT(30),NBT(30),TIX(35),TBX(35),
3 ATXFR(30),BTXFR(30),TAU(30),TCNV(30),TORAD(30),TVANISH(30),Q(30)
4 ,GOUT(30),ORAD(30),SMDY(30),REQ(35),ACOEFF,AENTHP,AMACH,AVELOX,
5 APPSURE,ARHO,ARN,ATEMP,CP1,CPSLUSH,CPV,DELX,DELY,DTIME,E,HF,HV,I,
6 J,MIDINT,MINT,NINT,NBBI,NXTRA,NZI,PRANDTL,RHO,STMLT,TML,THU,TV,
7 T1STMLT,TIME,VIS,XFROMLE,STOP,DELTIME
IF(AVELOX.EQ.0.0) GO TO 300
10 DO 200 I=1,MINT
    NBBI=NB(I)+1
    NZI=NZ(I)
    IF(NZI.LT.NBBI) GO TO 200
    NBPLUS2=NB(I)+2
15    NZI=NZ(I)-1
    SMDYLO=0.
    DO 1 J=NBBI,NZI
        SMDYLO=SMDYLO+DY(I,J)
20    IF(DY(I,NB(I))+SMDYLO.GT.1.5*DELY) GO TO 5
    C14 J=NBPLUS2,NZI
    T(I,NBBI)=(DY(I,NBBI)+T(I,NBBI)+DY(I,J)+T(I,J))/(DY(I,NBBI)+DY(I,J)
    : )
    DY(I,NBBI)=DY(I,NBBI)+DY(I,J)
    T(I,J)=0.0
25    4 DY(I,J)=0.0
    NZI=NBBI
    NZI=NBBI
    CALL FREEZE
    IF(DY(I,NZ(I)).GT.1.5*DELY) GO TO 140
    GO TO 200
30    5 IF(DY(I,NB(I))-DELY) 3,15,10
10    T(I,NBPLUS2)=(T(I,NBBI)+DY(I,NBBI)+T(I,NBPLUS2)+DY(I,NBPLUS2))/
    : (DY(I,NBBI)+DY(I,NBPLUS2))
    DY(I,NBPLUS2)=DY(I,NBBI)+DY(I,NBPLUS2)
35    T(I,NBBI)=T(I,NB(I))
    DY(I,NBBI)=DY(I,NB(I))-DELY
    DY(I,NB(I))=DELY
    NB(I)=NB(I)+1
    NBBI=NB(I)+1
40    NBPLUS2=NBPLUS2+1
    IF(T(I,NB(I)).LT.TML-E) NAT(I)=NAT(I)+1
    GO TO 3
15    DO 70 J=NBBI,NZI
        REQ(J)=DELY-DY(I,J)
45    IF(REQ(J)) 20,70,40
20    IF(J.EQ.NZ(I)) GO TO 70
    T(I,J+1)=THU+(DY(I,J+1)+(T(I,J+1)-THU)-REQ(J)+(T(I,J)-THU))/(DY(I,
    : J+1)-REQ(J))
    DY(I,J+1)=DY(I,J+1)-REQ(J)
50    DY(I,J)=DELY
    GO TO 70
40    JJ=J+1
    DO 60 K=JJ,NZI
        IF(DY(I,K).EQ.0.) GO TO 60
55    IF(DY(I,K).LT.REQ(J)) GO TO 50

```

SUBROUTINE SQUEEZE

PAGE 2

```

      DY(I,K)=DY(I,K)-REQ(J)
      T(I,J)=TMU*(DY(I,J)*(T(I,J)-TMU)+REQ(J)*(T(I,K)-TMU))/DELY
      DY(I,J)=DELY
      GO TO 70
60      50  T(I,J)=TMU*(DY(I,J)*(T(I,J)-TMU)+DY(I,K)*(T(I,K)-TMU))/(DY(I,J)+
      : DY(I,K))
      DY(I,J)=DY(I,J)+DY(I,K)
      DY(I,K)=0.0
      REQ(J)=DELY-DY(I,J)
65      60  CONTINUE
      70  CONTINUE
      DO 80 J=NB1,NZ1
      IF(DY(I,J).GT.0.) GO TO 80
      NZ1=J-1
70      IN=J
      GO TO 85
      80  CONTINUE
      GO TO 100
      85  DO 90 J=N,NZ1
75      90  T(I,J)=0.0
      100 IF(DY(I,NZ1).LT.0.5*DELY) GO TO 120
      IF(DY(I,NZ1).GT.1.5*DELY) GO TO 140
      GO TO 200
      120 IF(T(I,NZ1-1).GE.TMU-E) GO TO 125
80      CALL FREEZE
      GO TO 200
      125 T(I,NZ1-1)=TMU*(DELY*(T(I,NZ1-1)-TMU)+DY(I,NZ1)*(T(I,NZ1)-
      : TMU))/(DELY+DY(I,NZ1))
      DY(I,NZ1-1)=DELY+DY(I,NZ1)
85      DY(I,NZ1)=0.0
      T(I,NZ1)=0.0
      NZ1=NZ1-1
      GO TO 200
      140 NEXCESS=DY(I,NZ1)/DELY
90      IF(DY(I,NZ1)-NEXCESS*DELY.LE.0.5*DELY) NEXCESS=NEXCESS-1
      NZX=NZ1+NEXCESS
      NZ1=NZ1+1
      DO 130 K=NZ1,NZX
95      130 T(I,K)=T(I,NZ1)
      DY(I,NZX)=DY(I,NZ1)-DELY*NEXCESS
      DY(I,NZ1)=DELY
      NZ1=NZX
      200 CONTINUE
100      300 CONTINUE
      RETURN
      END

```

SUBROUTINE TRANSFRX

CDC 6600 FTM V3.0-320A OPT=1 11/15/72 11

```

SUBROUTINE TRANSFRX
COMMON T(30,35),YT(30,35),DY(30,35),CHDAXL(30,35),CHORDL(30,35),
2 TFR(30,35),NA(30),NB(30),NZ(30),NAT(30),NBT(30),TIX(35),TBX(35),
3 ATXFR(30),BTXFR(30),TAU(30),TODW(30),TORAD(30),TVANISH(30),Q(30),
4 QOUT(30),ORAD(30),SUNDY(30),REQ(35),ACOEFF,AENTHLP,AMACH,AVELCX,
5 APSURE,ARNO,ARN,ATEMP,CPI,CPSLUSH,CPV,DELX,DELY,DTIME,E,HF,HV,I,
6 J,MIDINT,MINT,MINT,NBB,NXTRA,NZI,PRANDL,RNO,STHET,TML,THU,TV,
7 TISTHET,TIME,VIS,XFROMLE,STOP,DELTIME
IF(AVELOX.EQ.0.0) GO TO 300
5 CONTINUE
DO 10 I=1,MINT
DO 10 J=1,NXTRA
10 TFR(I,J)=0.0
DO 30 I=1,MINT
15 NBB1=NB(I)+1
NZ1=NZ(I)
IF(NZ1.LT.NBB1) GO TO 30
VISY=0.0
DO 25 J=NBB1,NZ1
20 CALL VISCSTY(T(I,J))
VISY=VISY+DY(I,J)/VIS
16 TFRX=TAU(I)*DTIME*(VISY-0.5*DY(I,J)/VIS)
IF(TFRX.LT.DELX) GO TO 20
KSHIFT=TFRX/DELX
SHIFT2=(TFRX-KSHIFT*DELX)/DELX
25 SHIFT1=1.0-SHIFT2
IF(KSHIFT.EQ.1) GO TO 18
DY(I-KSHIFT+1,NZ(I-KSHIFT+1)+1)=DY(I,J)*SHIFT1
TFR(I-KSHIFT+1,NZ(I-KSHIFT+1)+1)=DY(I,J)*SHIFT1
30 T(I-KSHIFT+1,NZ(I-KSHIFT+1)+1)=T(I,J)
DY(I-KSHIFT,NZ(I-KSHIFT)+1)=DY(I,J)*SHIFT2
TFR(I-KSHIFT,NZ(I-KSHIFT)+1)=DY(I,J)*SHIFT2
T(I-KSHIFT,NZ(I-KSHIFT)+1)=T(I,J)
DY(I,J)=0.0
35 T(I,J)=0.0
NZ(I)=NZ(I)-1
NZ(I-KSHIFT)=NZ(I-KSHIFT)+1
NZ(I-KSHIFT+1)=NZ(I-KSHIFT)+1
GO TO 25
40 DY(I-1,NZ(I-1)+1)=SHIFT2*DY(I,J)
TFR(I-1,NZ(I-1)+1)=SHIFT2*DY(I,J)
T(I-1,NZ(I-1)+1)=T(I,J)
TFR(I,J)=SHIFT1*DY(I,J)
45 DY(I,J)=SHIFT1*DY(I,J)
NZ(I-1)=NZ(I-1)+1
GO TO 25
20 TFR(I,J)=TFRX/DELX*DY(I,J)
25 CONTINUE
30 CONTINUE
50 MINT=MINT-1
DO 60 I=1,MINT
N1LOD=NB(I)+1
N2LOD=NB(I)+NZ(I+1)-NB(I+1)
55 IF(NZ(I).LT.N1LOD).AND.(N2LOD.EQ.NB(I+1)) GO TO 60
IF(NZ(I).LT.N2LOD) NZ(I)=N2LOD
NZ1=NZ(I)
DO 50 J=N1LOD,NZ1
JJ=J-NB(I)+NB(I+1)
60 DENOM=DY(I,J)-TFR(I,J)+TFR(I+1,JJ)
IF(DENOM.NE.0.0) GO TO 40
T(I,J)=0.0
NZ(I)=NZ(I)-1
GO TO 50
40 T(I,J)=((DY(I,J)-TFR(I,J))+T(I,J)+TFR(I+1,JJ)+T(I+1,JJ))/DENOM
50 DY(I,J)=DENOM
60 CONTINUE
N1LOD=NB(MINT)+1
NZ1=NZ(MINT)
70 DO 70 J=N1LOD,NZ1
DY(MINT,J)=DY(MINT,J)-TFR(MINT,J)
300 CONTINUE
RETURN
END

```

SUBROUTINE VAPORIZ

CDC 6600 FTM V3 0-320A OPT=1 11/15/72

```

SUBROUTINE VAPORIZ
COMMON T(30,35),TY(30,35),DY(30,35),CNDAXL(30,35),CNDROL(30,35),
2 TFR(30,35),NA(30),NB(30),NZ(30),NAT(30),NBT(30),TIX(35),TBX(35),
3 ATXFR(30),BTXFR(30),TAU(30),TOCNV(30),TORAD(30),TVANISH(30),Q(30)
4 ,QOUT(30),ORAD(30),SUNDY(30),REQ(35),ACOEFF,AENTHLP,AMACH,AVELOX,
5 APPSURE,ARHO,ARN,ATEMP,CPI,CPSLUSH,CPV,DELX,DELY,DTIME,E,HF,HV,I,
6 J,MIDINT,MINT,NINT,NBT,NKTRA,NZI,PRANDTL,RHO,STHFLT,TML,THU,TV,
7 TISTML,TIME,VIS,XFRONLC,STOP,DELTIME
5 DO 100 I=1,MINT
10 IF(T(I),NZ(I)) LE TV) GO TO 100
VANISH=(T(I),NZ(I))-TV)*CPV*DY(I),NZ(I))/HV
IF(VANISH-DY(I),NZ(I)) LE 0.20,30
10 DY(I),NZ(I)=DY(I),NZ(I)-VANISH
T(I),NZ(I)=TV
15 TVANISH(I)=TVANISH(I)+VANISH
GO TO 100
20 DY(I),NZ(I)=0.0
T(I),NZ(I)=0.0
NZ(I)=NZ(I)-1
20 TVANISH(I)=TVANISH(I)+VANISH
GO TO 100
30 VANISH=VANISH-DY(I),NZ(I)
TVANISH(I)=TVANISH(I)+DY(I),NZ(I)
DY(I),NZ(I)=0.0
25 T(I),NZ(I)=0.0
NZ(I)=NZ(I)-1
T(I),NZ(I)=T(I),NZ(I)+VANISH*HV/CPV/DELY
GO TO 5
100 CONTINUE
30 RETURN
END

```

SUBROUTINE XACTIME

CDC 6600 FTM V3 0-320A OPT=1 11/15/72

```

SUBROUTINE XACTIME
COMMON T(30,35),TY(30,35),DY(30,35),CNDAXL(30,35),CNDROL(30,35),
2 TFR(30,35),NA(30),NB(30),NZ(30),NAT(30),NBT(30),TIX(35),TBX(35),
3 ATXFR(30),BTXFR(30),TAU(30),TOCNV(30),TORAD(30),TVANISH(30),Q(30)
4 ,QOUT(30),ORAD(30),SUNDY(30),REQ(35),ACOEFF,AENTHLP,AMACH,AVELOX,
5 APPSURE,ARHO,ARN,ATEMP,CPI,CPSLUSH,CPV,DELX,DELY,DTIME,E,HF,HV,I,
6 J,MIDINT,MINT,NINT,NBT,NKTRA,NZI,PRANDTL,RHO,STHFLT,TML,THU,TV,
7 TISTML,TIME,VIS,XFRONLC,STOP,DELTIME
9 DIMENSION DDTIME(30)
EQUIVALENCE (DDTIME,REQ)
10 DO 50 I=1,MINT
5 DDTIME(I)=DTIME+E
DTIME=DTIME+E
15 DTIMB=DTIME+E
NAT(I)=NAT(I)
NBT(I)=NBT(I)
10 IF(NAT(I) LE 0) GO TO 15
IF(T(I),NA(I)) GE TML-E) DTIMA=(TML-TT(I),NA(I))*ATXFR(I)
15 IF(T(I),NB(I)) GE THU-E) DTIMB=(THU-TT(I),NB(I))*BTXFR(I)
20 IF(DTIMA GT DTIMB OR DTIMA GT DTIME) GO TO 25
DDTIME(I)=DTIMA
NAT(I)=NAT(I)-1
IF(I EQ MIDINT OR NAT(I) LE NINT) GO TO 25
25 TISTML=TIME+DTIMB
STHFLT=TIME+DTIMA
IF(DTIMB GT DTIMA OR DTIMB GT DTIME) GO TO 50
DDTIME(I)=DTIMB
IF(I EQ MIDINT) TBX(NBT(I))=TIME+DDTIME(I)
IF(I EQ MIDINT) TIX(NBT(I))=TIX(I)
30 NBT(I)=NBT(I)-1
50 CONTINUE
DDTIME=DDTIME(I)
DO 60 I=2,MINT
60 DDTIME=AMINT(DDTIME,DDTIME(I))
IF(DDTIME GE DTIME) GO TO 80
DTIME=DDTIME
CALL XCHART
80 RETURN
END

```

[illegible]

TITANIUM	.1000000	CENTIMETERS THICK
TOTAL BEAM POWER=	15.0	KILOWATTS
BEAM RADIUS (2 SIGMA)=	1.79412	CM
AXIAL RADIUS OF CURVATURE=	1.79412	CM
AXIAL DIMENSION OF ELEMENTS=	.200000	CM
AXIAL DIMENSION OF ELEMENTS=	.005557	CM

DEYNOLDS NUMBER= 1775150:
 ALTITUDE= 0. FEET
 MACH NUMBER= .500
 DISTANCE FROM LEADING EDGE=

INITIAL TEMPERATURE =	300.00	DEGREES KELVIN
MELTING POINT =	1588.00	DEGREES KELVIN
BOILING POINT =	3550.00	DEGREES KELVIN

HEAT OF FUSION*	93.946 CALORIES(GM)/GRAM
HEAT OF VAPORIZATION*	560 CALORIES(GM)/GRAM

SPECIFIC HEAT	1	INITIAL T.	123.308	CALORIES/GRAM/DEG K
SPECIFIC HEAT	1	T MELT	221.080	CALORIES/GRAM/DEG K
SPECIFIC HEAT	1	T LIQUID	7.446459	CALORIES/GRAM/DEG K
SPECIFIC HEAT	1	T SLOSH	167.600	CALORIES/GRAM/DEG K

MAXIMUM CONDUCTIVITY= 070000 CALORIES/SEC/CM/DEG K

361	335	459	555	690	995	319	1564	1747	8776	952	1975	1976	1998	1979	1975	1952	647	1611	1347	1086	873	692	555	459	353	361
362	395	459	555	700	1001	324	1567	1749	8777	953	1975	1981	2000	2016	1976	1953	648	1612	1349	1087	874	693	559	459	353	362
363	396	460	556	707	1035	323	1573	1753	8800	954	1975	2025	2111	2072	1976	1954	651	1616	1352	1099	878	694	559	459	356	362
364	396	460	556	710	1051	347	1582	1758	8809	956	1975	2089	2185	2157	1978	1957	656	1621	1356	1103	878	698	559	460	356	362
365	397	461	561	725	1095	368	1608	1775	8894	959	1978	2160	2264	2212	2026	1960	662	1628	1362	1107	882	698	560	461	357	362
366	400	462	563	740	1134	414	1625	1785	902	966	2052	0	0	2079	1963	670	1637	1378	1120	886	700	560	461	357	362	366
367	400	462	563	740	1134	414	1625	1785	902	966	2052	0	0	2146	1963	670	1637	1378	1120	886	700	562	463	358	362	367
368	404	465	568	781	1179	444	1644	1799	910	971	2114	0	0	0	1972	689	1640	1400	1137	904	712	567	464	359	363	368
369	406	467	572	833	1266	513	1689	1828	959	982	2249	0	0	0	0	1972	689	1640	1400	1137	904	712	567	464	359	363
370	407	469	576	889	1347	551	1713	1844	1940	2027	0	0	0	0	0	2017	913	1589	1413	1147	911	723	574	469	401	364
371	407	469	576	889	1347	551	1713	1844	1940	2027	0	0	0	0	0	2017	913	1589	1413	1147	911	723	574	469	401	364
372	407	469	576	889	1347	551	1713	1844	1940	2027	0	0	0	0	0	2017	913	1589	1413	1147	911	723	574	469	401	364
373	407	469	576	889	1347	551	1713	1844	1940	2027	0	0	0	0	0	2017	913	1589	1413	1147	911	723	574	469	401	364
374	407	469	576	889	1347	551	1713	1844	1940	2027	0	0	0	0	0	2017	913	1589	1413	1147	911	723	574	469	401	364
375	407	469	576	889	1347	551	1713	1844	1940	2027	0	0	0	0	0	2017	913	1589	1413	1147	911	723	574	469	401	364
376	407	469	576	889	1347	551	1713	1844	1940	2027	0	0	0	0	0	2017	913	1589	1413	1147	911	723	574	469	401	364
377	407	469	576	889	1347	551	1713	1844	1940	2027	0	0	0	0	0	2017	913	1589	1413	1147	911	723	574	469	401	364
378	407	469	576	889	1347	551	1713	1844	1940	2027	0	0	0	0	0	2017	913	1589	1413	1147	911	723	574	469	401	364
379	407	469	576	889	1347	551	1713	1844	1940	2027	0	0	0	0	0	2017	913	1589	1413	1147	911	723	574	469	401	364
380	407	469	576	889	1347	551	1713	1844	1940	2027	0	0	0	0	0	2017	913	1589	1413	1147	911	723	574	469	401	364
381	407	469	576	889	1347	551	1713	1844	1940	2027	0	0	0	0	0	2017	913	1589	1413	1147	911	723	574	469	401	364
382	407	469	576	889	1347	551	1713	1844	1940	2027	0	0	0	0	0	2017	913	1589	1413	1147	911	723	574	469	401	364
383	407	469	576	889	1347	551	1713	1844	1940	2027	0	0	0	0	0	2017	913	1589	1413	1147	911	723	574	469	401	364
384	407	469	576	889	1347	551	1713	1844	1940	2027	0	0	0	0	0	2017	913	1589	1413	1147	911	723	574	469	401	364
385	407	469	576	889	1347	551	1713	1844	1940	2027	0	0	0	0	0	2017	913	1589	1413	1147	911	723	574	469	401	364
386	407	469	576	889	1347	551	1713	1844	1940	2027	0	0	0	0	0	2017	913	1589	1413	1147	911	723	574	469	401	364
387	407	469	576	889	1347	551	1713	1844	1940	2027	0	0	0	0	0	2017	913	1589	1413	1147	911	723	574	469	401	364
388	407	469	576	889	1347	551	1713	1844	1940	2027	0	0	0	0	0	2017	913	1589	1413	1147	911	723	574	469	401	364
389	407	469	576	889	1347	551	1713	1844	1940	2027	0	0	0	0	0	2017	913	1589	1413	1147	911	723	574	469	401	364
390	407	469	576	889	1347	551	1713	1844	1940	2027	0	0	0	0	0	2017	913	1589	1413	1147	911	723	574	469	401	364
391	407	469	576	889	1347	551	1713	1844	1940	2027	0	0	0	0	0	2017	913	1589	1413	1147	911	723	574	469	401	364
392	407	469	576	889	1347	551	1713	1844	1940	2027	0	0	0	0	0	2017	913	1589	1413	1147	911	723	574	469	401	364
393	407	469	576	889	1347	551	1713	1844	1940	2027	0	0	0	0	0	2017	913	1589	1413	1147	911	723	574	469	401	364
394	407	469	576	889	1347	551	1713	1844	1940	2027	0	0	0	0	0	2017	913	1589	1413	1147	911	723	574	469	401	364
395	407	469	576	889	1347	551	1713	1844	1940	2027	0	0	0	0	0	2017	913	1589	1413	1147	911	723	574	469	401	364
396	407	469	576	889	1347	551	1713	1844	1940	2027	0	0	0	0	0	2017	913	1589	1413	1147	911	723	574	469	401	364
397	407	469	576	889	1347	551	1713	1844	1940	2027	0	0	0	0	0	2017	913	1589	1413	1147	911	723	574	469	401	364
398	407	469	576	889	1347	551	1713	1844	1940	2027	0	0	0	0	0	2017	913	1589	1413	1147	911	723	574	469	401	364
399	407	469	576	889	1347	551	1713	1844	1940	2027	0	0	0	0	0	2017	913	1589	1413	1147	911	723	574	469	401	364
400	407	469	576	889	1347	551	1713	1844	1940	2027	0	0	0	0	0	2017	913	1589	1413	1147	911	723	574	469	401	364
401	407	469	576	889	1347	551	1713	1844	1940	2027	0	0	0	0	0	2017	913	1589	1413	1147	911	723	574	469	401	364
402	407	469	576	889	1347	551	1713	1844	1940	2027	0	0	0	0	0	2017	913	1589	1413	1147	911	723	574	469	401	364
403	407	469	576	889	1347	551	1713	1844	1940	2027	0	0	0	0	0	2017	913	1589	1413	1147	911	723	574	469	401	364
404	407	469	576	889	1347	551	1713	1844	1940	2027	0	0	0	0	0	2017	913	1589	1413	1147	911	723	574	469	401	364
405	407	469	576	889	1347	551	1713	1844	1940	2027	0	0	0	0	0	2017	913	1589	1413	1147	911	723	574	469	401	364
406	407	469	576	889	1347	551	1713	1844	1940	2027	0	0	0	0	0	2017	913	1589	1413	1147	911	723	574	469	401	364
407	407	469	576	889	1347	551	1713	1844	1940	2027	0	0	0	0	0	2017	913	1589	1413	1147	911	723	574	469	401	364
408	407	469	576	889	1347	551	1713	1844	1940	2027	0	0	0	0	0	2017	913	1589	1413	1147	911	723	574	469	401	364
409	407	469	576	889	1347	551	1713	1844	1940	2027	0	0	0	0	0	2017	913	1589	1413	1147	911	723	574	469	401	364
410	407	469	576	889	1347	551	1713	1844	1940	2027	0	0	0	0	0	2017	913	1589	1413	1147	911	723	574	469	401	364
411	407	469	576	889	1347	551	1713	1844	1940	2027	0	0	0	0	0	2017	913	1589	1413	1147	911	723	574	469	401	364
412	407	469	576	889	1347	551	1713	1844	1940	2027	0	0	0	0	0	2017	913	1589	1413	1147	911	723	574	469	401	364
413	407	469	576	889	1347	551	1713	1844	1940	2027	0	0	0	0	0	2017	913	1589	1413	1147	911	723	574	469	401	364
414	407	469	576	889	1347	551	1713	1844	1940	2027	0	0	0	0	0	2017	913	1589	1413	1147	911	723	574	469	401	364
415	407	469	576	889	1347	551	1713	1844	1940	2027	0	0	0	0	0	2017	913	1589	1413	1147	911	723	574	469	401	364
416	407	469	576	889	1347	551	1713	1844	1940	2027	0	0	0	0	0	2017	913	1589	1413	1147	911	723	574	469	401	364
417	407	469	576																							

WIND VECTOR IS TO THE LEFT (FOR TEMPERATURE ARRAY ABOVE) AND IS UPWARD (FOR PRINTOUT WHICH FOLLOWS)

ELEMENT	Q (IN)	Q (CNVC)	Q (RAD)	Q (VPR)	CMS VPRZD	CMS LEFT
1	.550392E+00	-.261762E-01	.194189E-03	0.	0.	.100000E+00
2	.103169E+01	-.435482E-01	.265799E-03	0.	0.	.100000E+00
3	.183905E+01	-.733469E-01	.455447E-03	0.	0.	.100000E+00
4	.311751E+01	-.116414E+00	.971993E-03	0.	0.	.100000E+00
5	.502566E+01	-.176773E+00	.347158E-02	0.	0.	.111036E+00
6	.770456E+01	-.259946E+00	.266716E-01	0.	0.	.166681E+00
7	.112324E+02	-.342051E+00	.596020E-01	0.	0.	.175486E+00
8	.155729E+02	-.416799E+00	.875976E-01	0.	0.	.168708E+00
9	.205321E+02	-.480625E+00	.144869E+00	0.	0.	.155243E+00
10	.257435E+02	-.531987E+00	.192334E+00	0.	0.	.128985E+00
11	.306954E+02	-.570479E+00	.238766E+00	0.	0.	.982911E-01
12	.348055E+02	-.595863E+00	.272630E+00	0.	0.	.677557E-01
13	.375313E+02	-.609859E+00	.292027E+00	0.	0.	.420222E-01
14	.384261E+02	-.612876E+00	.291617E+00	0.	0.	.303976E-01
15	.377313E+02	-.606155E+00	.273929E+00	0.	0.	.317120E-01
16	.348055E+02	-.586824E+00	.239684E+00	0.	0.	.473912E-01
17	.306954E+02	-.560102E+00	.193106E+00	0.	0.	.762714E-01
18	.257435E+02	-.516850E+00	.134371E+00	0.	0.	.999587E-01
19	.205321E+02	-.458016E+00	.755790E-01	0.	0.	.100000E+00
20	.155729E+02	-.389130E+00	.367989E-01	0.	0.	.100000E+00
21	.112324E+02	-.314939E+00	.162948E-01	0.	0.	.100000E+00
22	.770456E+01	-.240030E+00	.698017E-02	0.	0.	.100000E+00
23	.502566E+01	-.172976E+00	.248876E-02	0.	0.	.100000E+00
24	.311751E+01	-.116393E+00	.971441E-03	0.	0.	.100000E+00
25	.183905E+01	-.733442E-01	.455447E-03	0.	0.	.100000E+00
26	.103169E+01	-.435473E-01	.265800E-03	0.	0.	.100000E+00
27	.550392E+00	-.261758E-01	.194189E-03	0.	0.	.100000E+00

TOTAL INCIDENT ABSORBED ENERGY = 429.1900637087 CALORIES
 TOTAL CALORIES LOST DUE TO CONVECTION = 8.9640258259 CALORIES
 TOTAL ENERGY EMITTED DUE TO RADIATION = 2.6027915860 CALORIES
 CALORIES EXPENDED IN VAPORIZATION (TOTAL) = 0.0000000000

TIME TO MELT THROUGH = .4027470967 SECONDS

DISTANCE FROM C/L (CMS)	TOTAL THICKNESS (CMS)	NON-MOLTEN THICKNESS
-2.60000	.100000000000	.100000000000
-2.40000	.100000000000	.100000000000
-2.20000	.100000000000	.100000000000
-2.00000	.100000000000	.100000000000
-1.80000	.111096293659	.111096293659
-1.60000	.166682630527	.140000000000
-1.40000	.175485897822	.140000000000
-1.20000	.168707588854	.133333333333
-1.00000	.155242690182	.120000000000
-.80000	.128984950525	.093333333333
-.60000	.098291138188	.066666666667
-.40000	.067755664366	.033333333333
-.20000	.042022169830	.013333333333
0.00000	.030397570922	.000000000000
.20000	.031712024201	.006666666667
.40000	.047391247646	.026666666667
.60000	.076271423712	.060000000000
.80000	.099958709493	.093333333333
1.00000	.100000000000	.100000000000
1.20000	.100000000000	.100000000000
1.40000	.100000000000	.100000000000
1.60000	.100000000000	.100000000000
1.80000	.100000000000	.100000000000
2.00000	.100000000000	.100000000000
2.20000	.100000000000	.100000000000
2.40000	.100000000000	.100000000000
2.60000	.100000000000	.100000000000

TEMPERATURE OF BACK SURFACE (DEG.K) VS TIME (SECS)

TIME (SECONDS)	TEMPERATURE (DEGREES KELVIN)
0.	.300000000E+03
.2326489168E+00	.1640870551E+04
.2541348580E+00	.1746273851E+04
.2705067049E+00	.1809752677E+04
.2848945294E+00	.1856245751E+04
.2974831208E+00	.1890725483E+04
.3071397060E+00	.1917076529E+04
.320123572E+00	.1939616663E+04
.3304814706E+00	.1954518447E+04
.3403305217E+00	.1965472297E+04
.3497419220E+00	.1972005311E+04
.3589003868E+00	.1974701009E+04
.3679590042E+00	.1975002184E+04
.3769947281E+00	.1975056429E+04
.3860546573E+00	.1975448696E+04
.3952510094E+00	.1977981651E+04
.4027470967E+00	.1988219229E+04

SOLID-LIQUID INTERFACE POSITION (CMS) VS TIME (SECS)

TIME (SECONDS)	CMS FROM ORIGINAL SURFACE
.2326489168E+00	0.
.2541348580E+00	.666666667E-02
.2705067049E+00	.1333333333E-01
.2848945294E+00	.2000000000E-01
.2974831208E+00	.2666666667E-01
.3088397060E+00	.3333333333E-01
.320123572E+00	.4000000000E-01
.3304814706E+00	.4666666667E-01
.3403305217E+00	.5333333333E-01
.3497419220E+00	.6000000000E-01
.3589003868E+00	.6666666667E-01
.3679590042E+00	.7333333333E-01
.3769947281E+00	.8000000000E-01
.3860546573E+00	.8666666667E-01
.3952510094E+00	.9333333333E-01
.4027470967E+00	.1000000000E+00

SURFACE RECESSION RATE (CMS/SEC) VS TIME (SECS) AND POSITION OF SOLID-LIQUID INTERFACE

TIME (SECONDS)	VELOCITY (CMS/SEC)	CENTIMETERS
.2433818874E+00	.5102804120E+00	.333333333E-02
.2623207814E+00	.4072030906E+00	.1000000000E-01
.2776808172E+00	.4646465149E+00	.1666666667E-01
.2911688251E+00	.5279026376E+00	.2333333333E-01
.3031614134E+00	.5870309197E+00	.3000000000E-01
.3144816421E+00	.5908137372E+00	.3666666667E-01
.3253025244E+00	.6436315786E+00	.4333333333E-01
.3354059982E+00	.6768841592E+00	.5000000000E-01
.3450367219E+00	.7083607605E+00	.5666666667E-01
.3543211544E+00	.7279240412E+00	.6333333333E-01
.3634256795E+00	.7359474767E+00	.7000000000E-01
.3724788652E+00	.7378121200E+00	.7666666667E-01
.3815246927E+00	.7358409197E+00	.8333333333E-01
.3905328333E+00	.7249251269E+00	.9000000000E-01
.3995990530E+00	.6893528576E+00	.9666666667E-01

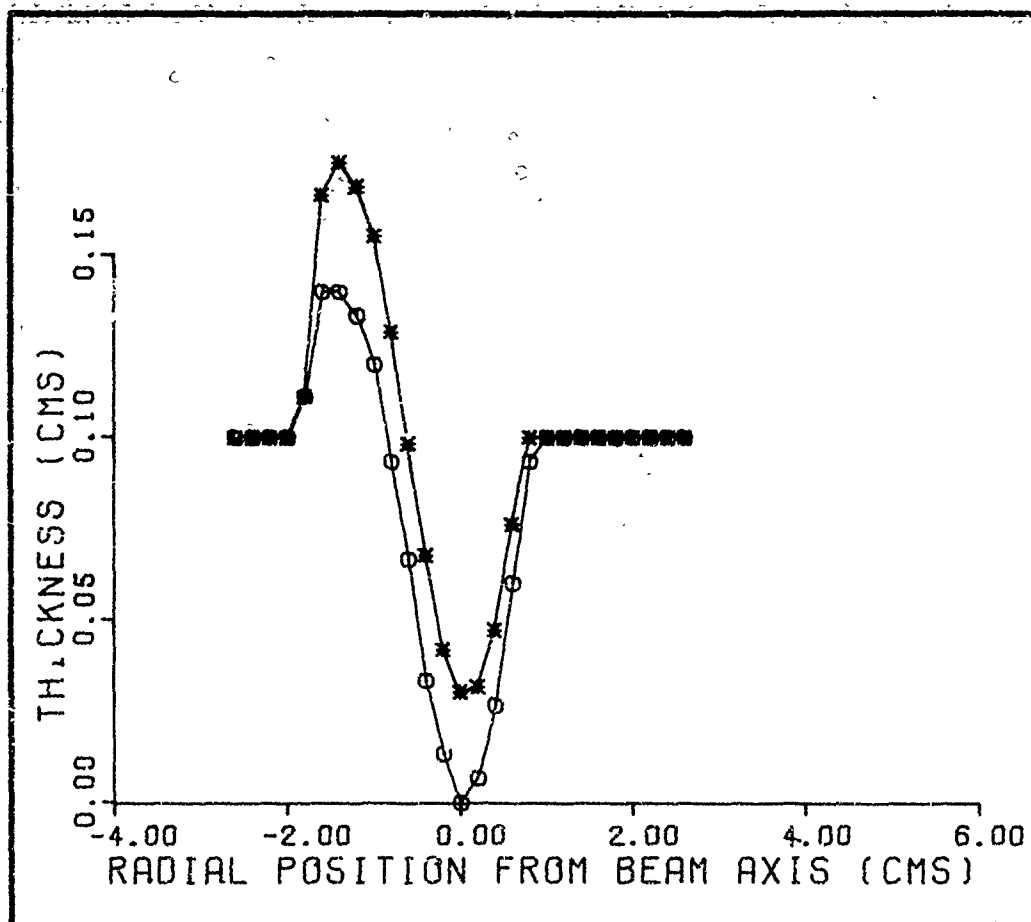


Fig. A-1. A Cross-Sectional View at Time of Melt-Through of a 0.01 cm Thick Titanium Sheet Subjected to a Mach 0.5 Sea-Level Wind and an Absorbed Gaussian-Distributed Flux of 10 kw Over a 10 cm² Spot.

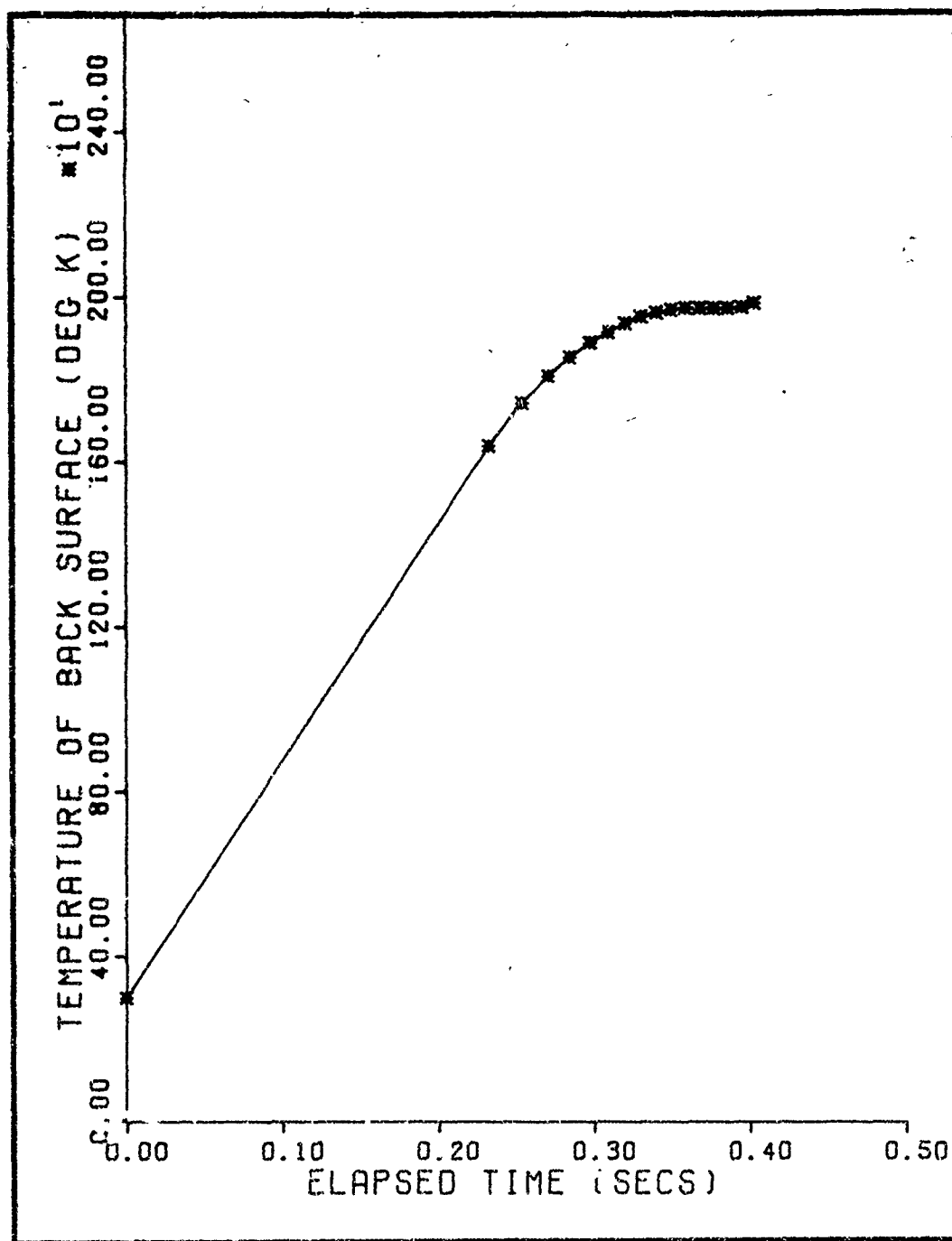


Fig. A-2. The Temperature History at the Back Surface (Opposite the Laser Beam Axis) of a 0.1 cm Thick Titanium Sheet in a Mach 0.5 Sea-Level Airstream Absorbing 10 kw of Laser Power Over a 10 cm² Spot

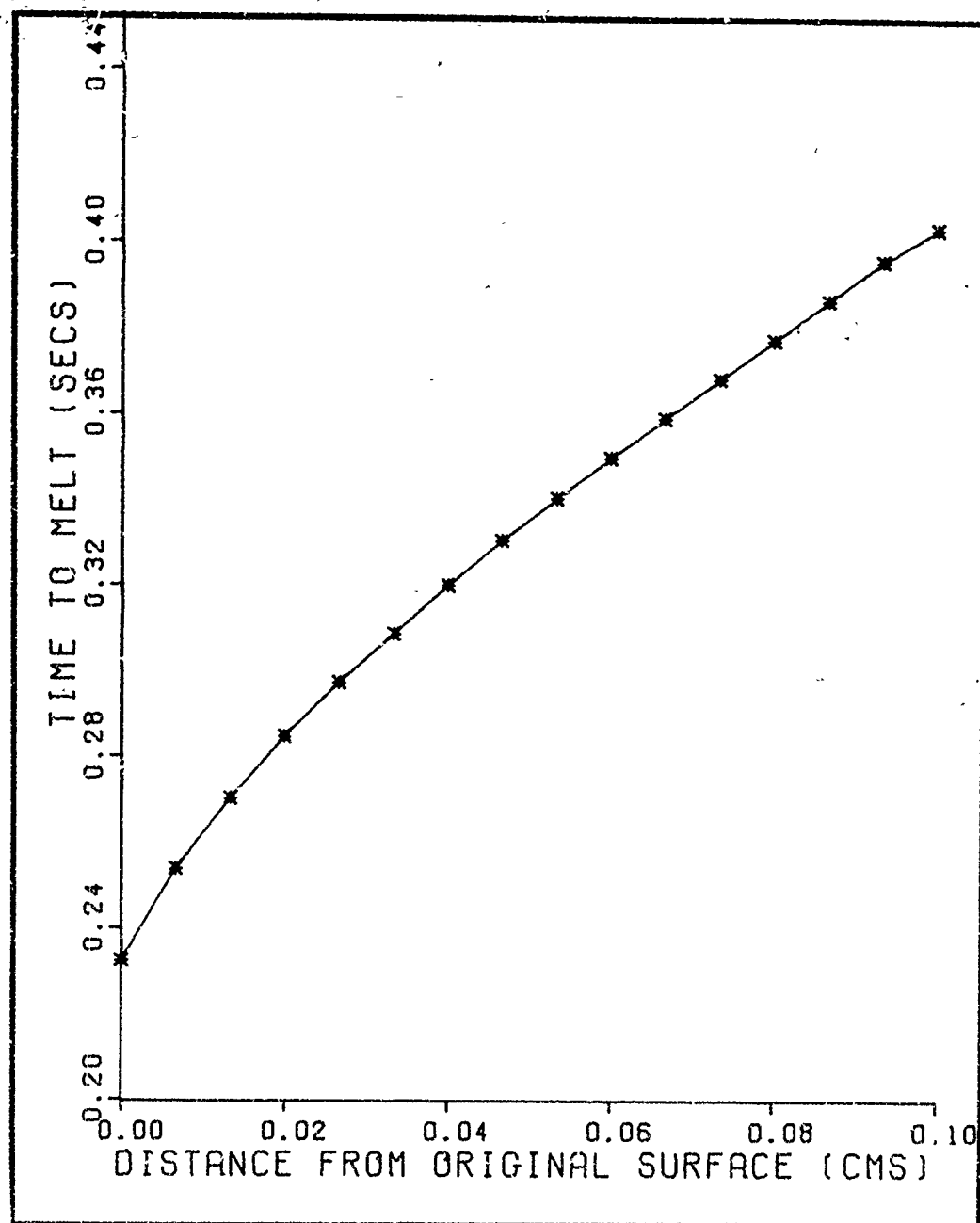


Fig. A-3. The Solid Surface Recession History at the Center of the Laser Beam Spot of a 0.10 cm Thick Titanium Sheet Absorbing 10 kw of Laser Power, Gaussian-Distributed, Over 10 cm² (Time vs. Axial Distance)

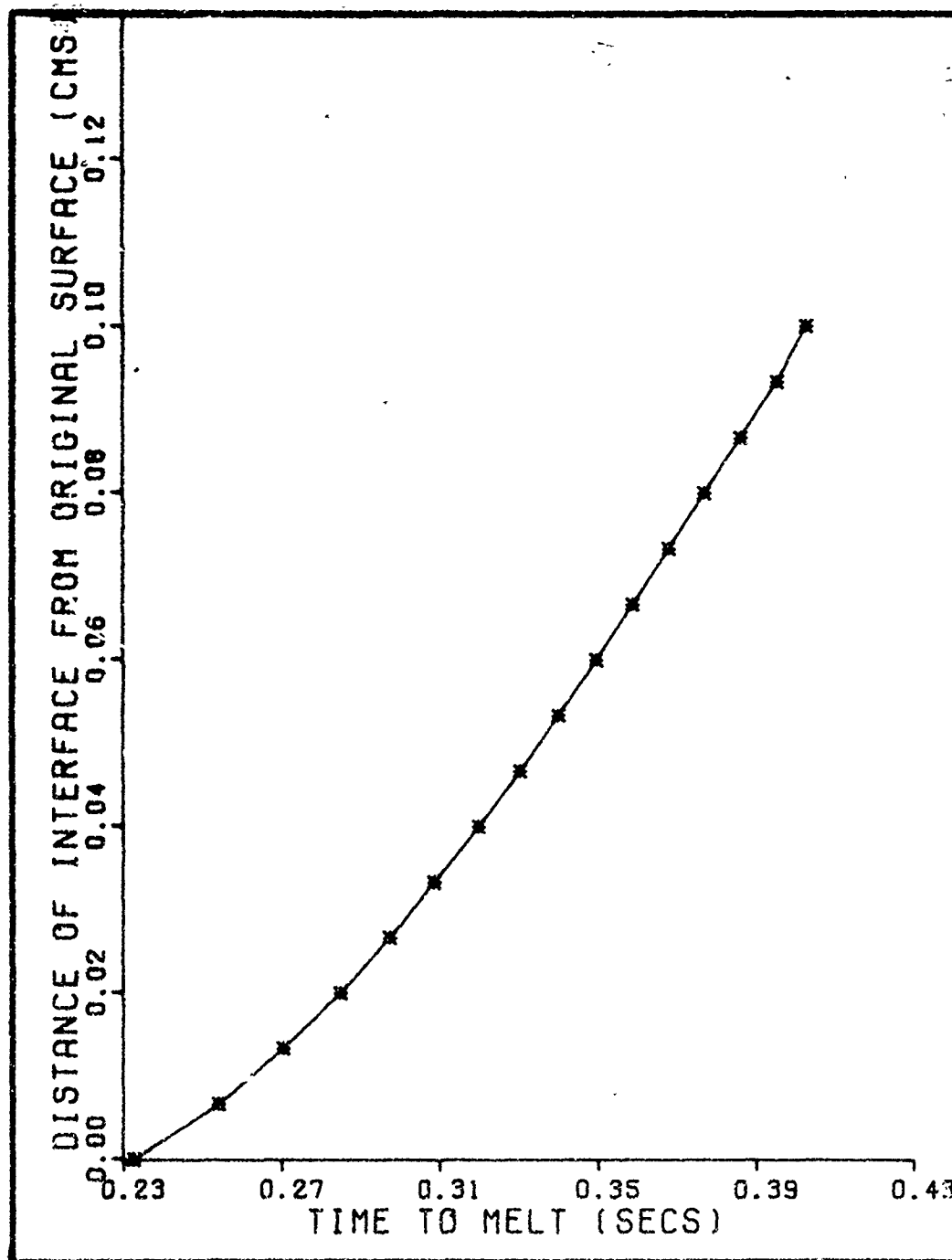


Fig. A-4. The Solid Surface Recession History at the Center of the Laser Beam Spot of a 0.10 cm Thick Titanium Sheet Absorbing 10 kw of Laser Power, Gaussian-Distributed, Over 10 cm² (Axial Distance vs. Time)

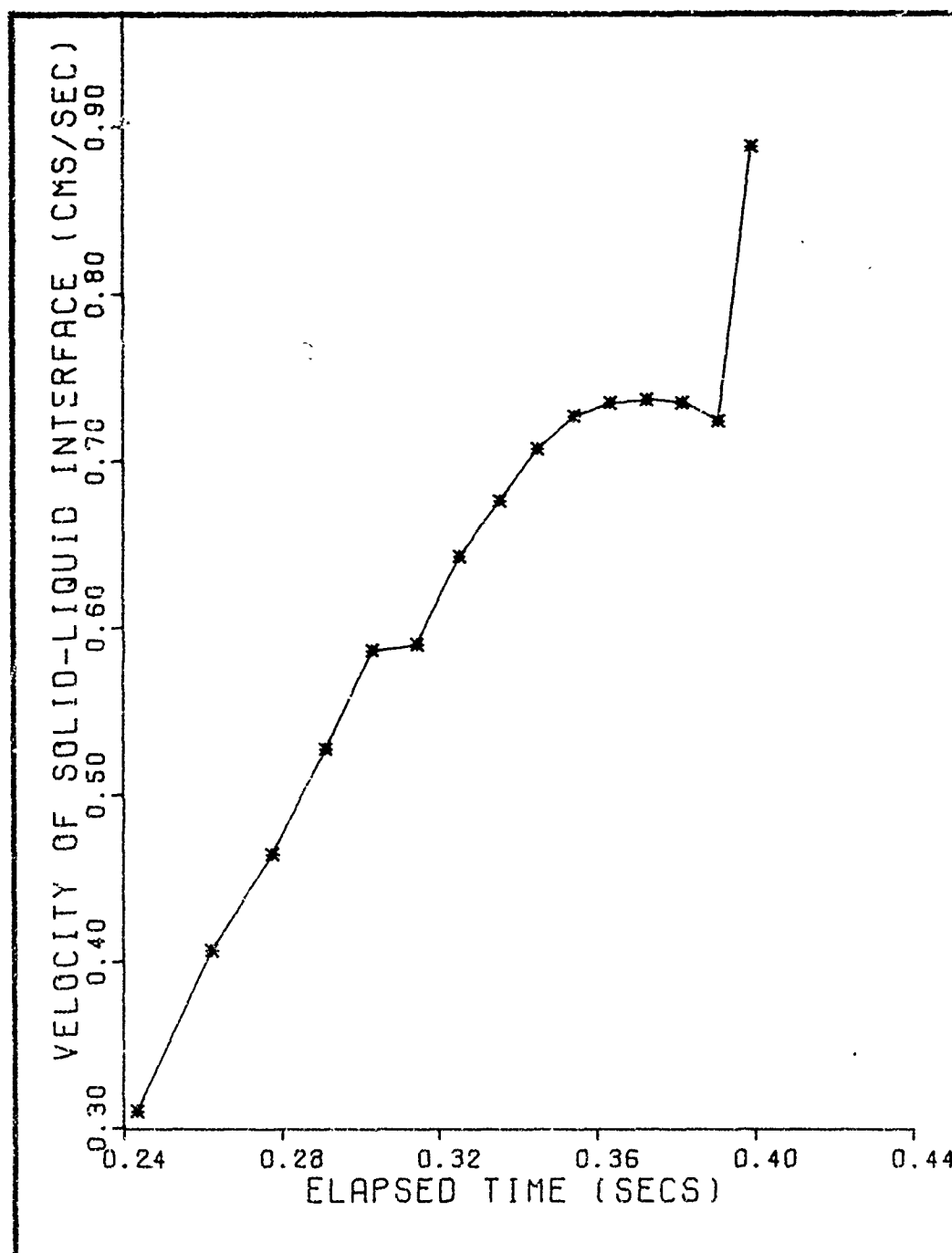


Fig. A-5. The Velocity History of the Nadir of the Liquid-Solid Interface in a Laser-Formed Pit in a 0.1 cm Thick Titanium Sheet Absorbing 10 kw of Gaussian-Distributed Power Over a 10 cm² Spot

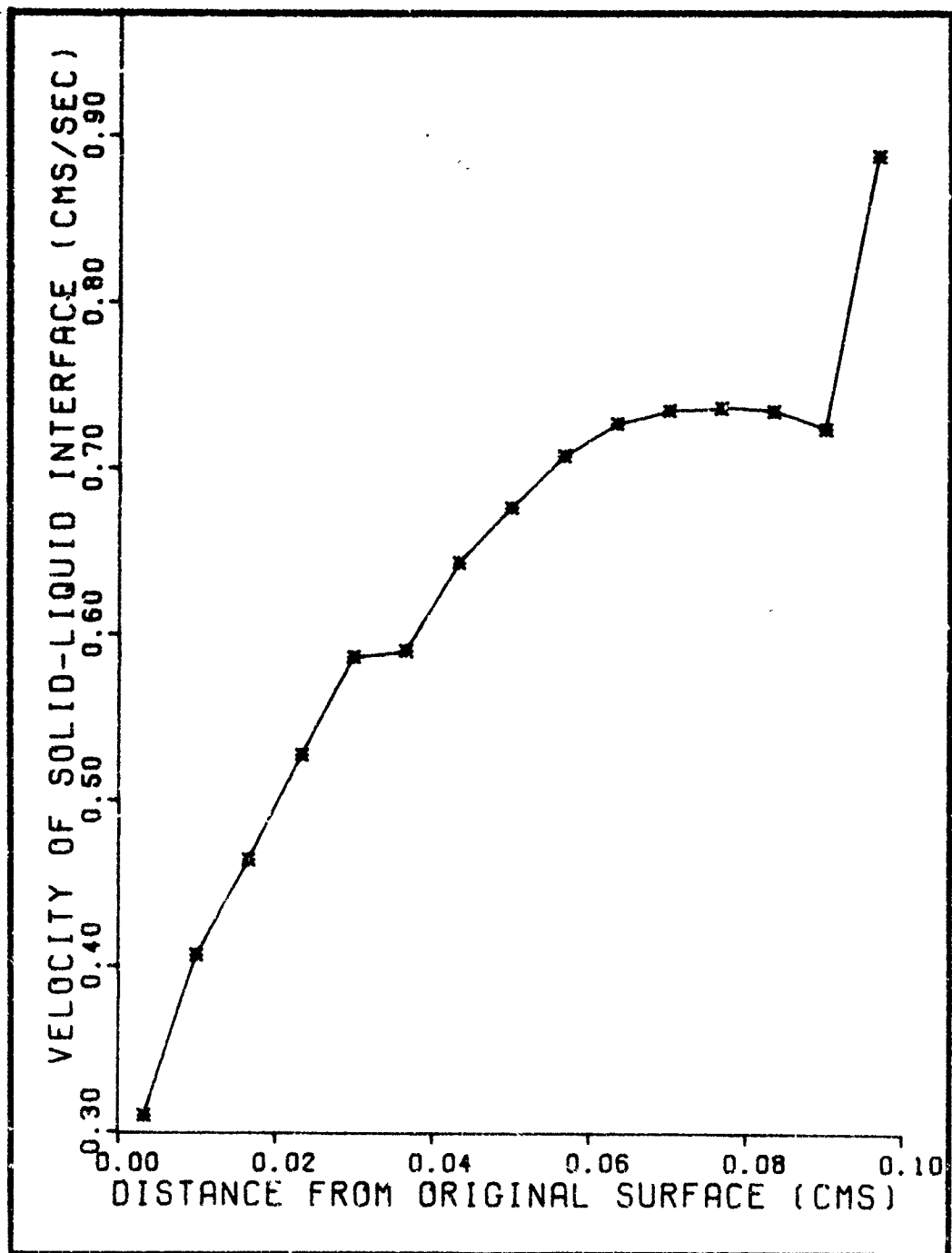
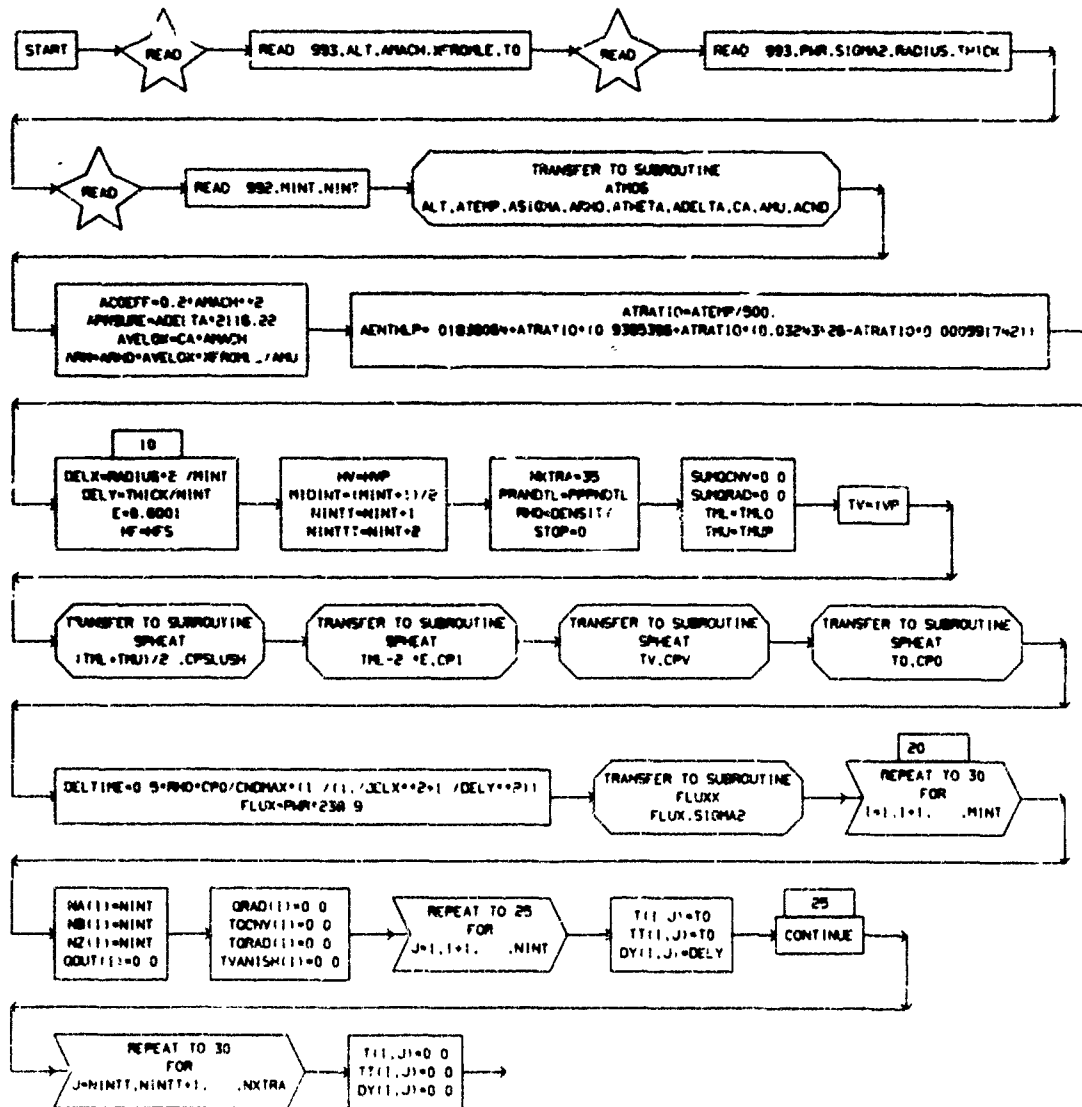


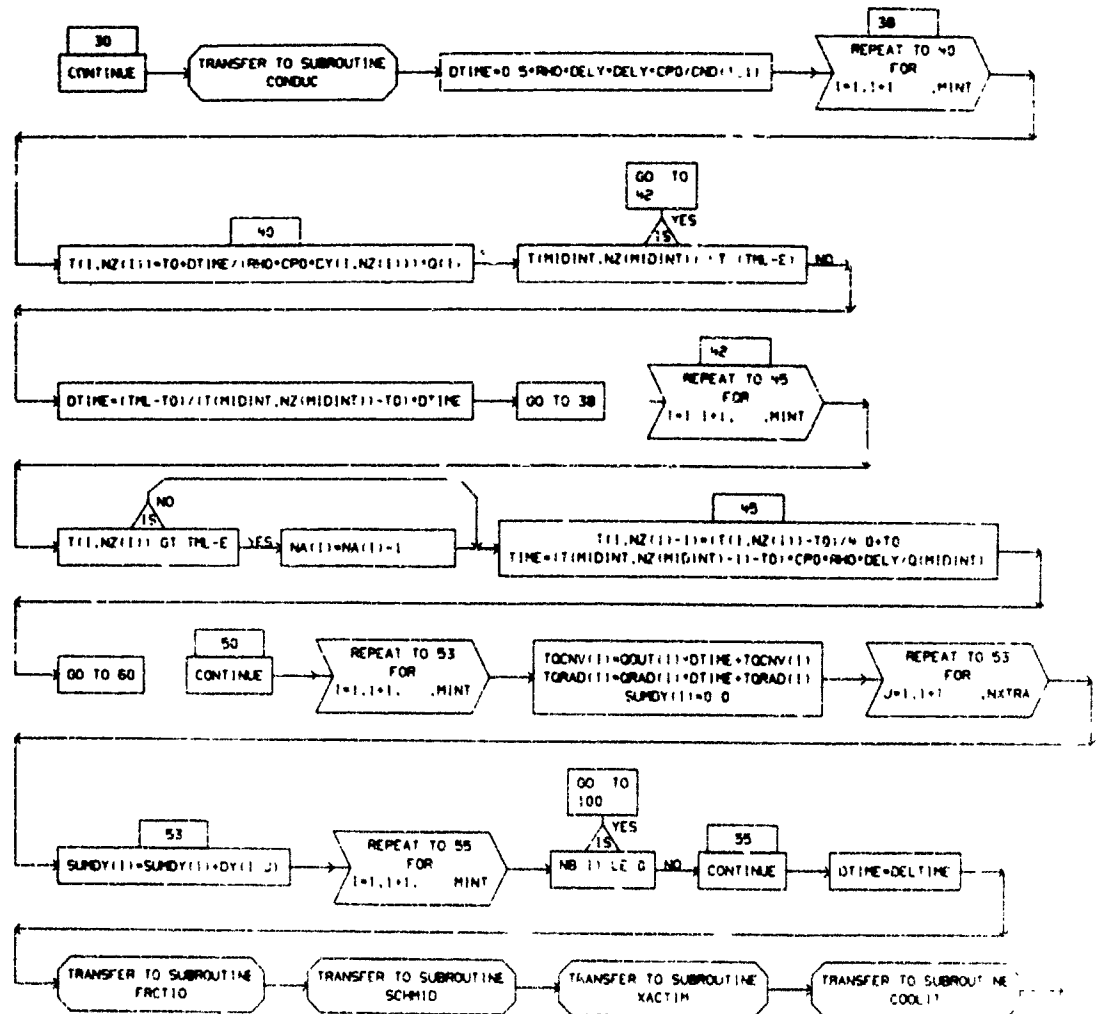
Fig. A-6. The Velocity as a Function of Axial Distance of the Radial of the Liquid-Solid Interface in a Laser-Formed Pit in a 0.1 cm Thick Titanium Sheet Absorbing 10 kw of Gaussian-Distributed Power Over 10 cm²

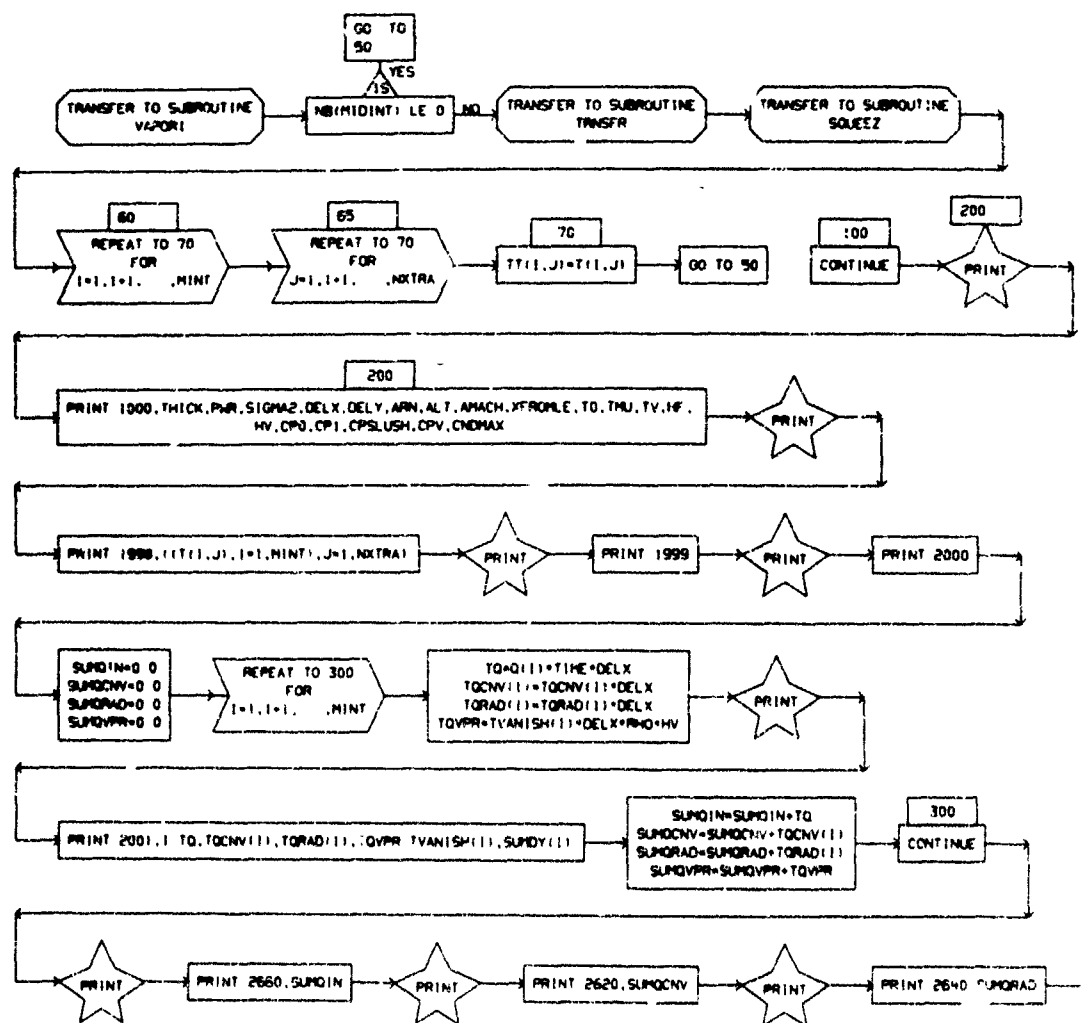
GAW/MC/72-17

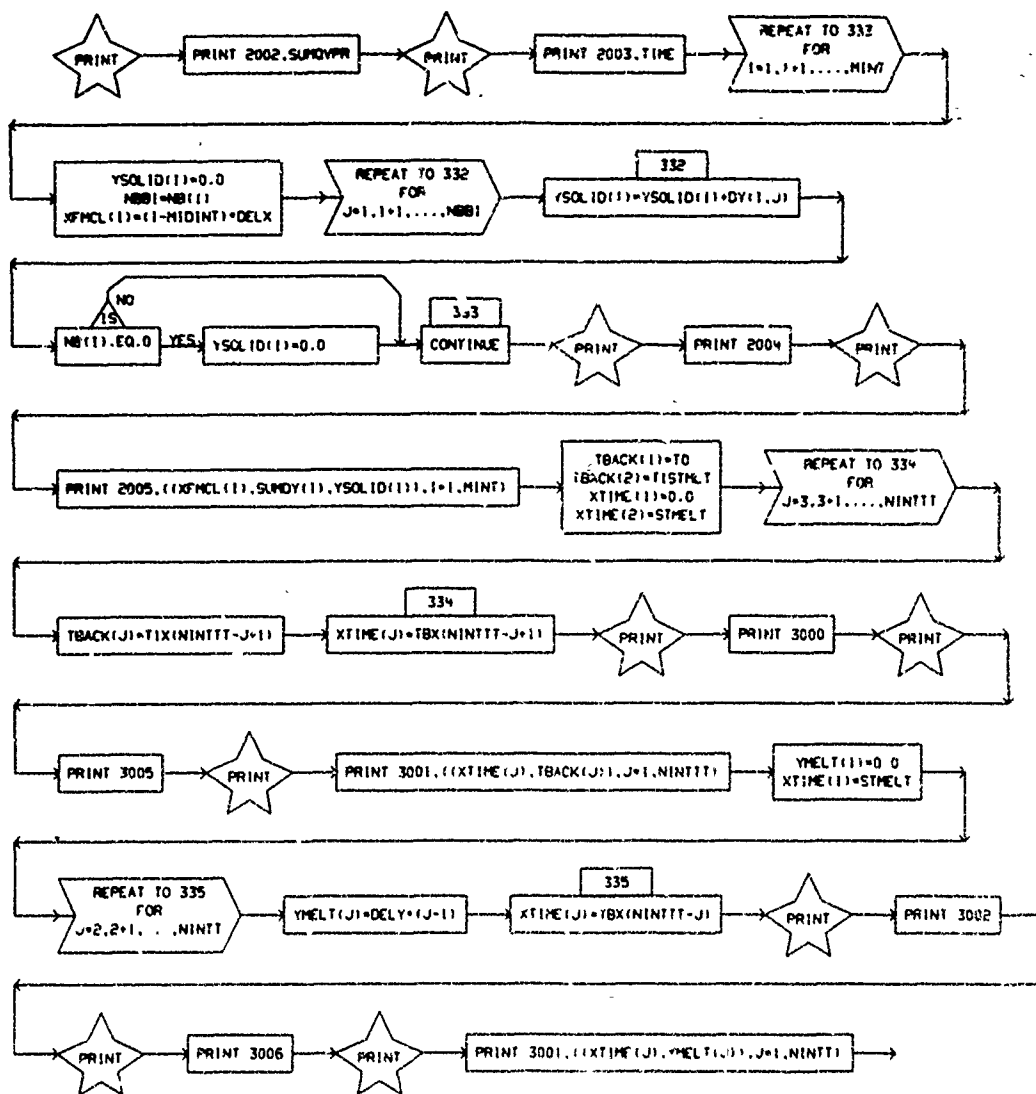
APPENDIX G

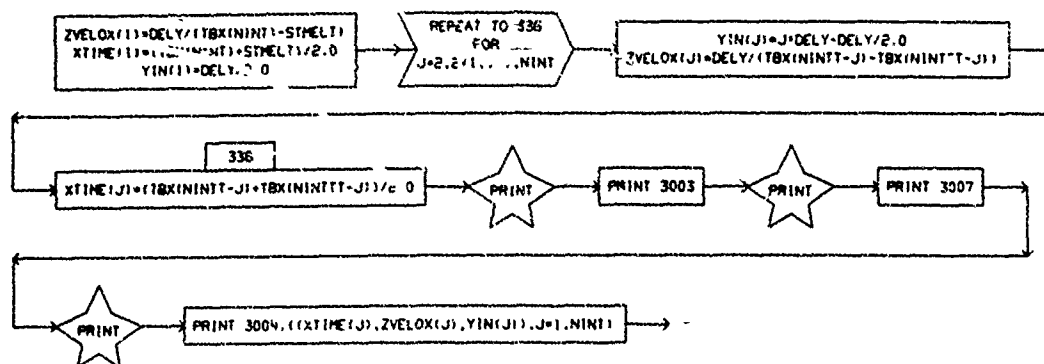
A Flow Diagram of QUEST

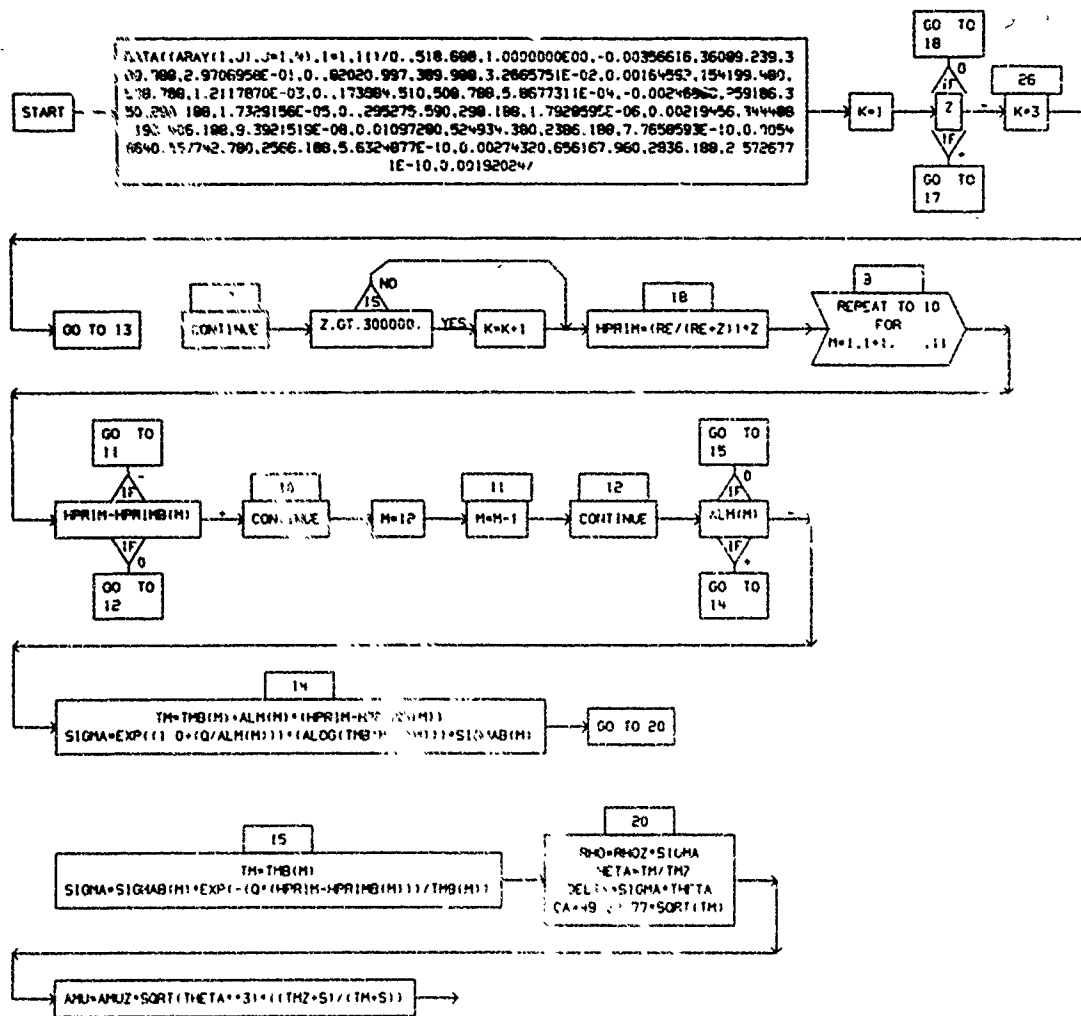






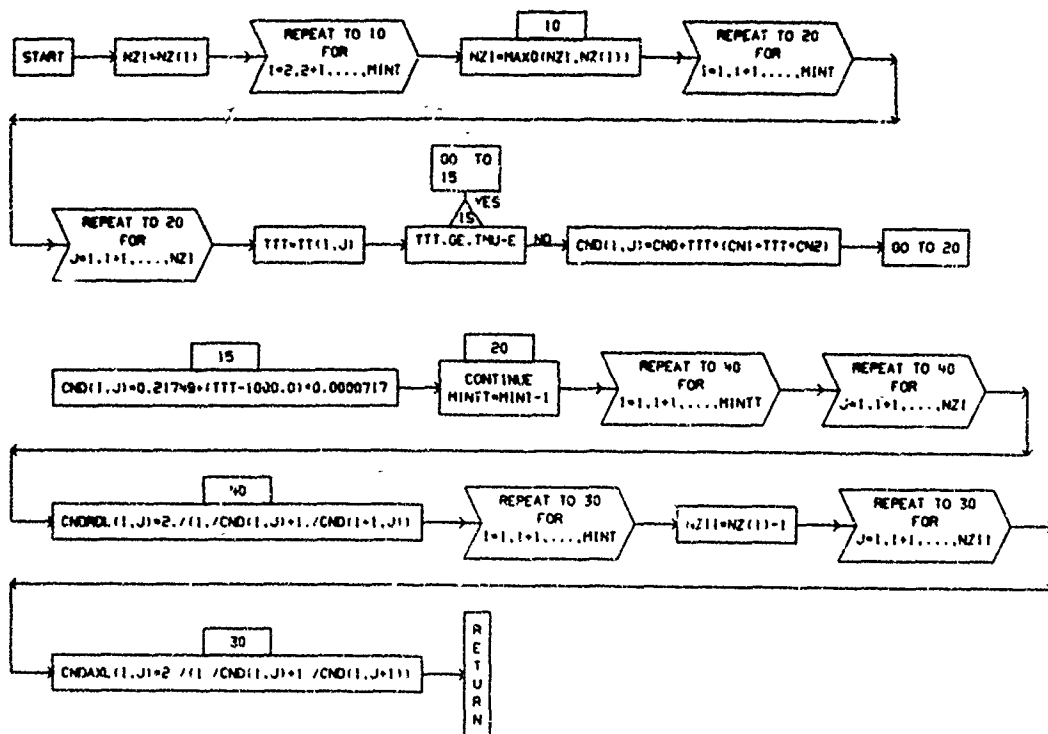


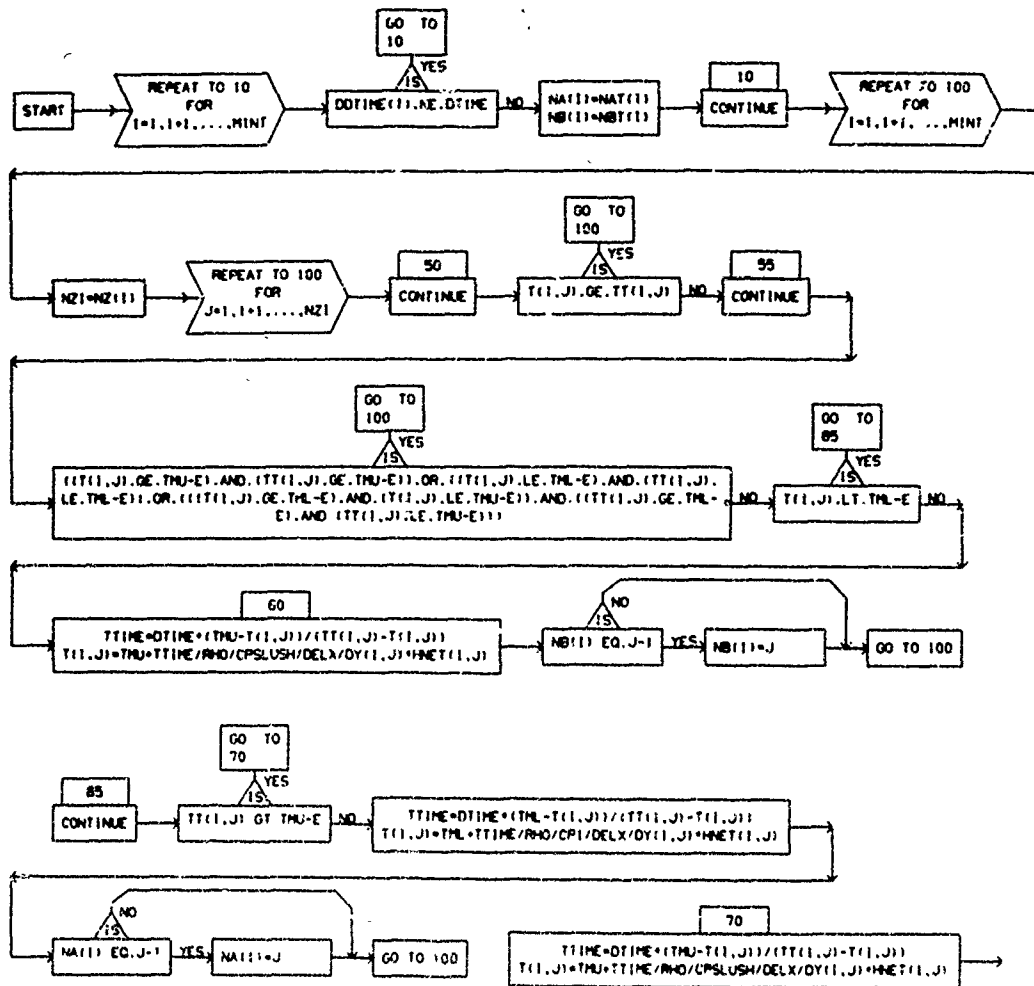


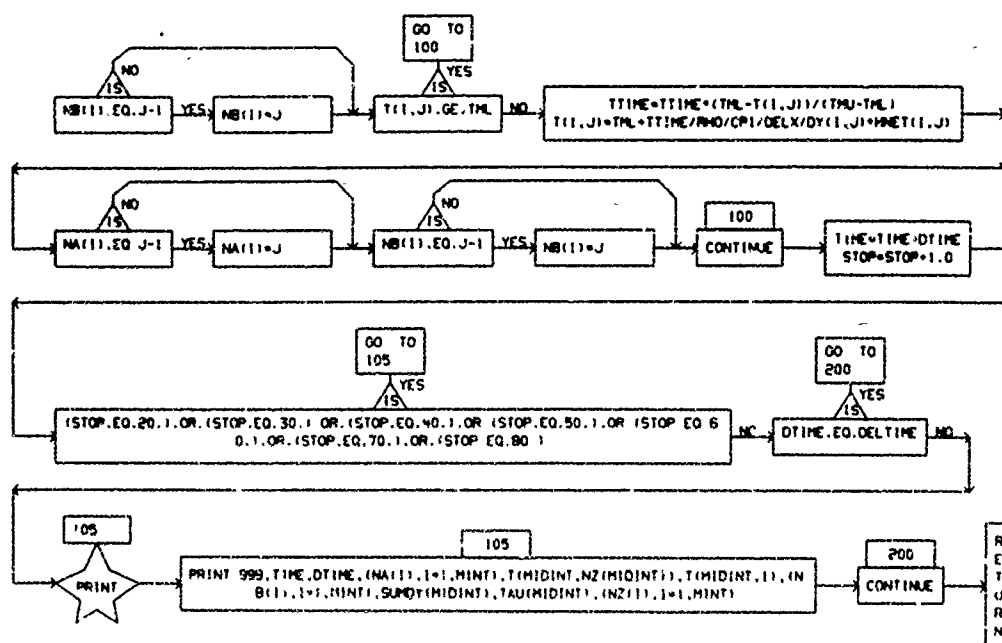


SUBROUTINE CONDUCT

PAGE 1

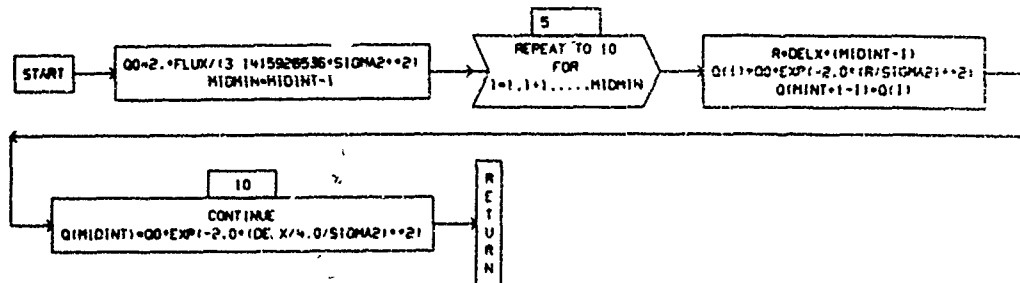






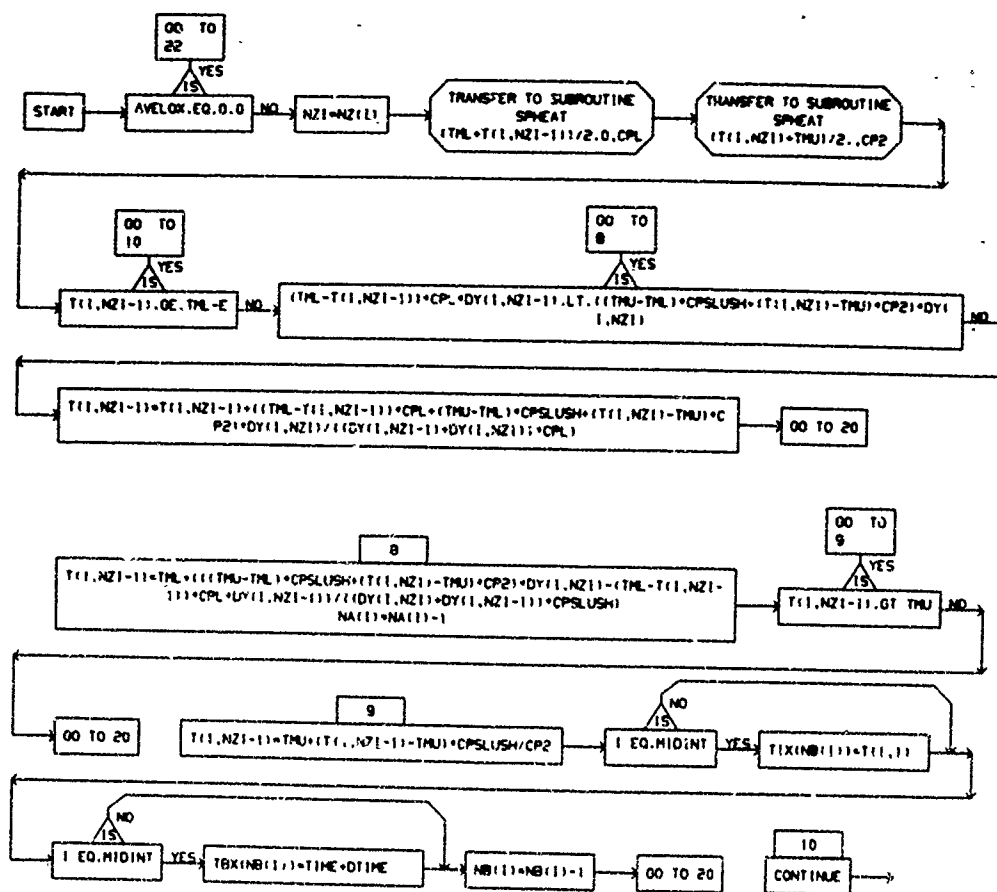
SUBROUTINE FLUX (FLUX, SIGMA2)

PAGE 1



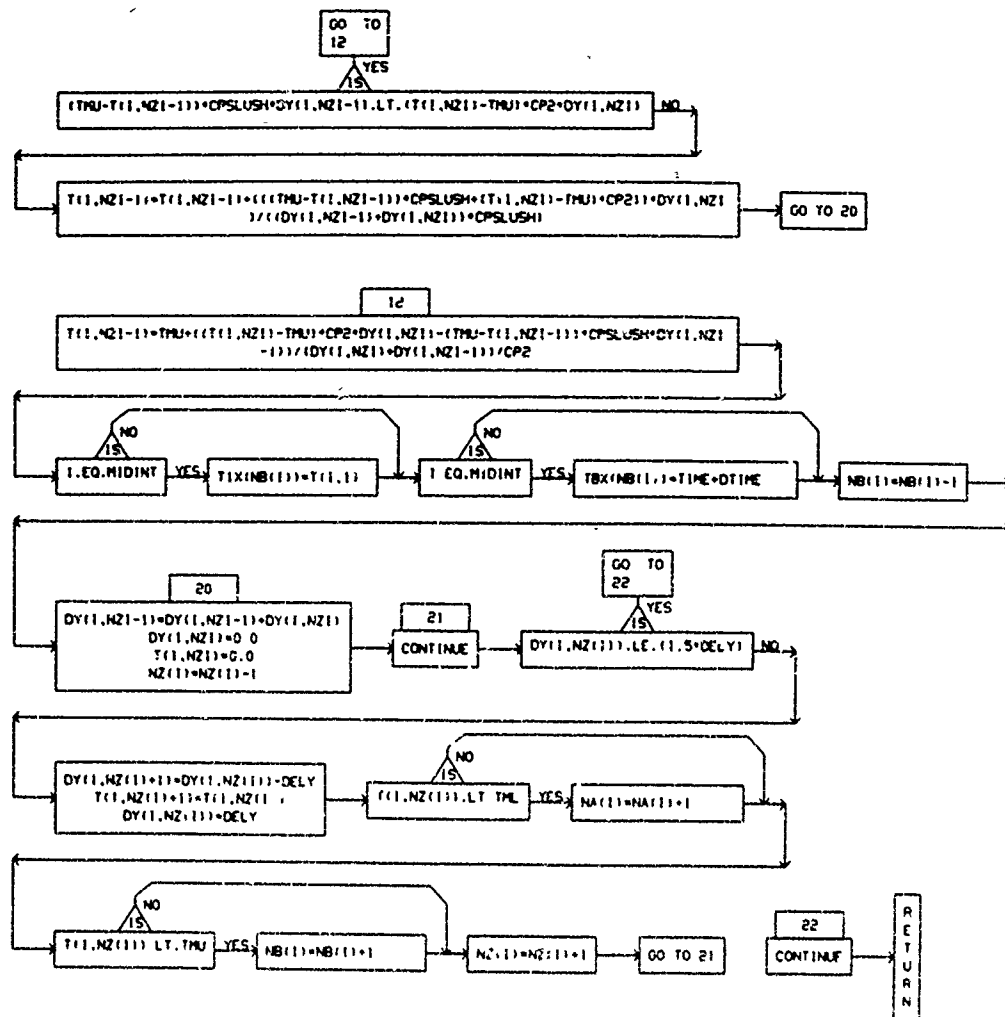
SUBROUTINE FREEZE

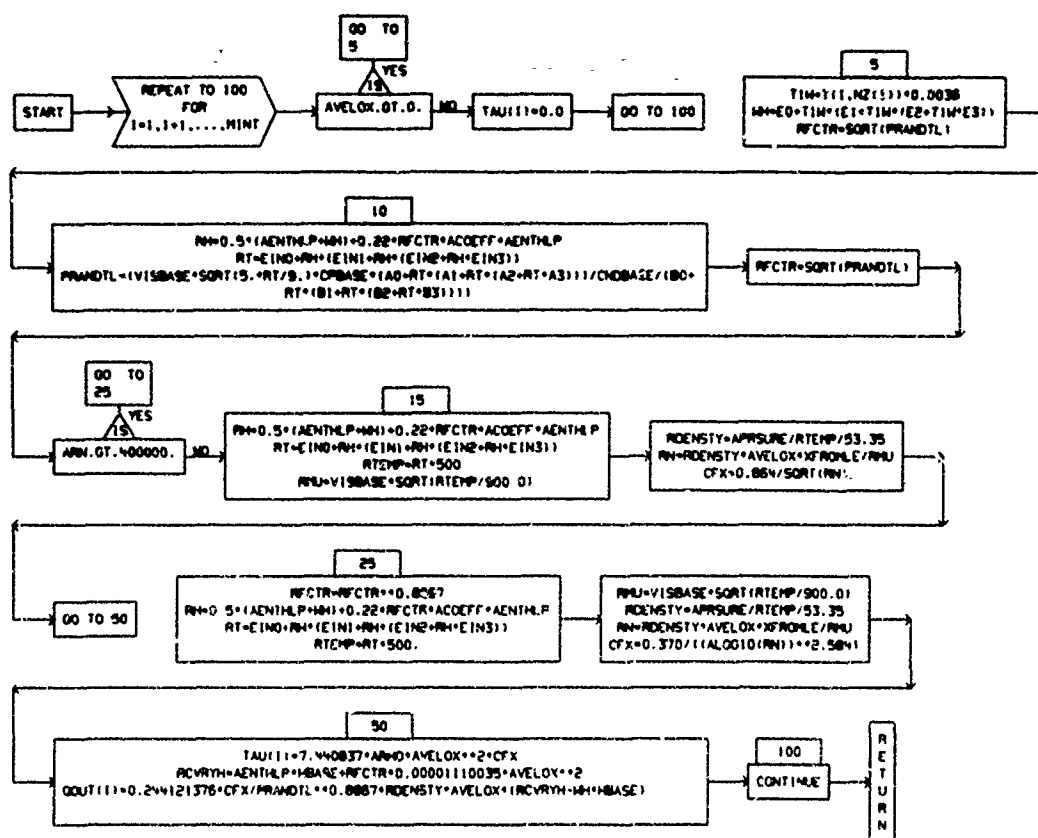
PAGE 1



SUBROUTINE FREEZE

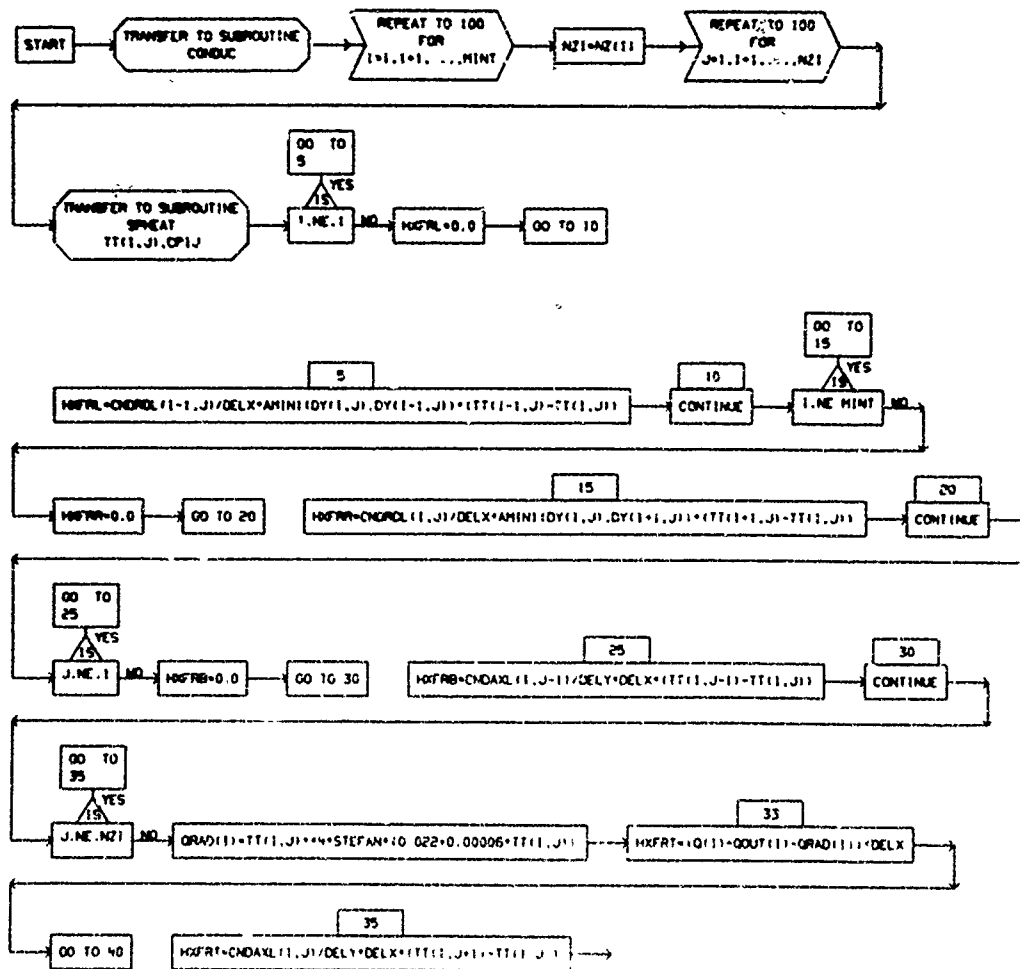
PAGE 2



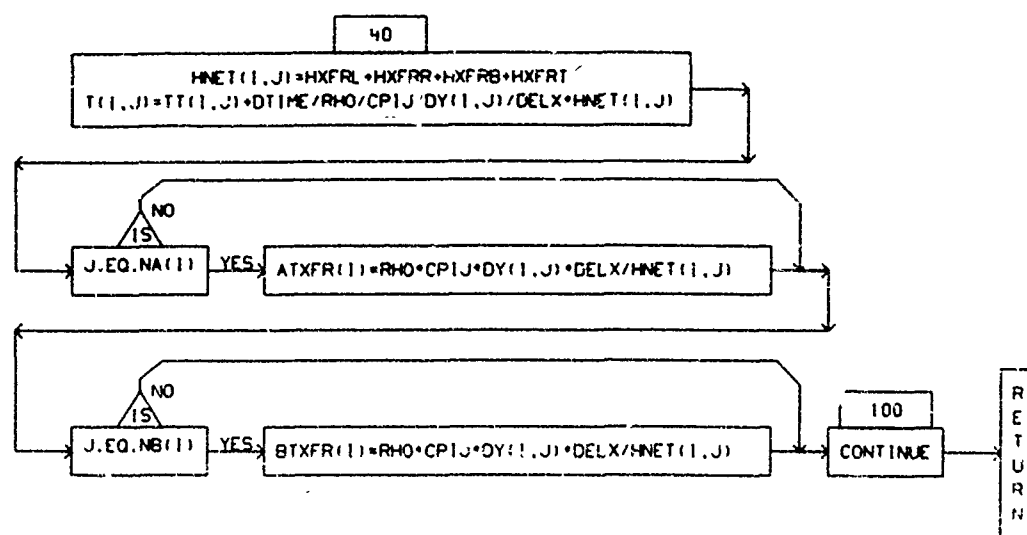


SUBROUTINE SCHMIDT

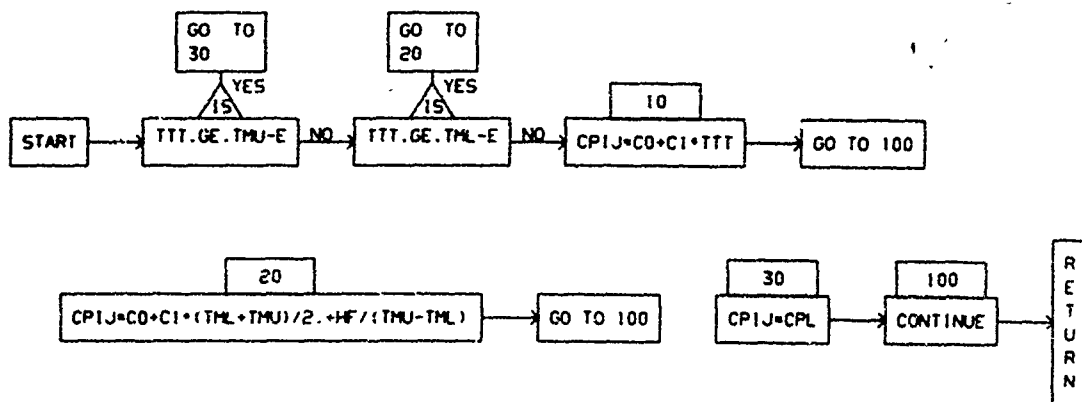
PAGE 1

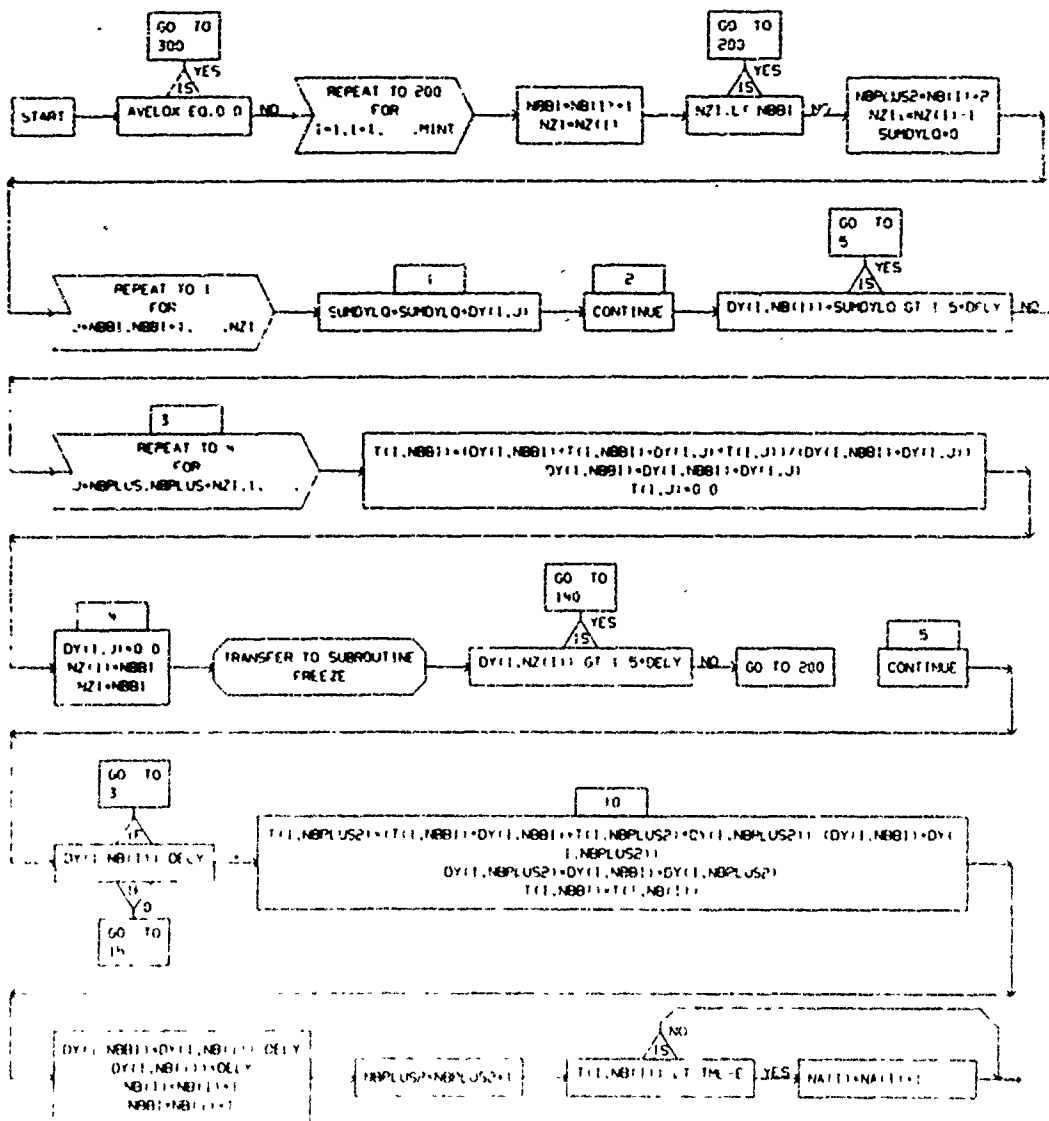


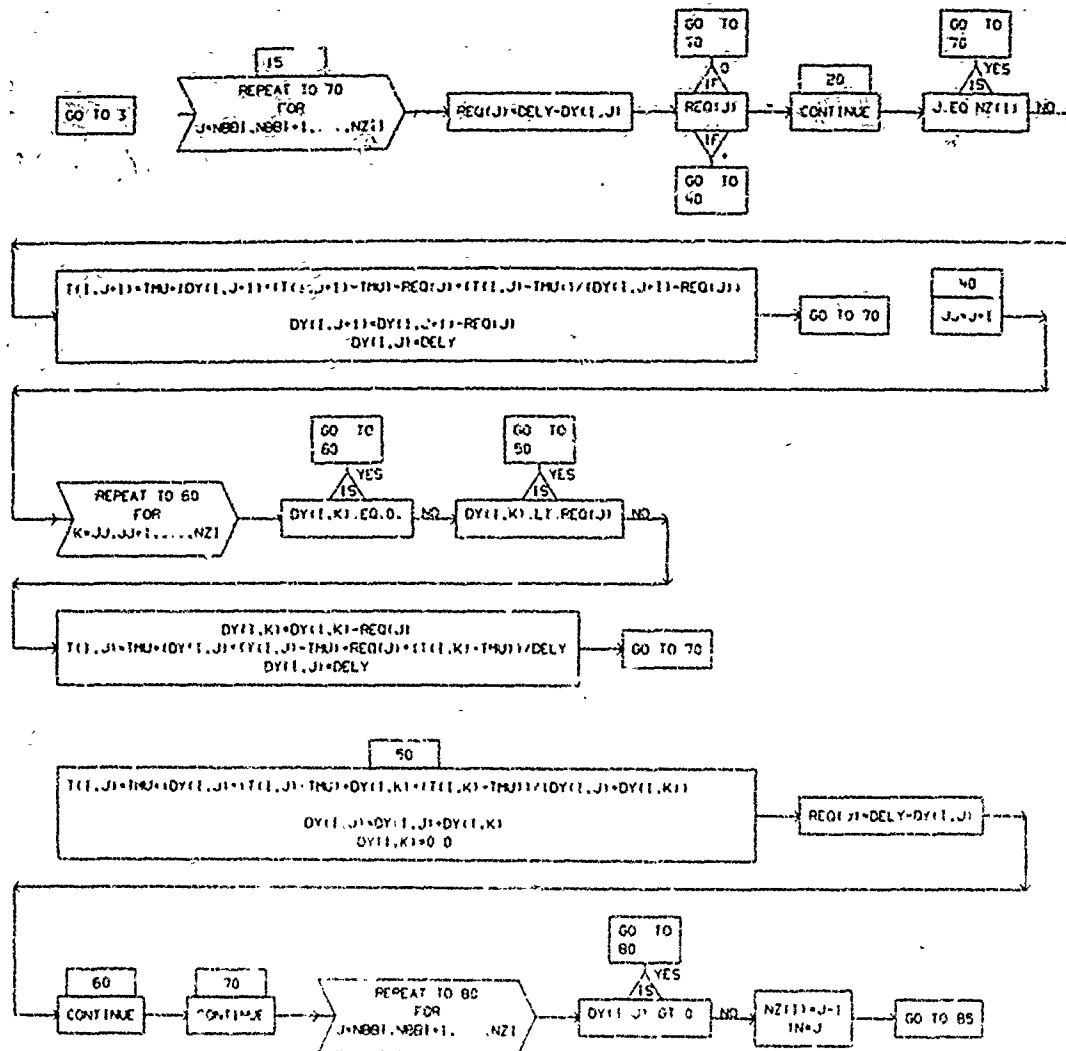
SUBROUTINE SCHM1DT

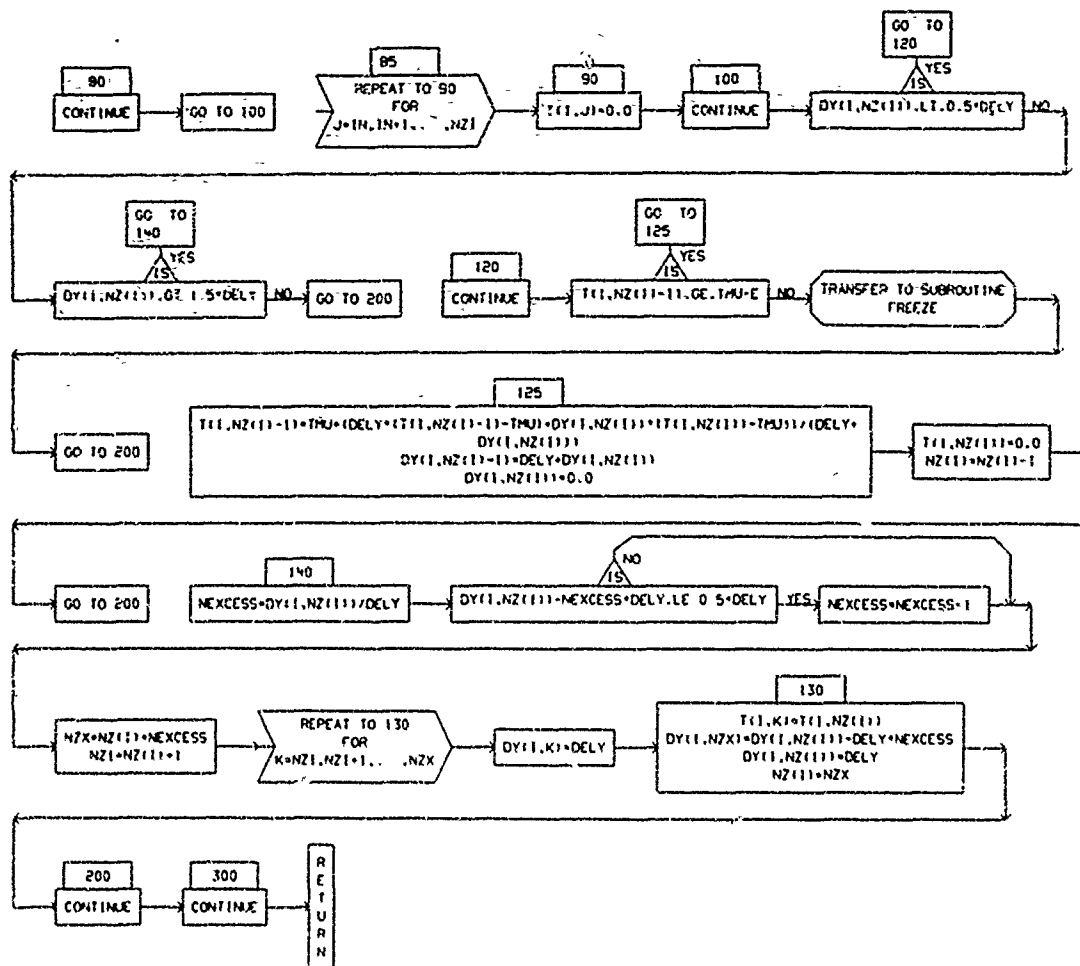


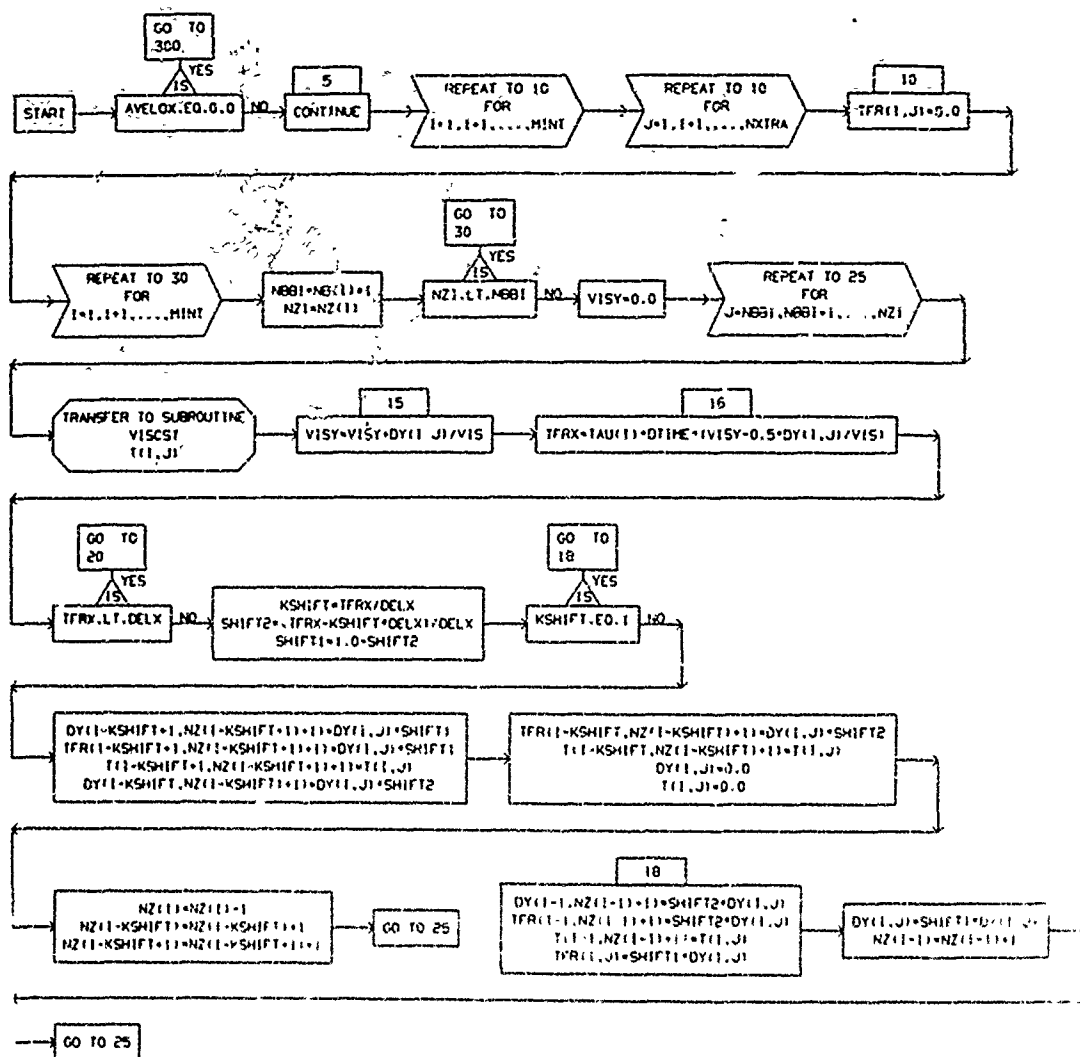
SUBROUTINE SPHEAT (TTT,CPIJ)





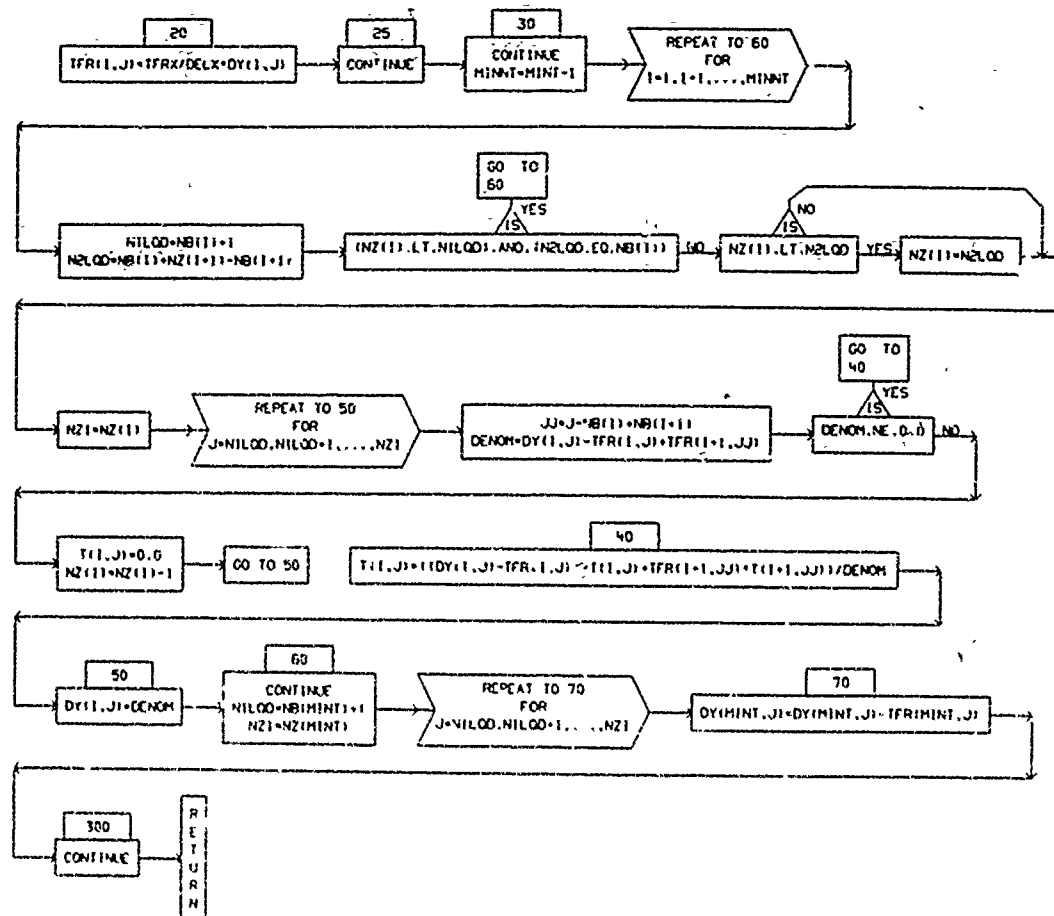






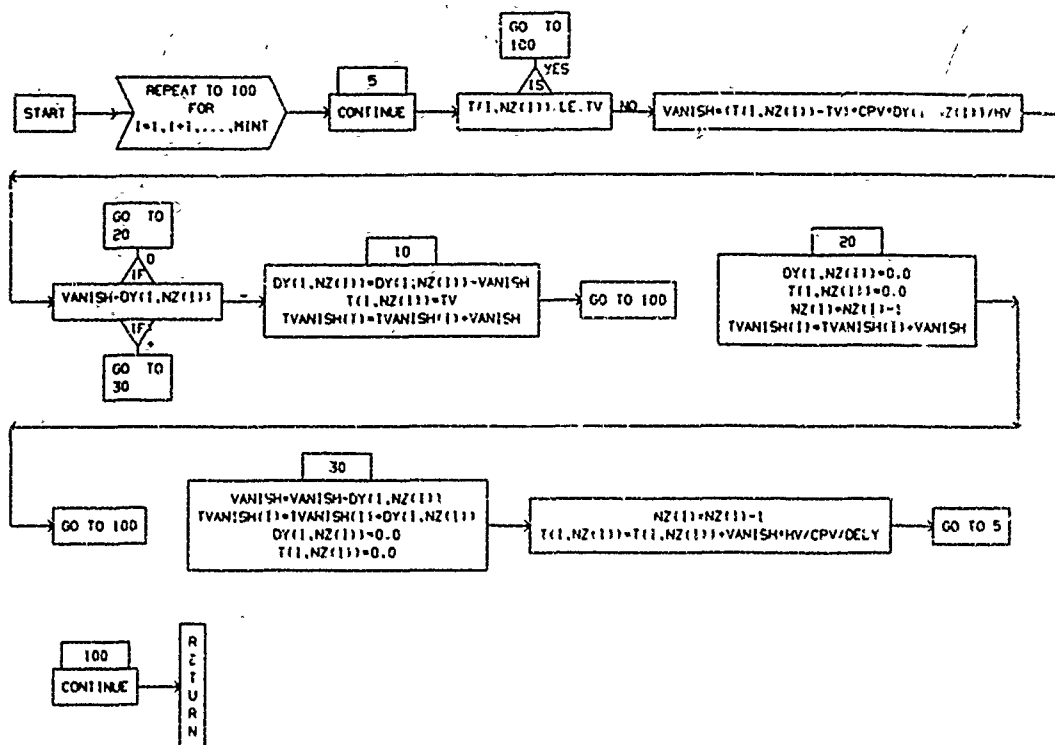
SUBROUTINE TRANSFX

PAGE 2



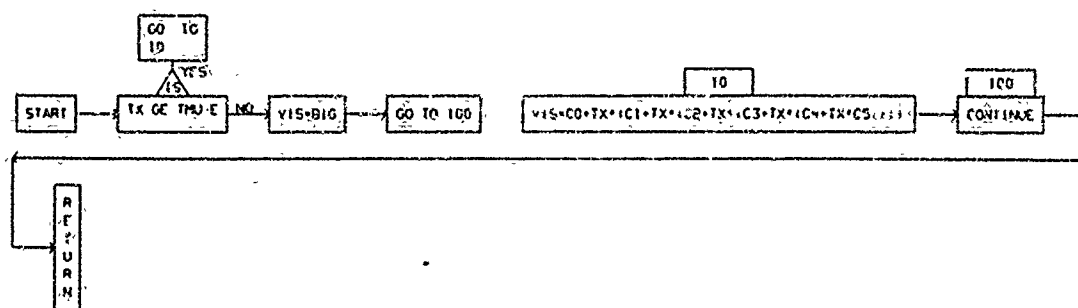
SUBROUTINE VAPORIZ

PAGE 1



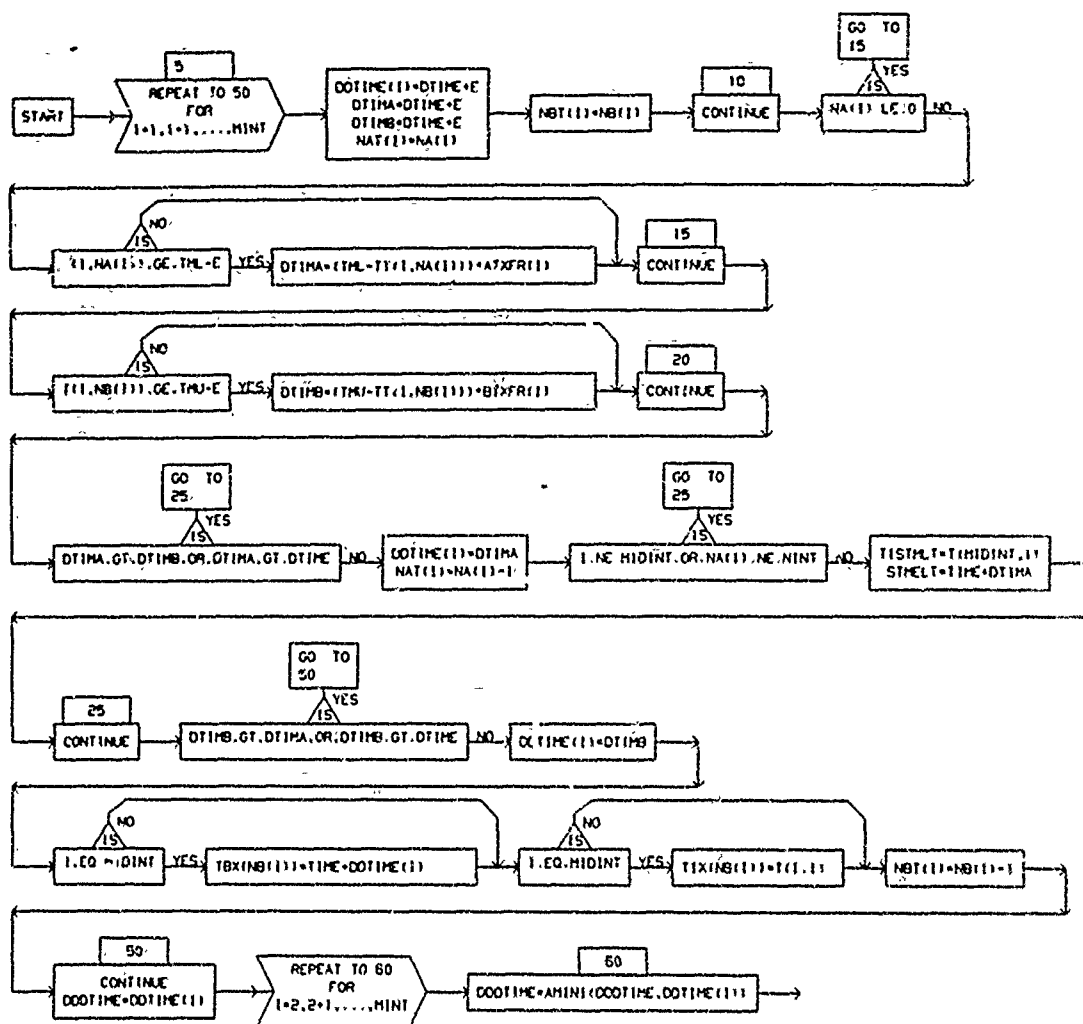
SUBROUTINE VISCSY (TX)

PAGE 1

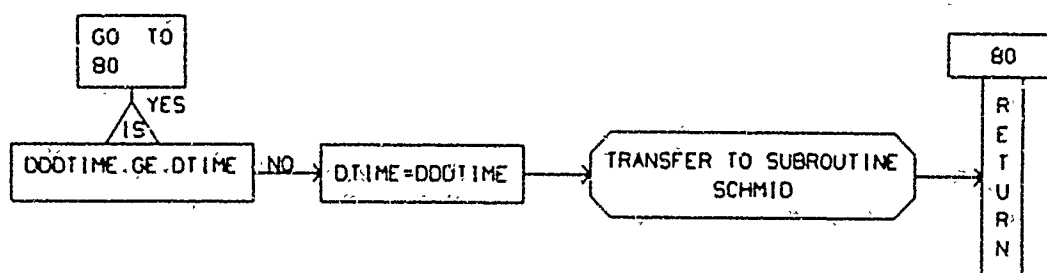


SUBROUTINE XACTIME

PAGE 1



SUBROUTINE XACTIME



APPENDIX C

Thermophysical and Thermodynamic Properties of Aluminum, Magnesium, Titanium, Stainless Steel (AISI 304), and Air as Used in QUEST

Two sources were primarily used in obtaining the thermodynamic and thermophysical properties of the four metals studied. The first (Ref 17), from which specific heats, heats of fusion, and heats of vaporization were taken, is Thermodynamic Properties of 65 Elements-- Their Oxides, Halides, Carbides, and Nitrides compiled by Charles E. Wicks and Frank E. Block and published in 1963 as Bureau of Mines Bulletin 605. This was considered as the most complete and authoritative source available for the calculation of heat content as a function of temperature from room temperature (300°K) through the boiling point. The second source (Ref 18), used to provide conductivities, densities, viscosities, and emissivities, is Recommended Values of the Thermophysical Properties of Eight Alloys, Major Constituents and Their Oxides assembled under the direction of Y. S. Touloukian of Purdue University. This was the most recent (1966), the most thorough, and in most cases the only, source that could be found which presented the listed properties as a function of temperature over the critical ranges of interest. However, extrapolation of this data from within the liquid state to the boiling temperature was necessary to cover any temperature, perhaps unlikely but theoretically possible, that might be encountered by QUEST.

Standard atmospheric properties were used for free stream air conditions. Although only sea level conditions were used in the cases tested thus far, the subroutine ATMOS (a library subprogram obtained

from the Computer Center, Aeronautical Systems Division, Wright-Patterson AFB, Ohio) possesses the capability to compute applicable properties of the atmosphere according to the 1959 ARDC Atmospheric Tables to altitudes of 300,000 feet. Property values of the air for boundary layer calculations, including conductivity, specific heat, enthalpy, and viscosity, were obtained from Refs 19, 20, and 21.

The property value of the metals as used within QUEST will warrant review as any future investigations and experiments which provide a better basis of estimation become available. The present estimates, however, obtained from the limited sources cited and while certainly in error to some extent, are deemed sufficient to provide meaningful trends and comparisons between the modeled metals.

The property values as used in QUEST for aluminum, magnesium, titanium, stainless steel, and air follow.

ALUMINUM

Density:	2.698 gm/cm ³
Melting Point (M.P.):	933°K
Boiling Point (B.P.):	2740°K
Heat of Fusion:	95.185 cal/gm
Heat of Vaporization:	2516.667 cal/gm

Conductivity

$$T < M.P. \quad k = [0.5325466 + T(1.839836 \times 10^{-4} + T(-2.360679 \times 10^{-7}))] \text{ cal}/(\text{sec} \cdot \text{cm} \cdot ^\circ\text{K})$$

$$M.P. < T < B.P. \quad k = [0.21749 + 0.000717(T - 1000^\circ\text{K})] \text{ cal}/(\text{sec} \cdot \text{cm} \cdot ^\circ\text{K})$$

Specific Heat

$$T < M.P. \quad C_p = [0.1831 + T(1.097048 \times 10^{-4})] \text{ cal}/(\text{gm} \cdot ^\circ\text{K})$$

$$T > M.P. \quad C_p = 0.259 \text{ cal}/(\text{gm} \cdot ^\circ\text{K})$$

Viscosity

$$\mu = 0.07612433 + T[-1.460141 \times 10^{-4} + T(1.24557 \times 10^{-7} + T\{-5.404153 \times 10^{-11} + T[1.181837 \times 10^{-14} + T(-1.035147 \times 10^{-18})]\})] \text{ poise}$$

Hemispherical Total Emissivity

$$\epsilon = 0.022 + 0.00006(T)$$

NOTE: T is temperature expressed in °K.

MAGNESIUM

Density:	1.738 gm/cm ³
Melting Point (M.P.):	923°K
Boiling Point (B.P.):	1393°K
Heat of Fusion:	88.845 cal/gm
Heat of Vaporization:	1295.656 cal/gm

Conductivity

$$T < M.P. \quad k = 0.37762 + T(-0.0000478) \text{ cal}/(\text{sec} \cdot \text{cm} \cdot ^\circ\text{K})$$

$$M.P. < T < B.P. \quad k = 0.1673 \text{ cal}/(\text{sec} \cdot \text{cm} \cdot ^\circ\text{K})$$

Specific Heat

$$T < M.P. \quad C_p = 0.25255 + T(6.1697927 \times 10^{-5}) + T^{-2}(3208.2922) \text{ cal}/(\text{gm} \cdot ^\circ\text{K})$$

$$T > M.P. \quad C_p = 0.32 \text{ cal}/(\text{gm} \cdot ^\circ\text{K})$$

Viscosity

$$\mu = 1.460654 \times 10^{-1} + T\{-2.911014 \times 10^{-4} + T[2.0358 \times 10^{-7} + T(-4.880739 \times 10^{-11})]\} \text{ poise}$$

Hemispherical Total Emissivity

$$\epsilon = 0.08 + 0.000178 (T)$$

NOTE: T is temperature expressed in °K.

TITANIUM

Density:	4.50 gm/cm ³
Melting Point (M.P.):	1988.0°K
Boiling Point (B.P.):	3550.0°K
Heat of Fusion:	93.946 cal/gm
Heat of Vaporization:	2108.56 cal/gm

Conductivity

$$\begin{aligned}
 T < M.P. \quad k = & 0.075251 + T(-0.00010874 + T[1.353216 \times 10^{-7} \\
 & + T[-6.294976 \times 10^{-11} + T(1.013052 \times 10^{-14})]]) \\
 & \cdot \text{cal}/(\text{sec} \cdot \text{cm} \cdot ^\circ\text{K})
 \end{aligned}$$

$$M.P. < T < B.P. \quad k = 0.035$$

Specific Heat

$$\begin{aligned}
 T < M.P. \quad C_p = & 0.071942 + T[0.0002821 + T(-5.009421 \times 10^{-7} \\
 & + T[5.059385 \times 10^{-10} + T[-2.400367 \times 10^{-13} \\
 & + T(4.327858 \times 10^{-17})]])] \text{ cal}/(\text{gm} \cdot ^\circ\text{K})
 \end{aligned}$$

$$T > M.P. \quad C_p = 0.167 \text{ cal}/(\text{gm} \cdot ^\circ\text{K})$$

Viscosity

$$\mu = 0.005 + 0.06e^{[(1915^\circ\text{K} - T)/125]} \text{ poise}$$

Hemispherical Total Emissivity

$$T < 950^\circ\text{K} \quad \epsilon = 0.08 + 1.818182T$$

$$T > 950^\circ\text{K} \quad \epsilon = 0.20 + 1.17647T$$

NOTE: T is temperature expressed in $^\circ\text{K}$

STAINLESS STEEL (AISI 304)

Density:	7.9 gm/cm ³
Melting Point (M.P.):	1730.0°K
Boiling Point (B.P.):	3000.0°K
Heat of Fusion:	66.252 cal/gm
Heat of Vaporization:	1515.211 cal/gm

Conductivity

$$T < M.P. \quad k = 0.0155816 + T[1.039741 \times 10^{-4} + T(-1.579824 \times 10^{-7} \\ + T[1.653638 \times 10^{-10} + T[-8.215264 \times 10^{-14} \\ + T(1.565207 \times 10^{-17})]])] \text{ cal/(sec} \cdot \text{cm} \cdot ^\circ\text{K)}$$

$$M.P. < T < B.P. \quad k = 0.05258 \text{ cal/(sec} \cdot \text{cm} \cdot ^\circ\text{K)}$$

Specific Heat

$$T < M.P. \quad C_p = 0.06496569 + T[1.696444 \times 10^{-4} + T[-1.119582 \times 10^{-7} \\ + T(2.769178 \times 10^{-11})]] \text{ cal/(gm} \cdot ^\circ\text{K)}$$

$$T > M.P. \quad C_p = 0.1791 \text{ cal/(gm} \cdot ^\circ\text{K)}$$

Viscosity

$$\mu = 2.448646 + T[-4.22152 \times 10^{-5} + T(2.987352 \times 10^{-6} + T[-1.067079 \times 10^{-9} \\ + T[1.911987 \times 10^{-13} + T(-1.369543 \times 10^{-17})]])] \text{ poise}$$

Hemispherical Total Emissivity

$$200^\circ\text{K} < T < 700^\circ\text{K} \quad \epsilon = 0.095 + 0.0002(T)$$

$$T > 700^\circ\text{K} \quad \epsilon = 0.165 + 0.0001(T)$$

NOTE: T is temperature expressed in °K.

AIR

Standard atmospheric properties at sea level:

$$T = 288.16^\circ\text{K}$$

$$\text{Speed of sound} = 340.29205 \text{ m/sec} = 1,116.89 \text{ ft/sec}$$

$$p = 10.1325 \text{ nt/cm}^2 = 14.696 \text{ lb/in}^2$$

$$\rho = 0.001225 \text{ gm/cm}^3 = 3.7457 \text{ slug/ft}^3$$

Conductivity

$$k_0 = 5.88218832 \text{ cal/}(\text{sec}\cdot\text{cm}\cdot^\circ\text{K})$$

$$T_0 = 500^\circ\text{R}$$

$$k = k_0[0.0306331 + 1.07642(T/T_0) - 0.113939(T/T_0)^2 \\ + 0.00679309(T/T_0)^3] \text{ cal/}(\text{sec}\cdot\text{cm}\cdot^\circ\text{K})$$

Specific Heat

$$c_{p0} = 0.2395 \text{ cal/}(\text{gm}\cdot^\circ\text{K})$$

$$T_0 = 500^\circ\text{K}$$

$$c_p = c_{p0}[0.979 + 0.00651928(T/T_0) + 0.0158536(T/T_0)^2 \\ - 0.00155636(T/T_0)^3] \text{ cal/}(\text{gm}\cdot^\circ\text{K})$$

Enthalpy

$$h_0 = 66.377778 \text{ cal/gm}$$

$$T_0 = 500^\circ\text{R}$$

$$h = 66.37778[0.01836064 + 0.9395396(T/T_0) \\ + 0.03243428(T/T_0)^2 - 9.91742\times 10^{-4}(T/T_0)^3] \text{ cal/gm}$$

Viscosity

$$\mu_0 = 2.55936\times 10^{-4} \text{ gm/}(\text{sec}\cdot\text{cm})$$

$$T_0 = 900^\circ\text{R}$$

$$\mu = \mu_0 \sqrt{T/T_0} \text{ gm/}(\text{sec}\cdot\text{cm})$$

APPENDIX D

Numerical Results from QUEST for 0.05, 0.10, and 0.20 cm Thick Aluminum,
Magnesium, Titanium, and Stainless Steel Irradiated by 1.0 and 10.0 kw
Power Over Spots of 1.0 and 10.0 cm² at Selected
Mach Numbers Between 0.0 and 4.0

TABLE D-I
Melt-Through Times (in Seconds) as Predicted by QUEST for Aluminum

Mach Number (at sea level)	Spot Size (cm ²)					
	1.0			10.0		
	Plate Thickness (cm)			Plate Thickness (cm)		
	0.05	0.10	0.20	0.05	0.10	0.20
1.0 kw Absorbed Power						
0.0	0.08535	0.20194	0.52967	0.82320	1.86313	4.41704
0.1	0.08540	0.19978	-	-	-	-
0.5	0.08477	0.19316	0.47043	-	-	4.92163
1.0	0.08444	0.19148	0.46699	-	2.19655	5.32153
1.5	-	-	-	-	2.24050	-
2.0	0.08377	0.18977	0.46090	-	2.17886	5.24222
3.0	-	-	-	-	1.77671	-
4.0	0.07939	0.17682	0.41828	-	1.31212	2.83614
10.0 kw Absorbed Power						
0.0	0.00934	0.02190	0.05554	0.07519	0.15718	0.34103
0.1	-	-	-	0.07533	0.15717	-
0.25	-	-	-	0.07540	-	-
0.5	0.00917	0.01997	0.04173	0.07531	0.153111	0.31521
2.0	0.00846	0.01678	0.03313	0.07448	0.15085	0.30828
4.0	0.00791	0.01582	0.03112	0.07121	0.14386	0.29477

TABLE D-II
Melt-Through Times (in Seconds) as Predicted by QUEST for Magnesium

Mach Number (at sea level)	Spot Size (cm ²)					
	1.0			10.0		
	Plate Thickness (cm)			Plate Thickness (cm)		
	0.05	0.10	0.20	0.05	0.10	0.20
1.0 kw Absorbed Power						
0.0	0.05846	0.13485	0.34751	0.55793	1.22602	2.89378
0.1	0.05850	0.13349	0.32574	-	-	-
0.5	0.05794	0.12797	-	0.60350	1.33226	3.16028
1.0	0.05750	0.12579	0.29493	-	1.40712	3.37728
1.5	-	-	-	0.64631	1.43397	-
2.0	0.05682	0.12434	0.28970	-	1.39618	3.30165
3.0	-	-	-	-	1.16482	2.60833
4.0	0.05400	0.11659	-	-	0.87862	1.87628
10.0 kw Absorbed Power						
0.0	0.00727	0.02108	0.06527	0.05332	0.11212	0.24451
0.1	-	-	-	0.05341	0.11210	-
0.5	0.00694	0.01540	0.03087	0.05332	0.10934	0.22138
2.0	0.00626	0.01232	0.02439	0.05238	0.10516	0.21158
4.0	0.00586	0.01156	0.02203	0.05005	0.10071	0.20484

TABLE D-III
Melt-Through Times (in Seconds) as Predicted by QUEST for Titanium

Mach Number (at sea level)	Spot Size (cm ²)					
	1.0			10.0		
	Plate Thickness (cm)			Plate Thickness (cm)		
	0.05	0.10	0.20	0.05	0.10	0.20
1.0 kw Absorbed Power						
0.0	0.20763	0.46671	1.15179	1.99589	4.22383	9.4575
0.1	0.20713	0.44930	0.99254	-	4.40521	9.7064
0.5	0.20257	0.42399	0.91670	2.36293	5.01379	11.2717
1.00	0.201312	0.421019	0.903722	2.73299	5.88005	13.7029
2.00	0.20065	0.41977	0.91325	3.51087	7.81713	20.3557
4.00	0.19664	0.41074	0.89954	3.23944	6.98538	-
6.00	-	-	-	-	3.16585	-
10.0 kw Absorbed Power						
0.0	0.03201	0.10184	0.30469	0.19696	0.41948	0.92913
0.1	-	-	-	0.19754	0.41346	-
0.25	-	-	-	0.19677	-	-
0.5	0.02577	0.05213	0.10236	0.19542	0.39231	0.77309
2.0	0.02141	0.04211	0.08358	0.19304	0.38146	0.76627
4.0	0.02075	0.04023	-	0.18873	0.37820	0.76285

TABLE D-IV

Melt-Through Times (in Seconds) as Predicted by QUEST for Stainless Steel

Mach Number (at sea level)	Spot Size (cm ²)					
	1.0			10.0		
	Plate Thickness (cm)			Plate Thickness (cm)		
	0.05	0.10	0.20	0.05	0.10	0.20
1.0 kw Absorbed Power						
0.0	0.26018	0.58389	1.43667	2.50173	5.28696	11.7950
0.1	0.26056	0.57556	1.30990	-	-	-
0.5	0.257121	0.54425	1.18365	2.90293	6.16154	13.7963
1.0	0.25493	0.53390	1.14413	3.27428	7.02708	16.2477
2.0	0.25276	0.53106	1.14560	3.91964	8.60810	21.2044
3.0	-	-	-	-	8.64554	21.2096
4.0	0.24664	0.51299	1.1120	3.21920	6.81835	15.3470
10.0 kw Absorbed Power						
0.0	0.03760	0.11804	0.36298	0.24689	0.52481	1.15785
0.1	-	-	-	0.24769	0.52489	-
0.5	0.03494	0.07705	0.14304	0.24729	0.50430	0.99877
1.0	-	-	-	-	-	0.96467
2.0	0.03023	0.06090	0.10138	0.24407	0.47639	0.95862
3.0	-	-	-	-	-	0.95426
4.0	0.02709	0.05197	0.09482	0.23533	0.467544	0.94398

VITA

Richard Glen Wigglesworth was born May 13, 1935, and raised on his parents' farm in Dane County, Wisconsin. After graduating from Lodi High School in 1953, he entered the University of Wisconsin from which, in 1957, he received the degree of Bachelor of Science in Agriculture and Education and a commission in the United States Air Force. He then served as a security police officer with Air Force units in France and New Mexico until entering the Air Force Institute of Technology in 1964 and where in 1966 he was awarded the degree of Bachelor of Science in Aerospace Engineering. After a four-year, intervening assignment with the Service Engineering Division, Ogden Air Materiel Area, Air Force Logistics Command, where he held several engineering-management positions, he returned to the Air Force Institute of Technology and is presently a candidate for the degree of Master of Science in Aerospace Engineering.

Permanent Address: 4232 Rushton Drive
Dayton, Ohio 45431

This thesis was typed by Mrs. Virginia Blakelock